PRIMARY PHOTOCHEMICAL PROCESSES IN HEXAFLUOROBIACETYL

by

William John Reid

B.A. (Moderatorship), Trinity College,

University of Dublin, Ireland, 1967

M.Sc., University of British Columbia, 1970

A THESIS SUBMITTED IN PARTIAL FULFILMENT OF

THE REQUIREMENTS FOR THE DEGREE OF

DOCTOR OF PHILOSOPHY

In the Department

of

CHEMISTRY

We accept this thesis as conforming to the

required standard.

THE UNIVERSITY OF BRITISH COLUMBIA

September, 1972

In presenting this thesis in partial fulfilment of the requirements for an advanced degree at the University of British Columbia, I agree that the Library shall make it freely available for reference and study. I further agree that permission for extensive copying of this thesis for scholarly purposes may be granted by the Head of my Department or by his representatives. It is understood that copying or publication of this thesis for financial gain shall not be allowed without my written permission.

Department of Chemistry

The University of British Columbia
Vancouver 8, Canada

Date 22nd September, 1972

ABSTRACT

Absolute photochemical quantum yields of hexafluorobiacetyl vapour have been obtained at various exciting wavelengths between 250 and 440 nm over the range 0.5 - 400 torr. The yields are strongly dependent on pressure demonstrating that vibrational relaxation is the dominant process competing with unimolecular dissociation.

It is found that two different states contribute to dissociation. One is identified as the excited singlet level reached on excitation. The other is attributed to the vibronic level reached on intersystem crossing from that initially formed vibronic state. The intersystem crossing rate constant has been shown to be a strong function of excitation energy. It is postulated that the first excited singlet state of hexafluorobiacetyl is photochemically inert unless it has at least 70 kcal of vibronic energy. This accounts for no decomposition being observed at the higher wavelengths. Temperature and quenching studies have shown that the equilibrated triplet state is unreactive photochemically. Phosphorescence lifetime measurements at very low pressures have confirmed

that wall-deactivation for the relatively long lived equilibrated triplet species is important when the average distance which the triplet molecule can diffuse is of the same magnitude as the cell radius.

The data from the various investigations are combined to give a description of the primary photochemical and photophysical events. From this information a mechanism for the primary process in hexafluorobiacetyl is proposed and critically evaluated. Estimates of the specific rate constants for the photochemical processes are given and discussed.

TABLE OF CONTENTS

Page

Title Page..... i

Abstract..... ii

Table of Contents..... iv

List of Figures..... vii

List of Tables..... ix

Acknowledgements..... x

CHAPTER I. INTRODUCTION..... 1

A. The Primary Process..... 1

B. Fluorinated Ketones..... 9

C. Previous Work on Hexafluorobiacetyl..... 11

D. Purpose of this Investigation..... 16

CHAPTER II. EXPERIMENTAL ARRANGEMENT AND PROCEDURE.. 18

A. Brief Synopsis of Experimental Procedure..... 18

B. Vacuum System..... 20

C. Preparation and Purification of Chemicals..... 21

D. Optical Arrangements..... 22

E. Reaction Cells..... 25

F. Temperature Control Systems..... 27

G. Gas Analysis..... 28

H. Actinometry..... 31

I. Measurement of the Fraction of Light Absorbed by the Sample..... 32

Page

J. Emission Spectroscopy..... 33

K. Lifetime Measurements..... 33

L. Errors..... 35

CHAPTER III. PHOTOCHEMISTRY OF HFB - RESULTS..... 36

A. Absorption..... 36

B. Ratio Experiments..... 36

C. Reliability of the Photolysis Data..... 38

D. Photolysis of HFB at 25° C..... 40

E. HFB Photolysis at Different Temperatures..... 50

F. HFB - HFAM System..... 51

(i) Quenching Study..... 51

(ii) Photolysis of HFB - HFAM Mixtures..... 53

CHAPTER IV. DISSOCIATION AND COLLISIONAL DEACTIVATION 58

A. Graphical Presentation of Results..... 58

B. General Observations..... 59

C. Proposed Mechanism..... 60

D. Discussion..... 75

(i) Collisional Deactivation..... 75

(ii) Mechanistic Considerations..... 76

(iii) Photochemical Inertness of Equilibrated Triplet..... 78

(iv) Triplet Dissociation..... 79

(v) Light Intensity..... 79

Page

(vi) Evaluation of Rate Constants..... 81

(vii) Simulation of Quantum Yield Results..... 84

(viii) Variation of k_1, k_2 and k_5 with Wavelength.. 85

(ix) Other Possible Mechanisms..... 90

(a) Involvement of the Vibrationally Excited Ground State..... 90

(b) Vibrational Energy Distribution Function.. 91

(x) Wall-Deactivation of the Equilibrated Triplet State..... 91

CHAPTER V. THE PRIMARY PROCESS..... 97

A. Detailed Mechanism..... 97

B. Independent Evaluation of $(k_1 + k_2)$..... 100

C. Evaluation of k_2 from the Full Mechanism..... 101

(i) Fluorescence/Photochemistry Ratio..... 101

(ii) Phosphorescence/Photochemistry Ratio..... 103

(iii) Discussion..... 105

D. Complementary Aspects of this and Previous Work.... 105

(i) Fluorescence and Intersystem Crossing..... 108

(ii) Limitations on Available Data..... 112

E. Concluding Remarks - Suggestions for Further Work.. 115

BIBLIOGRAPHY..... 118

APPENDIX..... 123

A. Window Corrections..... 124

B. Wall Deactivation..... 126

LIST OF FIGURES

Figure		Page
1.	Jablonski diagram of hexafluorobiacetyl.....	4
2.	Photolysis system.....	19
3.	Photolysis line shapes.....	23
4.	5-cm reaction cell and mixer.....	26
5.	Gas analysis system.....	29
6.	Absorption spectra of hexafluorobiacetyl at 25° C	37
7.	Stern-Volmer quenching of hexafluorobiacetyl phosphorescence.....	57
8.	Reciprocal quantum yields versus pressure - 254 nm, 25° C. High pressure region.....	61
9.	Reciprocal quantum yields versus pressure - 254 nm, 25° C. Low pressure region.....	62
10.	Reciprocal quantum yields versus pressure - 297 nm, 25° C. High pressure region.....	63
11.	Reciprocal quantum yields versus pressure - 297 nm, 25° C. Low pressure region.....	64
12.	Reciprocal quantum yields versus pressure - 313 nm, 25° C. High pressure region.....	65
13.	Reciprocal quantum yields versus pressure - 313 nm, 25° C. Low pressure region.....	66
14.	Reciprocal quantum yields versus pressure - 313 nm, 25° C. Low pressure region.....	67
15.	Reciprocal quantum yields versus pressure - 334 nm, 25° C. High pressure region.....	68
16.	Reciprocal quantum yields versus pressure - 334 nm, 25° C. Low pressure region.....	69

Figure		Page
17.	Reciprocal quantum yields versus pressure - 366 nm, 25° C. High pressure region.....	70
18.	Reciprocal quantum yields versus pressure - 297 nm, 25° C and -20° C.....	71
19.	Reciprocal quantum yields versus pressure - 313 nm, various temperatures.....	72
20.	Quantum yields versus reciprocal pressures - High pressure region.....	80
21.	Log of the various rate constants versus excitation energy.....	89
22.	Difference (γ) between the reciprocals of the observed lifetime (τ) at low pressures and the constant high pressure triplet lifetime (τ_0) versus HFB pressure.....	94
23.	Difference (γ) between the reciprocals of the observed lifetime (τ) at low pressures and the constant high pressure triplet lifetime (τ_0) versus reciprocal HFB pressure.....	95
24.	Ratio of fluorescence yield to photochemical yield versus HFB pressure at 313 nm. High pressure region	107
25.	Ratio of phosphorescence yield to photochemical yield versus HFB pressure at 313 nm. High pressure region.....	107
26.	Ratio of fluorescence yield to photochemical yield versus HFB pressure at 297 nm.....	110
27.	Ratio of fluorescence yield to photochemical yield versus HFB pressure at 313 nm.....	111
28.	Fluorescence quantum yield versus HFB pressure at 313 nm.....	113
29.	Phosphorescence quantum yield versus HFB pressure at 313 nm.....	114

LIST OF TABLES

Table		Page
1.	Mean molar absorption coefficients of HFB at the wavelengths used in photolysis at 25° C.....	39
2.	Ratio experiments.....	39
3.	Photolysis of HFA at 313 nm and 25° C.....	41
4.	Photolysis of HFB at 254 nm and 25° C.....	41
5.	Photolysis of HFB at 297 nm and 25° C.....	42
6.	Photolysis of HFB at 313 nm and 25° C.....	44
7.	Photolysis of HFB at 334 nm and 25° C.....	45
8.	Photolysis of HFB at 366 nm and 25° C.....	46
9.	Photolysis of HFB at 405 nm and 25° C.....	47
10.	Photolysis of HFB at 436 nm and 25° C.....	47
11.	Photolysis of HFB at 297 nm and -20° C.....	48
12.	Photolysis of HFB at 313 nm and 50° C.....	48
13.	Photolysis of HFB at 313 nm and 76° C.....	49
14.	Photolysis of HFB/HFAM mixtures at 25° C.....	55
15.	Rate constants for dissociation and intersystem crossing at 25° C.....	81
16.	Rate constants for dissociation and intersystem crossing at various temperatures.....	82
17.	Rate constants for the sum of singlet dissociation and intersystem crossing from the initially populated vibronic singlet state.....	102
18.	Rate constants for singlet dissociation.....	106

ACKNOWLEDGEMENTS

I wish to sincerely thank Dr. Gerald B. Porter for his guidance and understanding during the course of this work. His encouragement not only aided in the progress of this work but also in the development of this researcher.

I am indebted to Dr. N. Basco, Mr. J.E. Hunt, Dr. J.S.E. McIntosh and Dr. R. May for many helpful discussions relating to this research problem. In addition the excellent craftmanship of Mr. S. Rak and Mr. J. Molnar of the Glassblowing Shop and of Mr. B. Powell and his colleagues of the Mechanical Shop is warmly appreciated.

Finally, I wish to thank my wife, Pamela, whose infinite patience and constant encouragement made this thesis possible.

to the

REIDS

and

DILLS

CHAPTER ONE

INTRODUCTION

A. The Primary Process

Carbonyl compounds have probably attracted more attention in the photochemical field than any other class of compound. The production of radicals during photolysis has been a major interest. Accessibility of the long-wavelength absorption band in the near UV region of the spectrum has enabled detailed studies to be made. In particular, the photochemical and photophysical behavior of aliphatic ketones in the gas phase has been studied extensively. It has become obvious that the systems have considerable kinetic complexity.

The Primary Process comprises the initial act of absorption of a photon by a molecule to produce an excited electronic state, and all subsequent events which lead either to disappearance of the molecule (primary photochemical process), or to the return of the molecule to its thermally equilibrated ground electronic state (primary photophysical processes).

In the primary photochemical process there is usually a variety of paths for degradation of the electronic energy of excitation. Chemical paths include intramolecular rearrangements (e.g. cis-trans isomerization of olefins) and the formation of free radicals which combine with each other, (e.g. $CF_3 + CF_3 \rightarrow C_2F_6$ in hexafluoroacetone) or which combine with other molecules in secondary processes to form new products. Frequently the unknown nature and magnitude of these latter processes tend to obscure the primary process.

The first absorption band of ketones, which generally has a maximum around 280 nm, results from excitation of one of the non-bonding electrons of the carbonyl oxygen into an antibonding orbital i.e. an $\pi^* \leftarrow n$ transition. The excited singlet state so produced is designated S_1. Other electronic states are abbreviated thus: S_0 (ground); S_2, S_3 ... (excited singlets); T_1, T_2 ... (excited triplets).

Absorption of light produces a species containing part of the excitation energy as excess vibrational energy. The stationary state concentration of excited species is, under normal circumstances, so small that they are essentially

surrounded by a heat bath of unexcited molecules. In principle, the vibrationally excited molecule in an upper electronic state can attain vibrational equilibrium by two mechanisms. Either this degradation of vibrational energy is accomplished by a single-step deactivation from high to low vibrational levels or by a multistep cascade from one group of vibrational levels to the next lower group.[1-6] Recent studies on hexafluoroacetone[4,7] and also on the isomerization of 1,3,5-cycloheptatriene[8,9] support a multistage process. In the latter study the photochemical isomerization to toluene occurs via the vibrationally excited ground state molecule. Atkinson and Thrush[8,9] obtained the amount of vibrational energy removed per collision when quenching of isomerization by various added gases was studied at a variety of wavelengths. Nevertheless, much of the contemporary kinetic data lends support to the concept of strong collisional transfer.

The paths that exist for energy dissipation from the photoexcited molecule are illustrated schematically by the Jablonski diagram for hexafluorobiacetyl (Figure 1).

FIG.1

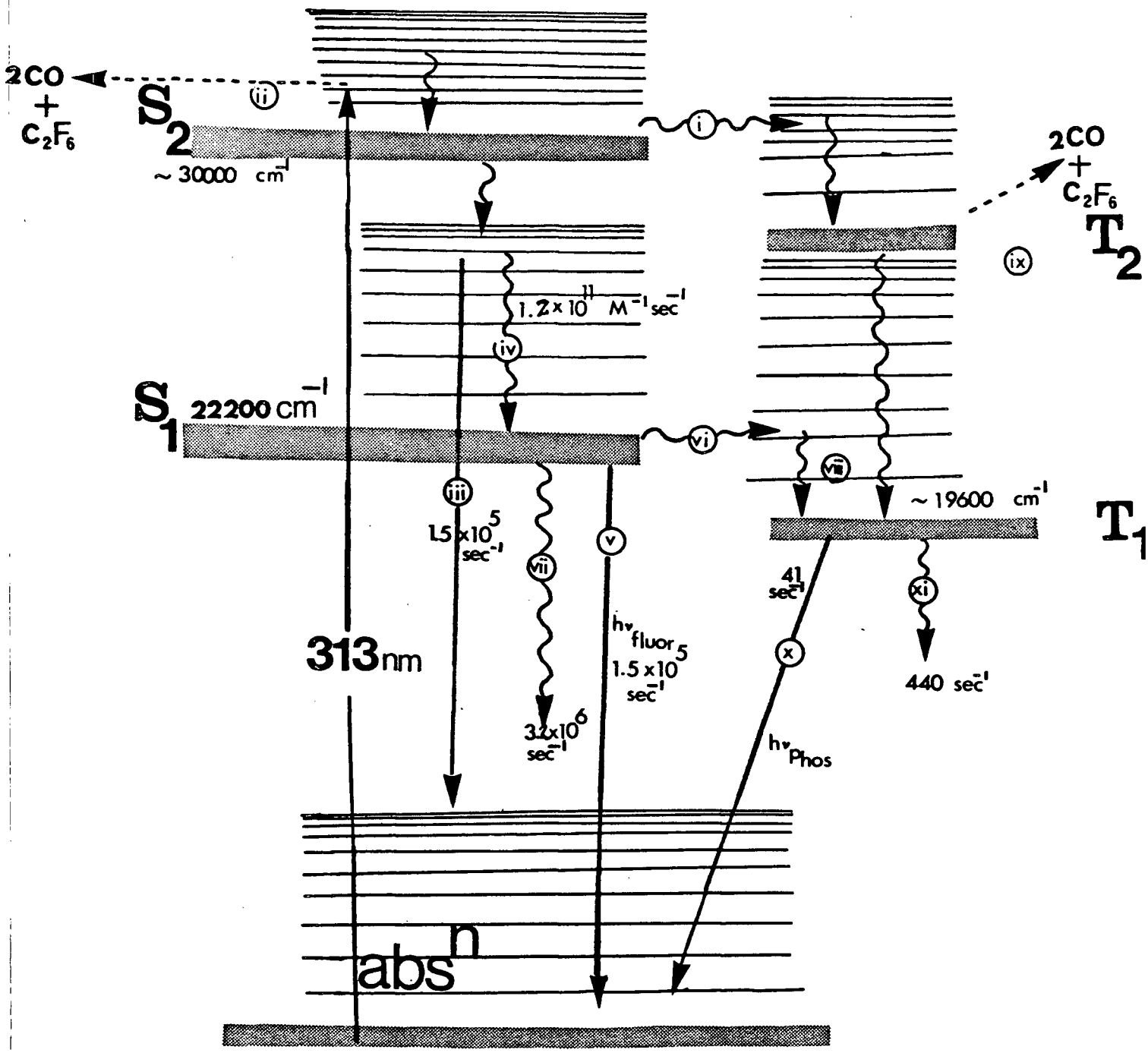

JABLONSKI DIAGRAM OF HEXAFLUOROBIACETYL

Processes (ii) and (ix), photodissociation, will both occur in the general case. They must take place rapidly to compete with internal conversion and loss of vibrational energy by collisions. Dissociation from the triplet will occur from the vibrational level reached from intersystem crossing. Although it seems that T_1^o (lowest vibrational level of first excited triplet state) may be long-lived enough to be re-energized by collision and dissociate in certain molecules (e.g. hexafluoroacetone), this thermal dissociation should be absent in HFB as the phosphorescence lifetime is both temperature independent and pressure independent near room temperature. Process (ii) will have a very small temperature dependence due to the Boltzmann vibrational energy distribution in the ground state. Both (ii) and (ix) should be wavelength dependent.

From level 0 of S_1, the molecule can return to any one of the vibration-rotation levels of the ground state with the emission of fluorescence. Fluorescence is a radiative transition between states of like multiplicity. With some molecules it seems that fluorescence is coming also from non-equilibrated levels of S_1 (e.g. HFB)[1].

In the absence of quenchers the fluorescence quantum yield depends on the relative rates of the radiative process on the one hand, and the radiationless processes of intersystem crossing (process (vi)) and internal conversion (process (vii)) on the other.

These radiationless processes between electronic states are poorly understood although they are receiving much theoretical interest at present.[10] Internal conversion (a spin allowed transition) ---process (vii)--- is an adiabatic crossing from the lowest excited singlet state to high vibrational levels of the ground state, followed by vibrational relaxation. This appears to be an important route in some systems, such as large dye molecules.[11] whereas in simple aromatics[12] and aliphatic carbonyl systems[13] its contribution is relatively minor.

The singlet-triplet intersystem crossing processes, (i) and (vi), although spin forbidden, occur with rates comparable to that of an allowed radiative transition (k_{isc} = $2.4 \pm 0.4 \times 10^8$ sec^{-1} in biacetyl).[14] As with internal conversion to the ground state, the rate of intersystem crossing increases rapidly as the separation of the levels decreases and, in addition, it depends on the degree of mixing

of the states i.e. the degree of triplet character in the singlet state and vice-versa.[15] In $\pi^* \leftarrow n$ transitions, intersystem crossing is rapid, the energy separation of S_1 and T_1 being small owing to the small overlap of the orbitals. Since the competing radiative transition from upper singlet to ground state is symmetry forbidden, the quantum efficiency of triplet formation often approaches unity (e.g. biacetyl,[16-17] acetone,[13] hexafluoroacetone[4]). Moreover, Calvert and co-workers[14] have recently confirmed Parmenter and Poland's[18] contention that an isolated excited singlet molecule (for biacetyl at least) undergoes a truly unimolecular intersystem crossing reaction with the same efficiency as in the collisionally perturbed system at high pressures.

Radiative transitions between states of different multiplicity (e.g. triplet-singlet) can take place. This luminescence is called phosphorescence.

In addition, however, a molecule in a vibrationally and electronically excited state has a small but finite radiative transition probability to other vibrational states of the same electronic state. A system of such molecules should emit the infrared photons corresponding to these transitions. This effect has been reported for the triplet

state of biacetyl.[19]

The importance of fluorescence and phosphorescence lies not in their absolute magnitude (usually less than 20% of excited molecules lose energy via emission in carbonyl compounds) but in their diagnostic value. For example, if intersystem crossing to the triplet manifold is only via process (vi) which competes with fluorescence from the equilibrated singlet state, pressure dependencies in the fluorescence yields should be reflected by the phosphorescence yields too. This was found to be the case in biacetyl.[17] An increase in the fluorescence yield as the pressure is raised indicates that photochemistry is quenched from a higher vibrational level.

Although it is a spin forbidden transition, conversion from the lowest triplet to ground state, process (xi), seems to be more important than conversion from the lowest singlet level. This is a result of the competing radiative process being very much slower. Radiationless conversion from the lowest triplet to ground state appears to be a major pathway for energy dissipation in ketones unless the primary photochemical yield is large.[15]

B. Fluorinated Ketones

Aliphatic ketones have been the subject of innumerable gas phase photochemical investigations.[13,20] There are principally two reasons for this attention. Firstly, these ketones are structurally simple and therefore would seem to offer the easiest examples for quantitative study of the primary process. Secondly, their longest wavelength absorption ($\pi^* \leftarrow n$) lies at about 300 nm and is readily accessible both in terms of excitation sources and optical instrumentation.

Unfortunately, however, the photochemistry of aliphatic ketones can be complicated by the large number of products formed.[20] The simplest member of the series, acetone, can give as products carbon monoxide, ethane, methane, biacetyl, methyl ethyl ketone, ketene and acetaldehyde depending on the conditions of photolysis.[13]

Biacetyl (butane -2,3-dione), the first member of the homologous series of the diketones, is equally complex. These compounds fail to be photochemically simple due to the relative weakness of the C-H bond (82 kcal/mole). Radicals formed in the primary photochemical act readily abstract hydrogen atoms from the parent ketone, producing many final products. Acetone has the added disadvantage that one of its

products, biacetyl, quenches its emission. Other members of the acetone and biacetyl homologous series are plagued by similar complications.

The situation is not much improved in fully chlorinated[13] or partially chlorinated ketones.[21,22] For fully fluorinated ketones, however, the strong C-F bond (114 kcal/mole) results in a suppression of secondary reactions over a wide range of conditions. For example, the primary photochemical act in hexafluoroacetone results solely in the formation of CF_3 and CO in a 2:1 molar ratio at temperatures up to 370° C.[23]

A great deal of photochemical as well as photophysical studies have been done on HFA.[2,4] It both fluoresces and phosphoresces, so it would seem to be an ideal molecule in which to observe details of the primary process. However it has one drawback: its equilibrated triplet state is long-lived enough to dissociate thermally at room temperature. This complicates the diagnosis of the primary process as it is a relatively large effect. Any photochemistry originating from an excited vibronic triplet state would probably be obscured by its magnitude. It appears that in HFB, this pathway (analogous to thermal dissociation) is absent at a similar temperature.[1]

C. Previous Work on Hexafluorobiacetyl

Whittemore and Szwarc[24] in 1963 published a short note on the gas phase photolysis of HFB at 25° C and 150° C. They found carbon monoxide and hexafluoroethane produced in a 2:1 molar ratio. Subsequently some preliminary photochemical quantum yields were obtained at 313 nm.[25] McIntosh[1] studied the phosphorescence and fluorescence quantum yields of HFB vapour at various exciting wavelengths between 290 and 440 nm, thereby showing, in a quantitative manner, the importance of emission processes in energy dissipation. Furthermore, he showed the importance of vibrational relaxation processes and how they affect other parameters. He was also able to make assignments regarding the observed electronic transitions from the absorption and emission spectra. Interestingly, he observed that the phosphorescence lifetime of HFB vapour was independent of temperature from 27° to -57° C. within experimental error.

Details of McIntosh's work: to explain his emission results quantitatively he assumed only three species were of importance, namely, the vibrationally hot singlet state reached on excitation and the thermally equilibrated excited singlet

and triplet states which result after vibrational relaxation. Such a "strong" collisional mechanism is not altogether realistic in view of recent work by Kutschke and co-workers[4] and Halpern and Ware.[7]

A kinetic description of the primary process, which includes a complete multistage vibrational degradation, becomes algebraically unmanageable in the sense of an actual evaluation of rate-constants, or even in terms of a quantitative test of the mechanism via various graphical plots. Actually, the strong collision approach is already complicated even though it is a gross simplification. The processes necessary to account for the observed results are as follows:

$$B + h\nu \longrightarrow {}^1B^*$$

$${}^1B^* \xrightarrow{k_1} {}^3B^* \qquad \text{(i)}$$

$${}^1B^* \xrightarrow{k_2} 2CO + C_2F_6 \qquad \text{(ii)}$$

$${}^1B^* \xrightarrow{k_f^*} B + h\nu_f \qquad \text{(iii)}$$

$${}^1B^* + M \xrightarrow{\omega} {}^1B^0 + M^* \qquad \text{(iv)}$$

$${}^1B^0 \xrightarrow{k_f} B + h\nu_{fluor} \qquad \text{(v)}$$

$${}^1B^0 \xrightarrow{k_{isc}} {}^3B^* \qquad \text{(vi)}$$

$${}^1B^0 \xrightarrow{k_6} B \qquad \text{(vii)}$$

$${}^3B^* + M \xrightarrow{\omega} {}^3B^0 + M \qquad \text{(viii)}$$

$$^3B^* \xrightarrow{k_5} 2CO + C_2F_6 \qquad \text{(ix)}$$

$$^3B^0 \xrightarrow{k_p} B + h\nu_{phos} \qquad \text{(x)}$$

$$^3B^0 \xrightarrow{k_{11}} B \qquad \text{(xi)}$$

$$^3B^0 + {}^3B^0 \xrightarrow{k_{12}} ? \qquad \text{(xii)}$$

with B a ground state hexafluorobiacetyl molecule, and M, any molecule which causes vibrational equilibration. The superscripts 1 and 3 refer to the multiplicity of the excited molecules and the superscripts 0 and an asterisk denote molecules in equilibrium and non-equilibrium vibrational states respectively.* It should be noted that McIntosh assumed that the state involved for processes (viii) and (ix) was a vibrationally excited triplet.

From a steady-state treatment of the mechanism, the emission yields were given by the expressions

$$\phi_f = \frac{k_f \ \omega M}{(k_f + k_{isc} + k_6)\ (k_f^* + k_1 + k_2 + \omega M)} + \frac{k_f^*}{(k_f^* + k_1 + k_2 + \omega M)} \qquad (1)$$

$$\phi_p = \frac{\beta \ \omega M}{(\omega M + k_5)} \cdot \frac{k_{isc}}{(k_f + k_{isc} + k_6)} \cdot \frac{\omega M}{(k_f^* + k_1 + k_2 + \omega M)}$$

*The notation and numbering scheme used here will be continued throughout the thesis.

$$+ \frac{\beta \quad \omega M}{(\omega M + k_5)} \qquad \frac{k_1}{(k_f^* + k_1 + k_2 + \omega M)} \qquad \text{---------(2)}$$

$$\text{with } \beta = \frac{k_p}{k_p + k_{11}} \quad .$$

It follows from equations (1) and (2) that when M = 0,

$$\phi_f = \phi_f^0 \doteq \frac{k_f^*}{(k_f^* + k_1 + k_2)} \qquad \text{----------(3)}$$

a constant, and $\phi_p^0 = 0$.

At infinite pressure the limiting yields become:

$$\phi_f^\infty = \frac{k_f}{(k_f + k_{isc} + k_6)} \qquad \text{-----(4)} \qquad \text{and} \qquad \phi_p^\infty = \frac{\beta \quad k_{isc}}{(k_f + k_{isc} + k_6)} \qquad \text{----(5}$$

i.e. ϕ_f^∞ and ϕ_p^∞ are constant, independent of pressure and wavelength.

In the intermediate pressure range the pattern is more complex. However, the shape the emission yields should take are shown below. McIntosh's results showed these general trends.

PREDICTED FORM OF THE EMISSION YIELDS

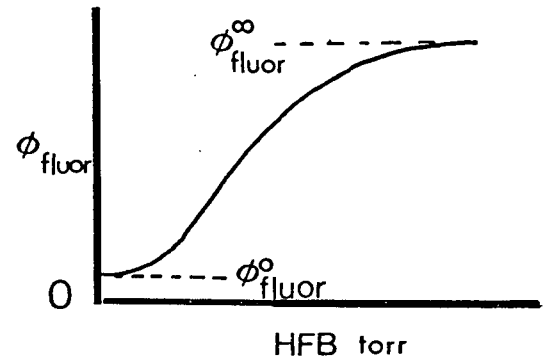

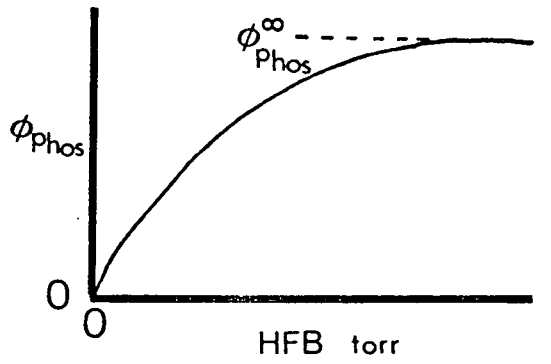

He rationalized the different pressure dependencies of ϕ_{phos}^{*} and ϕ_{fluor}^{*} in the lower pressure region as evidence for:

(a) Fluorescence from non-equilibrated $^{1}B^{*}$ levels (process (iii)).

(b) Intersystem crossing to the triplet manifold from excited singlet levels (process (i)) as well as from equilibrated levels (process (vi)).

(c) Dissociation from the vibronic triplet state reached by intersystem crossing (process (ix)).

Moreover, he found that the ϕ_{fluor} extrapolates smoothly to a finite limit at zero pressure. This residual fluorescence yield decreases with increasing excitation energy as process (ii) presumably becomes dominant. Kutschke and co-workers have observed this effect in HFA.[4]

D. Purpose of this Investigation

Quantitative documentation of the primary process is virtually unknown in aliphatic systems. Biacetyl and HFA are possibly the only compounds for which the necessary evidence exists. In both cases however, complications arise which are

* ϕ_{phos} and ϕ_{p} as well as ϕ_{fluor} and ϕ_{f} are used interchangeably throughout this thesis.

specific to that particular system: triplet-triplet interaction to give products in biacetyl[26] and thermal-like dissociation for HFA.[4]

It appears that these peculiarities are absent in HFB. Moreover, McIntosh[1] has recently determined the absolute emission quantum yield at 250 torr of HFB and has put his yields, obtained as a function of pressure and excitation energy, on an absolute basis.

It is now necessary to assess the role of dissociation in energy dissipation in the primary process. By determining absolute photochemical quantum yields of HFB over a range of conditions information regarding the roles of singlet and triplet dissociation could be obtained.

The aims of this work have been to provide such a study. Absolute photochemical quantum yields of HFB are obtained at various exciting wavelengths between 250 and 440 nm over a wide range of pressures. The effects of temperature and of phosphorescence quenching on photochemistry are also ascertained. These results elucidate the importance of dissociative processes and their relationship to vibrational relaxation in the primary process.

Finally the photochemical and photophysical data are combined and a kinetic description of the primary process is formulated.

CHAPTER II

Experimental Arrangement and Procedure

A. Brief Synopsis of Experimental Procedure

A block diagram of the setup for photolysis is shown in Figure 2. Basically three quantities are necessary for the evaluation of a product quantum yield - the fraction of light absorbed by the sample, the intensity of light and the amount of product formed in a specified time.

After filling the cell at the desired pressure of gas, the fraction of light absorbed was determined by a phototube (PT2). During the photolysis run the intensity of light was continuously monitored by another phototube (PT1) which had previously been calibrated absolutely. After photolysis the non-condensable product (carbon monoxide) was transferred quantitatively from the cell to a small volume (V). The latter could then form part of the gas chromatographic circuit (GC). Emission spectra could also be monitored during a photolysis run.

FIGURE 2
PHOTOLYSIS SYSTEM

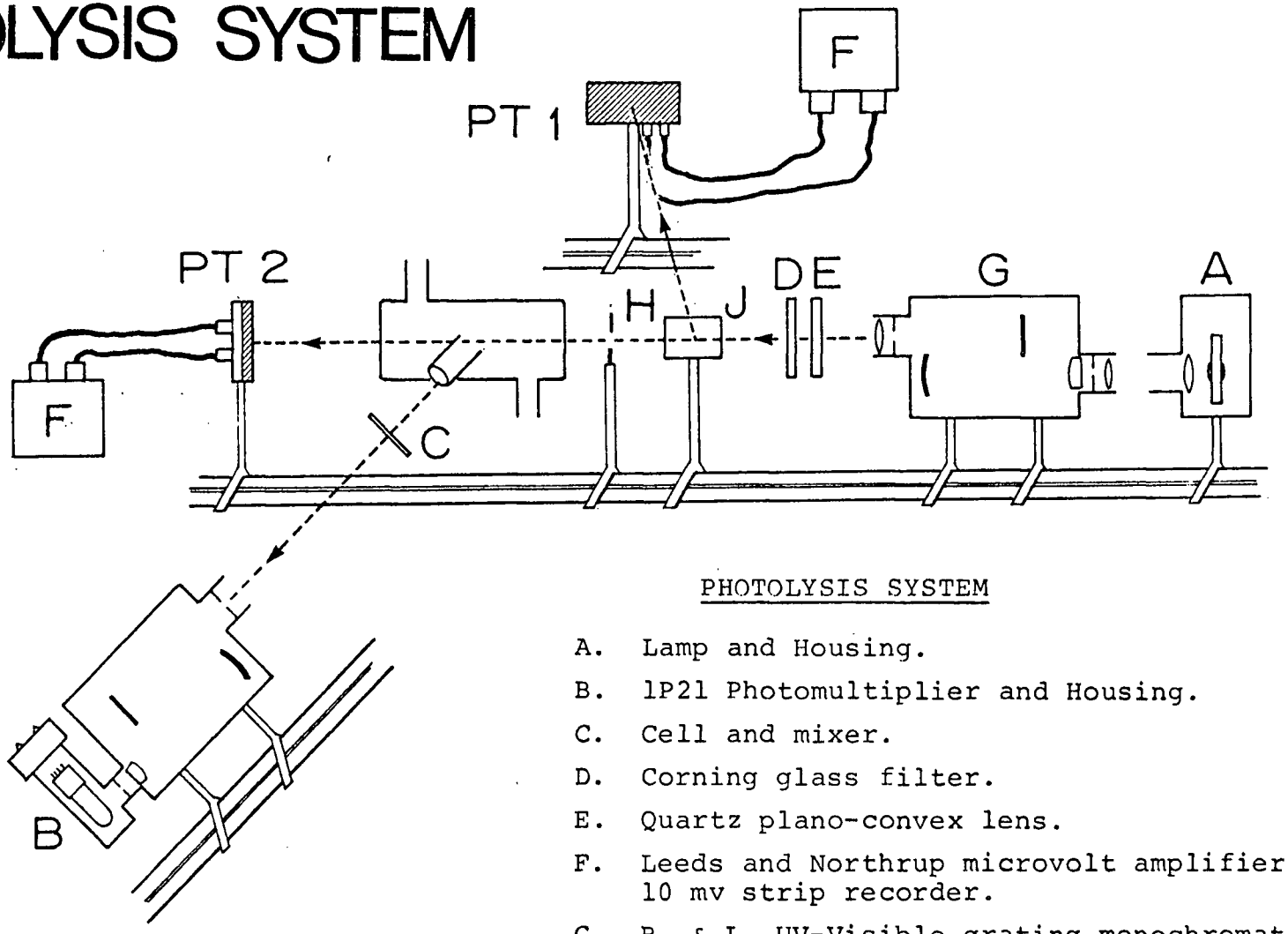

PHOTOLYSIS SYSTEM

A. Lamp and Housing.

B. 1P21 Photomultiplier and Housing.

C. Cell and mixer.

D. Corning glass filter.

E. Quartz plano-convex lens.

F. Leeds and Northrup microvolt amplifier and 10 mv strip recorder.

G. B. & L. UV-Visible grating monochromator.

H. Light stops.

J. Light beam splitter.

PT1 and PT2: Phototubes (RCA 935 vacuum photodiode, S-5 response).

B. Vacuum System

In view of the fact that mercury is an efficient quencher of hexafluoroacetone triplet state[4,27] it was thought advisable to build a mercury-free system to handle hexafluorobiacetyl.

The vacuum system was of standard, all glass construction consisting of a gallery of storage globes, a section leading to the photolysis cell and a manifold with a series of traps for purification together with a Le Roy-Ward still. The temperature of the still was measured with Cu-constantan thermocouples placed at the top and bottom and two intermediate positions. Apiezon N grease was used on the greaseable stopcocks. High Vacuum Teflon stopcocks (Kontes, Vineland, New Jersey) were used, however, to connect the cell to the vacuum system. This type of greaseless stopcock was also used throughout the analytical section of the apparatus.

The pumping system consisted of a standard rotary oil pump and a metal two-stage diffusion pump (Edwards E01) operated with Silicone 704 oil (Dow Corning). The system could be evacuated to 3×10^{-6} torr with a reliable working vacuum of 4×10^{-5} torr after isolation from the pump. Pressures were

measured with an NRC thermocouple, an NRC 538P ionization gauge, and a pyrex spiral gauge accurate to ± 0.5 torr.

C. Preparation and Purification of Chemicals

(i) Hexafluorobiacetyl (HFB)

HFB was prepared by the chromic acid oxidation of 2,3-dichloro-1,1,1,4,4,4-hexafluoro-2-butene following the modification by McIntosh[1] of Moore and Clark's method.[28] The crude condensate containing the HFB was partially purified by trap-to-trap distillation in vacuo from -78° C (methanol/CO_2) to -96° C (toluene/liquid N_2) slush baths. This procedure was repeated several times. The majority of this semi-pure material was stored in break-seals at -78° C. The portion of HFB to be used in the series of experiments was further purified by distillation through a Le Roy-Ward still set at -65° C and then stored in the side arm of a blackened 1-litre globe at -196° C. Immediately prior to use the sample was degassed at -196° C. A phosphorescence lifetime determination served as a criterion of adequate degassing.

(ii) Hexafluoroacetone (HFA)

HFA, obtained from Allied Chemical was purified by outgassing from the liquid held at the temperature of an ether

mush;[27] the m.p. of HFA is several degrees lower than that of ether. A phosphorescence lifetime determination again served as a criterion of purity. All HFA samples used had a $\tau_p \geq 3.1$ msec.

(iii) Hexafluoroethane (HFE)

HFE, supplied by Matheson Co. (Freon -116) was degassed at -196° C by trap-to-trap distillation.

(iv) Hexafluoroazomethane (HFAM)

HFAM, supplied by Merck, Sharp & Dohme (Isotopic Products Division, Montreal) was degassed at -196° C by trap-to-trap distillation.

(v) Carbon Monoxide

Carbon monoxide, supplied by Matheson Co. (C.P. Grade) was used without further purification.

D. Optical Arrangement

The excitation source for the experiments consisted of a PEK 110 mercury arc lamp operated at 100 watts from a stabilized DC power supply (PEK Model 401). A Bausch and Lomb

FIGURE 3

PHOTOLYSIS LINE SHAPES

(Relative intensities have no significance)

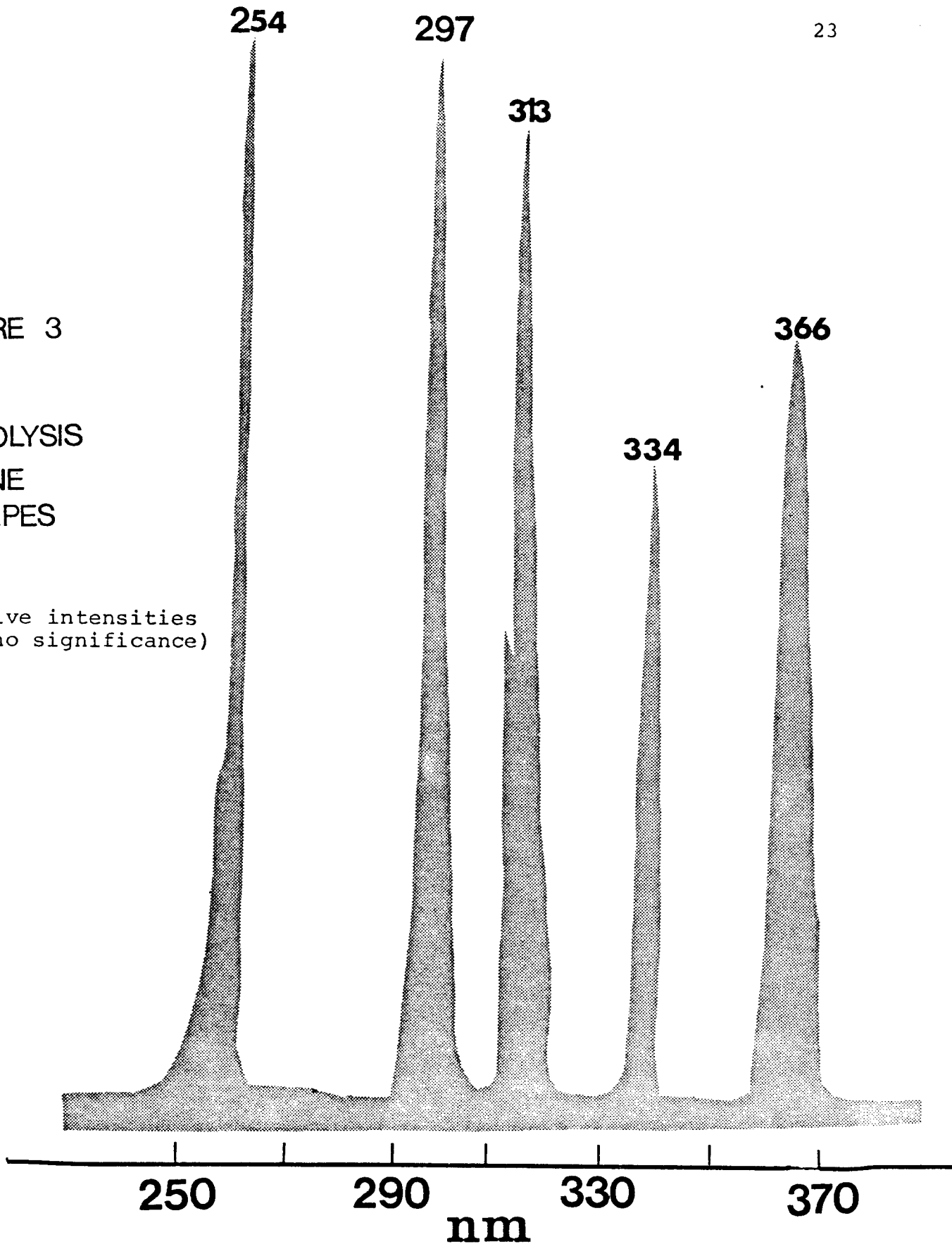

Monochromator(33-86-25) was used for isolation of the exciting wavelengths. They were the 436, 405, 366, 334, 313, 297 and 254 nm Hg lines. A UV-visible grating (33-86-07) 1200 grooves/mm blazed at 250 nm, reciprocal linear dispersion of 7.2 nm/mm was used in conjunction with a pair of variable slits. With 254 nm radiation the exit slit was set at 3.0 mm, while a 1.0 mm exit slit was used at all other wavelengths.

The divergent beam was passed through a combination of two quartz plano-convex lenses which produced a parallel beam of radiation.

A Corning 7-54 visible absorbing filter was used with these lenses at 254, 297, 313, 334 and 366 nm. At 405 nm and 436 nm Corning 3-75 and Corning 3-73 filters were used respectively. This parallel, filtered beam then entered the reaction cell.

The spectral characteristics of the "monochromatic" radiation used in the photolysis were ascertained using a second (Bausch and Lomb) grating monochromator, placed at the far end of the cell. Emergent light from this analyser (100μ exit slit) fell on to a RCA 1P28 photomultiplier coupled with a Leeds and Northrup microvolt amplifier and a 10 mV recorder.

The line shapes are summarized in Figure 3. The half-widths could only be bettered at the expense of considerable loss in intensity, and this last factor determined the practicability of quantitative photolysis under most conditions.

The intensity of light was measured before it entered the cell by having a quartz window in the optical train set at a slight angle so as to reflect a small proportion of the light onto an RCA 935 photocell (PT1). The latter was used with a Leeds and Northrup microvolt amplifier and a 10 mV recorder. It was calibrated absolutely by actinometry (section H).

The light intensity was also measured by a different photocell (PT2) after it traversed the cell. This detector was used primarily to determine the fraction of light absorbed (in situ) for each photolysis run (section I).

E. Reaction Cells

Cylindrical reaction vessels were of pyrex, with quartz windows whose transmission properties at various wavelengths had been measured before attachment to the cell with "Araldite" resin cement.

FIGURE 4

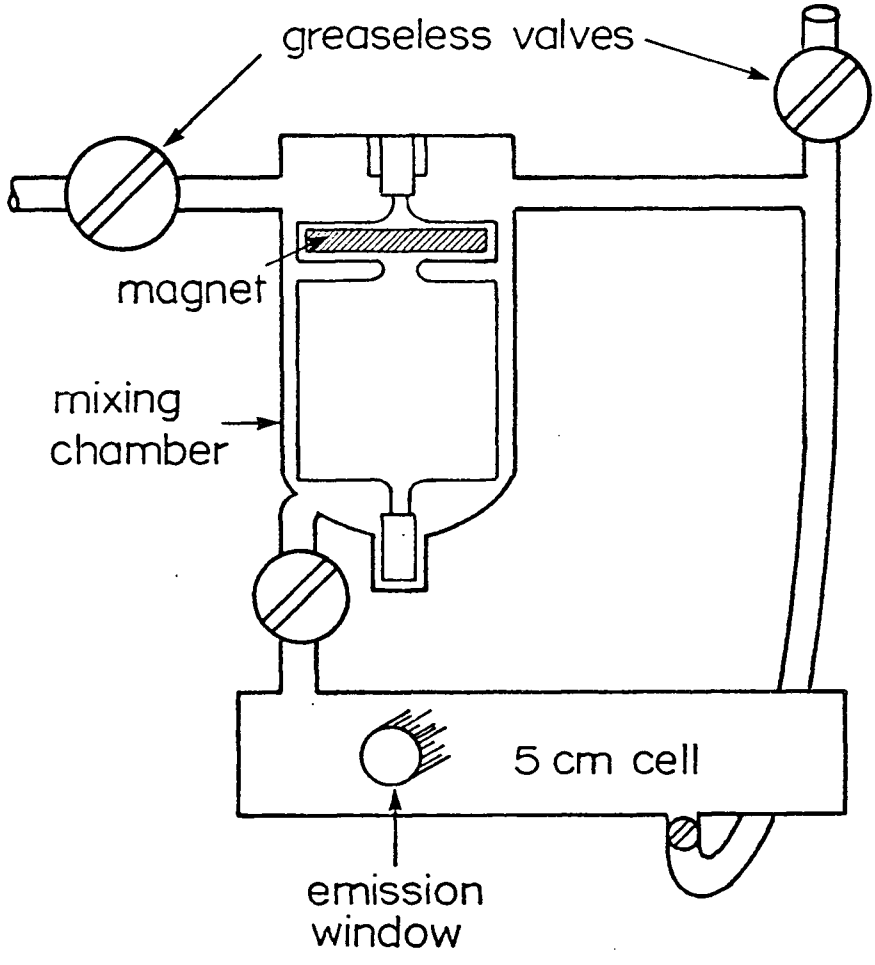

5-cm reaction cell and mixer

Photochemical experiments were done in either of two cells, both of which had an internal diameter of 2 cms. One of the cells was 30 cm long while the other was 5 cm long. Both were attached by CAJON (Cajon Company, Solon, Ohio 44139) stainless steel flexible tubing (½" O.D.) to the vacuum system at one end and the analysis system at the other end. This allowed for adjustments to be made in the position of the cell on the optical train without having to cut any of the connecting glass tubing.

The 30 cm. cell was fitted with a thermostatic jacket for temperature controlled runs.

The 5 cm cell was attached to a glass magnetically-driven mixing chamber (Figure 4). A quartz window was fitted to one side of this cell with "Araldite" for emission measurements.

F. Temperature Control Systems

A Lauda Constant Temperature Bath and Circulator, Series N (Brinkmann Instruments Inc., N.Y.) was used with the 30 cm cell. For temperatures below 25^{o} a dry ice heat exchanger was connected "in-series"with the circulator. Above room temperature, tap-water was circulated through the built-

in cooling coil.

The cell was well insulated with cotton batting. The temperature gradient along its length was measured with Cu-constantan thermocouples and was found to be constant $\pm 1^{\circ}$ C.

G. Gas Analysis

The analysis system is shown schematically in Figure 5.

(i) Normal Procedure

After photolysis the contents of the reaction cell were allowed to flow through two successive traps at -190° (liquid N_2). These condensed out C_2F_6 and unchanged HFB, and carbon monoxide was measured as the only non-condensable product. One re-evaporation of the condensed products was necessary to release occluded CO. The latter was then transferred by a Delmar-Urry Automatic Topler Pump[29] (Delmar Scientific Laboratories) to a small isolateable volume. The carrier gas of the chromatograph was then diverted so that this volume formed part of its circuit. Subsequently the CO was flushed onto the chromatographic column. The latter was a 5', ¼" molecular sieve column (13X) operated at 100° C and

FIG. 5

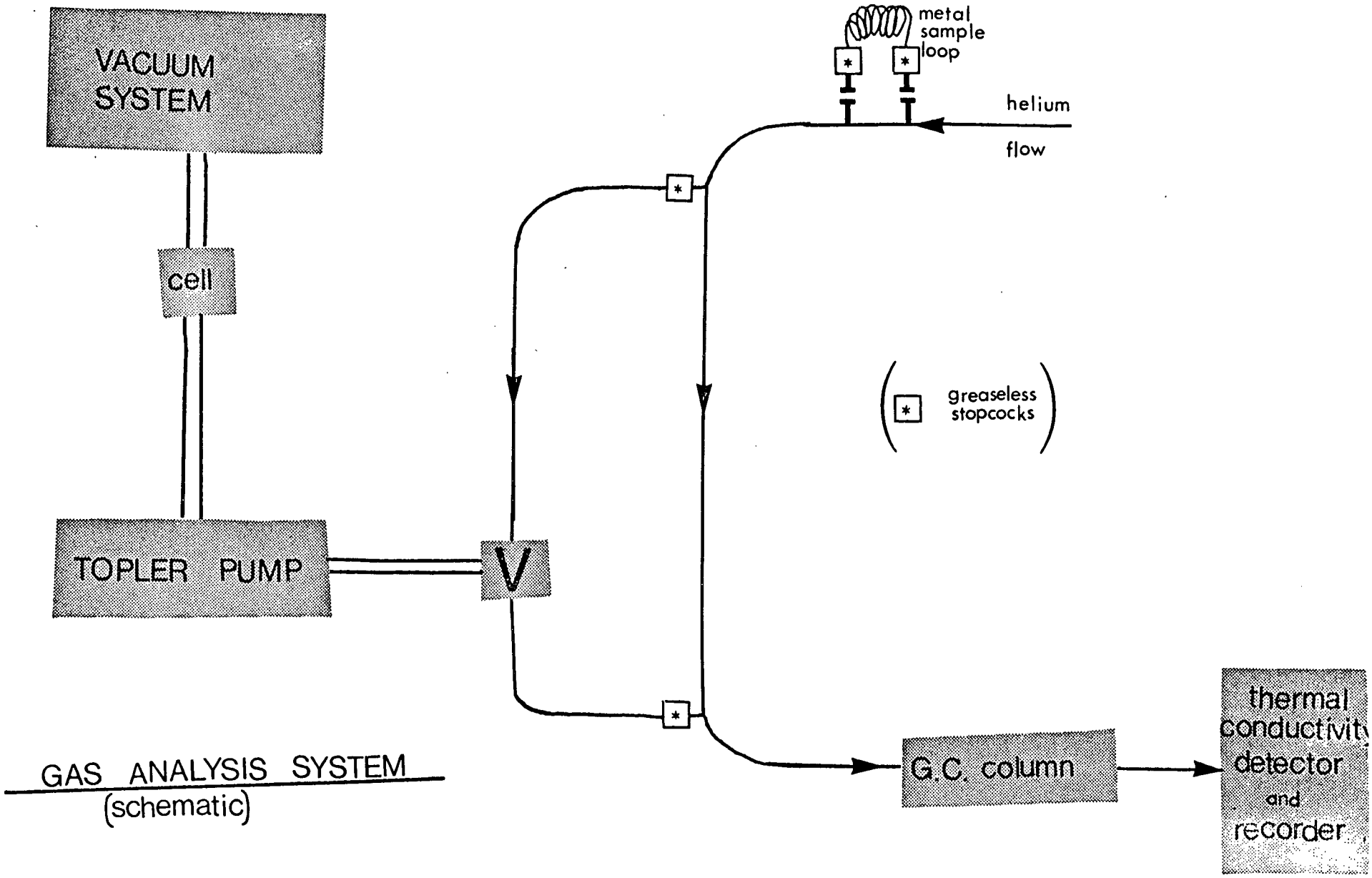

GAS ANALYSIS SYSTEM
(schematic)

at a flow of 75 ml/min. The detector was a Varian Aerograph Thermal Conductivity Detector (No. 01-000334-00) with two matched pairs of 30 ohm. tungsten rhenium (WX) filaments. They were operated at 150 mA and at ambient temperature. The power supply was a Kepco regulated DC supply (Model PAT 21-1T). Great care was taken to shield the various components from external noise. The detector block was housed in a copper box which was then filled up with mica chips to keep temperature fluctuations at a minimum. The reference and sensing resistance elements were incorporated into a Wheatstone bridge, and the out-of-balance signal was applied to a Leeds and Northrup microvolt amplifier coupled to a Brown (MH) Recorder (Model 143 x 58) equipped with a Disc Chart Integrator (Model 201). The chromatograph was calibrated using known samples of CO after every run.

(ii) Procedure for Ratio-Determining Runs

After photolysis, the contents of the cell were expanded into the evacuated glass tubing and metal sample loop. The loop was then removed and placed in position, by means of B10 glass sockets, in the helium stream. The sample was subsequently flushed onto a 5', ¼" Porapak Q (50/80 mesh) column

operated at 0^{o} C and a flow of 75 ml/min. The chromatograph was calibrated using known synthetic mixtures of C_2F_6 and CO.

H. Actinometry

The intensity of the absorbed radiation at the various pressures was monitored by means of a phototube (PT1) (RCA 935 vacuum photodiode, S-5 response) operated at 90 volts. It was calibrated against the potassium ferrioxalate actinometer of Hatchard and Parker.[30-31] The quartz actinometer cell, diameter 2.5 cm, depth 1.0 cm, was placed immediately behind the reaction vessel. Optical densities of exposed and developed solutions were determined on a Cary 14 spectrophotometer at 510 nm. The usual blank correction was made with an unexposed solution.

Because of the large transmission losses from the silica-air interfaces of the reaction vessel and the actinometer cell, it was necessary to apply a correction factor to obtain the absolute intensity of the absorbed radiation.[32-33] For convenience all windows were assumed to have identical losses from reflection (Appendix 1).

The phototube, in conjunction with a Leeds and Northrup microvolt amplifier and 10 mV strip chart recorder

was found to have a linear response over the range of intensities required for the series of experiments. This was done using a set of calibrated neutral density filters (Oriel Optics Corporation).

Actinometry was frequently done to check the phototube (PT1) calibration. No change was found for the latter over a period of 9 months.

I. Measurement of the Fraction of Light Absorbed by the Sample

The fraction of light absorbed (FLA) by the sample was measured by phototube (PT2). Before each run, with the cell empty, PT1 and PT2 were simultaneously read. When the run had begun PT1 and PT2 were again read. This way, if the absolute intensity of the light had changed then the PT2 reading could be corrected for it. This procedure was followed for every run where the FLA was between circa 0.85 and 0.30. When it lay outside this range (normally at pressures below 5 mm in the 30 cm cell) the value of the extinction coefficient (ε) from the higher pressure runs was used and the FLA was computed from this. This procedure was justified by the fact that at intermediate pressures, where measurements could be made with both cells, Lambert's Law was found

to hold exactly. Beer's law was obeyed at all wavelengths in either cell over the complete range of pressures used.

J. Emission Spectroscopy

Figure 2 shows the arrangement used for observing emission spectra with the 5 cm cell. The entrance slit of the analysing Bausch and Lomb monochromator (33-86-25) was placed as near to the observing window as possible. A visible grating (33-86-02) 1350 grooves/mm, blazed at 250 nm, reciprocal linear dispersion of 6.4 nm/mm was used. The emission was recorded using a 1P21 photomultiplier operated at approximately 1000 volts.

K. Lifetime Measurements

(i) Flash lamp

Phosphorescence lifetime measurements were made with an argon filled coaxial capillary flash lamp operated at 4-5 kv. This lamp dissipates 16 to 25 J and has a peak rise time of 3 μsec and a half-width of 8 μsec.[34] The argon discharge produces a continuum throughout the visible and ultraviolet, down to the silica cut-off. The emission

emerging from one end of the capillary was passed through a Corning C.S. 7-54 (3 mm thick) filter and was focused with a silica lens into the cell. Generally due to the long lifetime of the emission being studied and to the cell geometry, scattered exciting radiation presented no difficulties. For low pressures (< 5 torr), however, considerable care had to be taken. Correction for scattered light was made by condensing the contents of the cell in a side arm or by evacuating the cell completely.

(ii) Lifetime Cell

A conventional T-shaped cell with a Wood's horn for a light trap was used. The main body of the cell (5.0 cm long) was constructed from 30 mm Pyrex tubing, with 20 mm tubing used for the light trap and viewing port which were at right angles to the main cell arm. Silica windows were attached using epoxy resin and the outside surfaces of the cells were covered with a flat black paint.

(iii) Detection System

The ketone emission was monitored perpendicular to the lamp discharge. Emitted light was recorded with a

1P28 photomultiplier (using a 10 k load resistor) on the exit slit of one of the Bausch & Lomb visible monochromators. A glass collective lens (33-85-33) was used on the entrance slit. Slit widths used were: exit 3.00 mm; entrance 5.36 mm, (i.e., band pass 19.2 nm). The voltage output from the photomultiplier was displayed either on a Tektronix 542B or 547 oscilloscope and photographed with a Tektronix C-27 Trace-Recording Camera with Polaroid Type 47 (ASA 3000) film. A 0.003 μf capacitor was placed in parallel with the oscilloscope and photomultiplier as a noise filter. This filter had a negligible effect on the measured emission decay times. To improve accuracy of the analysis the decay curves were enlarged by approximately four times with a delineascope. The lifetimes obtained in this way were reproducible to within 5%.

L. Errors

The error limits are given as ± one standard deviation.

CHAPTER III

Photochemistry of HFB

RESULTS

The majority of results of the investigation are given in this chapter. Where appropriate, they are discussed briefly.

A. Absorption

The mean molar absorption coefficients of HFB found by measuring the percent transmission in situ (Page32) are listed in Table 1. The absorption spectrum obtained on a Cary 14 recording spectrophotometer[35] is reproduced in Figure 6.

B. Ratio Experiments

Although Whittemore and Szwarc[24] reported in a short note that the gas phase photolysis of HFB at 25° and 150° C produced only CO and C_2F_6 in a 2:1 molar ratio they gave no

fig. 6

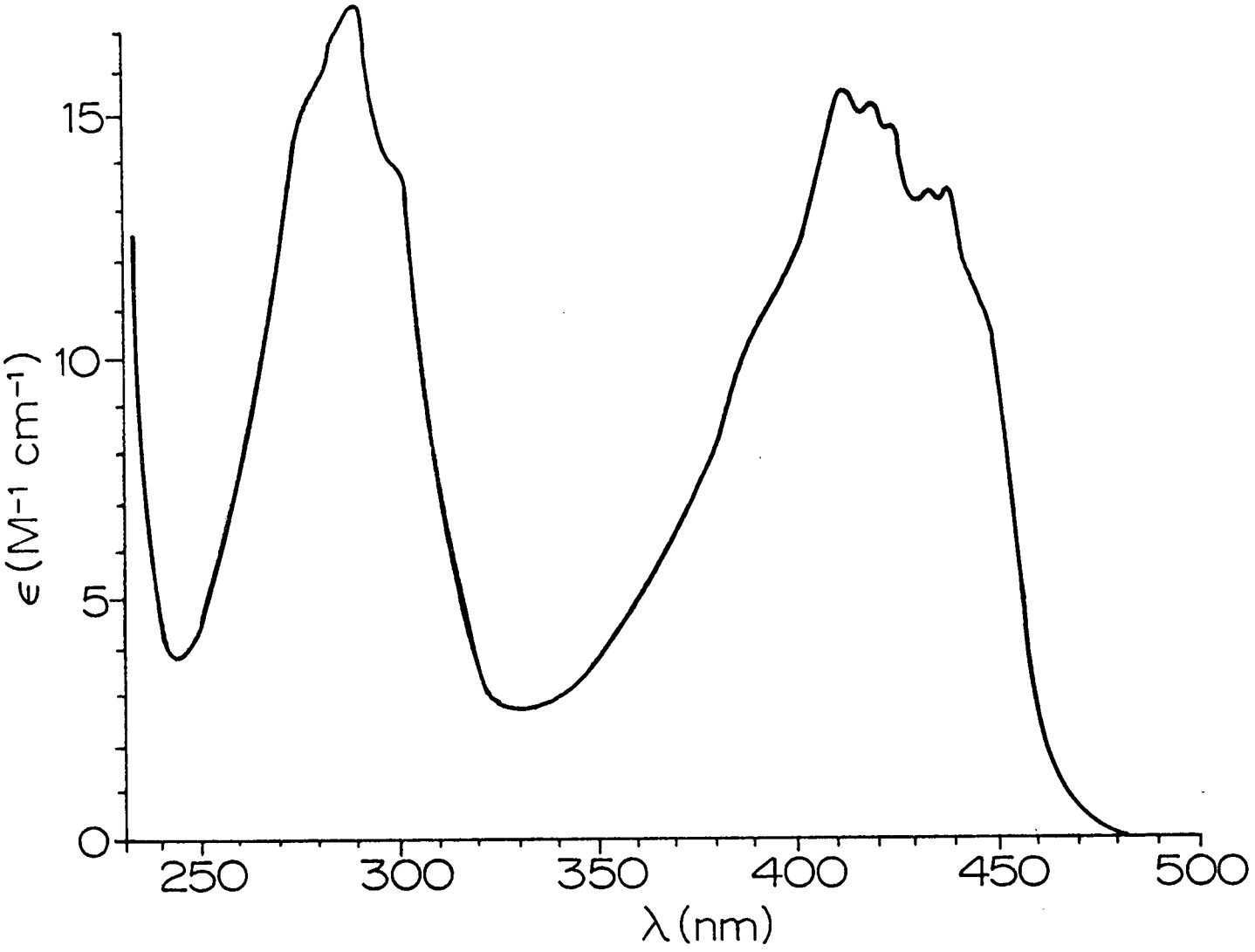

Absorption spectra of hexafluorobiacetyl vapour at 25 °C

error limits for their results. If their observations were quantitatively correct, then our analysis would be considerably simplified.

Table 2 shows the conditions used and results obtained in this work. CF_4, a possible photochemical product was not detected under any of our conditions.

Discussion:

Although extreme conditions were used it was found that CO and C_2F_6 were indeed produced in 2:1 molar ratio within our experimental error. On this basis, therefore, carbon monoxide only was determined thereafter for each photolysis run.

C. Reliability of the Photolysis Data

Experimental quantum yields are notoriously prone to large random and systematic errors. Chief sources of random error are in measuring the fraction of light absorbed and in reading the spiral gauge. Unlike the case of HFA^2, small temperature fluctuations ($\pm 2^{\circ}$ C) would not contribute a noticeable random error. These random errors are fairly

Table 1. Mean molar absorption coefficients of HFB at the wavelengths used in photolysis, at 25° C.

(nm)	(M^{-1} cm^{-1})
254	6.60
297	11.9
313	5.26
334	2.42
366	4.89
405	12.9
436	12.2

Table 2. Ratio experiments

	Pressure	Irrad.Time	CO	C_2F_6	Ratio	% Decomposition
297	5 mm	1200 secs	0.628	0.326	1.93 ±0.20	3%
297	10 mm	18 hours	0.604	0.286	2.12	25%
297	20 mm	4.75 hours	0.530	0.265	2.00	2.5%
313	1 mm	20 hours			2.17	35%
Full Hg arc	5 mm	5 hours			1.94	25%

reflected in the scatter of points on $1/\phi_{PP.}$ vs. (HFB) plots (e.g. Figure 10) and normally amount to about ±10%. Systematic errors were harder to point to. To this end HFA was put into the system and the photochemical quantum yields obtained were compared with Kutschke's[4] published data (obtained by interpolation of his graphical data). The results are given in Table 3. There is seen to be reasonably good agreement between the two studies. He used acetone as an actinometer. It seemed therefore that the system was free of major systematic errors although the possibility of both studies being incorrect could not be ruled out. Finally it should be noted that the "absolute" value of a particular quantum yield is rarely as important as its relative value with respect to other quantum yields.

D. Photolysis of HFB at 25° C.

The exposure time for a run at room temperature varied from 30 minutes to 36 hours, and was generally around 2 hours. At low absorptions (e.g. with 334 nm radiation and low pressure) or with low quantum yields (e.g. with 366 nm radiation and high pressure) this time was determined by the

Table 3 Photolysis of HFA at 313 nm

Cell length: 30 cm
Temperature: 25° C

HFA Concentration (mm Hg)	ϕ_{CO} (a)	ϕ_{CO} (b)
50	0.32_0	0.33_0
20	0.37_1	0.40_7

(a) This work (b) Kutschke[4]

Table 4 Photolysis of HFB at 254 nm

Temperature: 25° C

HFB Conc (torr)	ϕ_{CO}	$\phi_{P.P.}$	$1/\phi_{P.P.}$
5	1.154	0.577	1.73
10	0.869	0.435	2.30
20	0.732	0.366	2.73
50	0.608	0.304	3.29
100	0.470	0.235	4.26
200	0.395	0.197	5.07
300	0.466	0.233	4.30
400	0.378	0.189	5.30

Table 5

Photolysis of HFB at 297 nm

Temperature 25° C

HFB Conc (torr)	ϕ_{CO}	$\phi_{P.P.}$	$1/\phi_{P.P.}$
0.5	1.280	0.640	1.56
0.5	1.226	0.613	1.63
0.5	1.226	0.613	1.63
1.0	1.130	0.565	1.77
1.47	1.035	0.518	1.93
2.0	0.860	0.430	2.33
2.0	0.880	0.440	2.27
2.79	0.790	0.395	2.53
4.0	0.777	0.388	2.58
5.0	0.742	0.371	2.69
5.0	0.742	0.371	2.69
7.5	0.642	0.321	3.12
10.0	0.620	0.310	3.23
15.0	0.589	0.295	3.39
20.0	0.541	0.271	3.70
30.0	0.440	0.220	4.55
40.0	0.418	0.209	4.79

Table 5 (continued)

Temperature 25°C

HFB Conc (torr)	ϕ_{CO}	$\phi_{P.P.}$	$1/\phi_{P.P.}$
50.0	0.402	0.201	4.97
50.0	0.394	0.197	5.07
100.0	0.306	0.153	6.55
200.0	0.217	0.109	9.22
400.0	0.137	0.068	14.6

Table 6

Photolysis of HFB at 313 nm

Temperature 25° C

HFB Conc (torr)	ϕ_{CO}	$\phi_{P.P.}$	$1/\phi_{P.P.}$
0.5	1.091	0.546	1.83
1.0	0.657	0.329	3.04
2.0	0.813	0.407	2.46
3.5	0.824	0.412	2.43
5.0	0.652	0.326	3.07
10.0*	0.569	0.284	3.52
10.0**	0.578	0.289	3.46
15.0	0.580	0.290	3.45
20.0	0.462	0.231	4.33
20.0	0.474	0.237	4.22
50.0	0.333	0.166	6.01
50.0	0.350	0.175	5.71
75.0	0.284	0.142	7.04
100.0	0.223	0.112	8.98
100.0	0.216	0.108	9.26
125.0	0.186	0.093	10.8
125.0	0.192	0.096	10.4
200.0	0.152	0.076	13.1
340.0	0.101	0.051	19.8

*Intensity of exciting light, 0.48×10^{15} photons/cm^2/sec.
**Intensity of exciting light, 1.45×10^{15} photons/cm^2/sec.

Table 7

Photolysis of HFB at 334 nm

Temperature 25° C

HFB Conc (torr)	ϕ_{CO}	$\phi_{P.P.}$	$1/\phi_{P.P.}$
2.0	1.035	0.517	1.93
3.0	0.900	0.450	2.22
4.0	0.811	0.406	2.46
5.0	0.999	0.499	2.00
5.0	0.824	0.412	2.43
5.0	0.803	0.402	2.49
7.5	0.621	0.311	3.22
10.0	0.544	0.272	3.68
15.0	0.511	0.256	3.92
20.0	0.413	0.207	4.83
50.0	0.211	0.106	9.49
100.0	0.121	0.061	16.5
100.0	0.125	0.062	16.0
150.0	0.095	0.048	21.0
200.0	0.0692	0.0346	28.9
200.0	0.0904	0.0452	22.1
300.0	0.0527	0.0264	37.9
400.0	0.0386	0.0193	51.8

Table 8

Photolysis of HFB at 366 nm

Temperature 25° C

HFB Conc (torr)	ϕ_{CO}	$\phi_{P.P.}$	$1/\phi_{P.P.}$
0.5	1.028	0.514	1.95
1.0	0.794	0.397	2.52
2.0	0.504	0.252	3.97
5.0	0.255	0.128	7.84
5.0	0.261	0.131	7.65
10.0	0.128	0.064	15.7
15.0	0.0904	0.0452	22.1
20.0	0.0612	0.0306	32.7
30.0	0.0384	0.0192	52
40.0	0.0285	0.0142	70
50.0	0.0277	0.0139	72
50.0	0.0240	0.0120	83
75.0	0.0186	0.0093	108
100.0	0.0153	0.0077	131
100.0	0.0185	0.0092	108
200.0	0.0126	0.0063	160
400.0	0.0081	0.0041	246

Table 9

Photolysis of HFB at 405 nm*

Temperature 25° C

HFB Conc (torr)	ϕ_{CO}	$\phi_{P.P.}$	$1/\phi_{P.P.}$
1.0	$\leq$ 0.0038	$\leq$ 0.0019	$\geq$ 530
2.0	$\leq$ 0.0032	$\leq$ 0.0016	$\geq$ 630

Table 10

Photolysis of HFB at 436 nm*

Temperature 25° C

HFB Conc (torr)	ϕ_{CO}	$\phi_{P.P.}$	$1/\phi_{P.P.}$
0.5	$\leq$ 0.050	$\leq$ 0.025	$\geq$ 40
0.5	$\leq$ 0.028	$\leq$ 0.0014	$\geq$ 71
2.0	$\leq$ 0.0014	$\leq$ 0.00072	$\geq$ 1400
5.0	$\leq$ 0.00064	$\leq$ 0.00032	$\geq$ 3100

*No product detected at these wavelengths under any conditions.

Table 11

Photolysis of HFB at 297 nm

Temperature -20° C

HFB Conc (torr)	ϕ_{CO}	$\phi_{P.P.}$	$1/\phi_{P.P.}$
42.5	0.302	0.151	6.62
34.0	0.326	0.163	6.13
25.5	0.364	0.182	5.49

Table 12

Photolysis of HFB at 313 nm

Temperature 50° C

HFB Conc (torr)	ϕ_{CO}	$\phi_{P.P.}$	$1/\phi_{P.P.}$
10.8	0.598	0.299	3.34
21.7	0.522	0.261	3.83
32.5	0.441	0.220	4.54
54.2	0.377	0.189	5.29
108.4	0.266	0.133	7.51

Table 13

Photolysis of HFB at 313 nm

Temperature 76° C

HFB Conc (torr)	ϕ_{CO}	$\phi_{P.P.}$	$1/\phi_{P.P.}$
5.8	0.767	0.384	2.60
11.7	0.678	0.339	2.95
23.0	0.569	0.285	3.51
41.2	0.491	0.245	4.08
58.6	0.413	0.207	4.83
87.8	0.383	0.192	5.22
117.1	0.334	0.167	5.99
146.4	0.304	0.152	6.58

minimum amount of CO which could be measured to within ±1% (2×10^{-7} moles). Normally less than 1% of the HFB was decomposed. On rare occasions (e.g. 0.5 and 1.0 mm experiments) this percentage was larger and corrections to the quantum yields were applied to allow for this.

The parameters measured in each run are related by,

$$\phi_{\substack{\text{Primary} \\ \text{process} \\ \text{(P.P.)}}} = \frac{\frac{1}{2} \text{ (Moles of CO produced)}}{\text{Einsteins absorbed}}$$

where "Einsteins absorbed" = F x I x t

and F = Fraction of light absorbed

I = Intensity of light

t = Irradiation time

The results for all seven wavelengths are presented in Tables 4 through 10.

E. HFB Photolysis at Different Temperatures

A measured pressure of HFB was dosed into the 30 cm cell before it was heated or cooled. Half an hour was allowed for the gas to equilibrate to the new temperature. The results

for the two wavelengths (297 nm at -20° C and 313 nm at 50° and 76° C) are given in Tables 11 through 13.

F. HFB - HFAM System

When it became clear that the dissociation of HFB was due to two or more states an attempt was made to differentiate between them. Although the "temperature runs" indicated that no thermalised triplet state was involved in dissociation (c.f. as in HFA[4]), conclusive evidence had to await photochemical runs in which the phosphorescence was completely quenched. Available evidence on a similar system, biacetyl-azomethane,[36] indicated that hexafluoroazomethane (HFAM) should have a triplet state lower than HFB.

(i) Quenching study

It was found that HFAM was a very efficient quencher of HFB phosphorescence. 50 torr HFB were dosed into the 5 cm cell and the emission spectrum recorded. Known amounts of HFAM were subsequently added by expansion from known volumes and the spectrum again recorded after each addition. No sensitized HFAM phosphorescence was observed at any pressure within the spectral range of the photomultiplier (300 nm to 650 nm).

With the HFAM pressures used here (0 - 35 torr), only the HFB phosphorescence is quenched. If one considers the triplet state only, the processes of importance are

$$^3HFB^0 \xrightarrow{k_p} HFB^* + h\nu_{phos}$$

$$^3HFB^0 \xrightarrow{k_{11}} HFB^*$$

$$^3HFB^0 + HFAM \xrightarrow{k_{ET}} HFB^* + {}^3HFAM^*$$

in which the superscript 3 refers to the multiplicity of the excited state molecule, the superscript 0 and an asterisk denote molecules in equilibrium and non-equilibrium vibrational states, respectively.

A steady-state treatment of the mechanism yields the familiar Stern-Volmer relationship

$$\frac{\phi^o_{phos}}{\phi_{phos}} = 1 + \tau_{phos} k_{ET} [HFAM]$$

with ϕ^o_{phos} being the HFB phosphorescence yield in the absence of HFAM, and the mean triplet lifetime τ_{phos} (2.1 msec) equal to the reciprocal of the sum $k_{phos} + k_{11}$. The data so

plotted are shown in Figure 7. The slope is 320 $torr^{-1}$ or 6.0×10^6 liter/mole, hence the bimolecular rate constant $k_{ET} = 3.52 \times 10^9$ liter/mole sec. The pressure of HFAM required for half quenching is 0.0025 torr, and about 0.2 torr are needed to completely remove the HFB phosphorescence. HFAM is therefore an extremely efficient quencher of HFB phosphorescence. The fluorescence of HFB remained unchanged even at the highest pressure of HFAM used (35 torr).

(ii) Photolysis of HFB - HFAM mixtures

A measured pressure of HFAM was expanded from calibrated volumes into the 5 cm cell which was then isolated from the mixer. The mixer was filled with the desired HFB pressure. The two gases were then allowed to mix, aided by the magnetically driven stirrer, for at least 30 minutes. The stirrer was also kept in operation and the HFB emission was monitored throughout the entire run. The results for the three wavelengths used are given in Table 14. Previous results for the same total pressures, but of pure HFB, are also given for comparison.

Direct photolysis of HFAM was observed when high pressures of the quencher were used. For example, ϕ_{N_2} was found to be 0.7 (based on the quanta absorbed by HFAM only) with 313 nm radiation and a total pressure of 60 torr (i.e. 25 torr HFB and 35 torr HFAM). Wu and Rice[37] have found ϕ_{N_2} to be 0.72 with 40 torr HFAM and 366 nm radiation.

In experiments where direct absorption by HFAM was negligible, little or no nitrogen product was observed. This observation implies that if the quenching mechanism is electronic energy transfer from the triplet state of HFB to the triplet state of HFAM then the latter is unreactive photochemically. For example, the sensitized photochemical quantum yield of HFAM can be calculated if it is assumed that the energy transfer process is 100% efficient. The ISC yield in HFB is known to be 0.9.[1] For 10 torr HFB and 0.2 torr HFAM with 297 nm radiation at 25° C the ϕ_{N_2} (sensitized) was found to be 0.02 ± 0.02. In the direct photolysis of 20 torr HFAM, with 366 nm radiation at 28.7° C, Wu and Rice[37] determined ϕ_{N_2} to be 0.830.

Table 14

Photolysis of HFB/HFAM Mixtures

Temperature 25° C Cell Length 5.0 cm

λ (nm)	HFB (mmHg)	HFAM (mmHg)	Total pressure (mmHg)	ϕ_{CO}	$\phi_{P.P.}$	$1/\phi_{P.P.}$
297	10.0	0.201	10.2	.586	.293	3.41
	10.0	-	10.0	.620	.310	3.23
	45.7	0.201	45.9	.371	.186	5.39
	50.0	-	50.0	.398	.199	5.00
	100.0	0.201	100.2	.344	.172	5.82
	100.0	-	100.0	.306	.153	6.55
	0.5	1.5	2.0	1.04	.520	1.93
	0.5	1.5	2.0	0.875	.438	2.28
	2.0	-	2.0	0.880	.440	2.27
	2.0	-	2.0	0.860	.430	2.33
	2.0	-	2.0	0.874	.422	2.28

Table 14(Continued)

λ (nm)	HFB (mmHg)	HFAM (mmHg)	Total pressure (mmHg)	ϕ_{CO}	$\phi_{P.P.}$	$1/\phi_{P.P.}$
313	25.0	35.0	60.0	0.342	.171	5.85
	60.0	-	60.0	0.304	.152	6.6
366	50.0	0.201	50.2	.0233	.0117	85.5
	50.0	-	50.0	.0240	.0120	83.3
	50.0	-	50.0	.0277	.0139	71.9

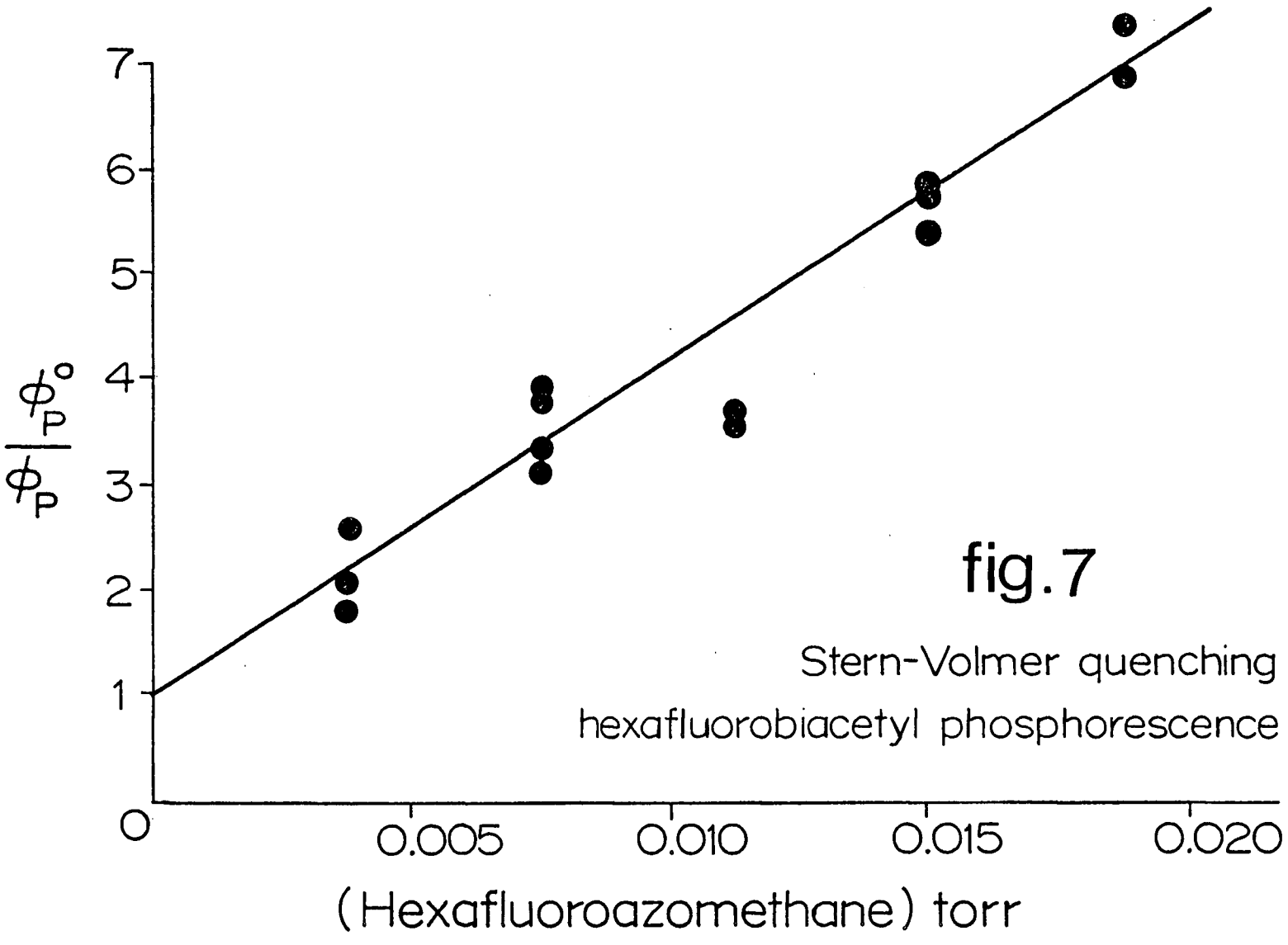

fig.7

Stern-Volmer quenching
hexafluorobiacetyl phosphorescence

CHAPTER IV

Dissociation and Collisional Deactivation

In this chapter a mechanism is presented which successfully accounts for the photochemical results. Each step is discussed critically and its implications fully rationalized. The various rate constants are then evaluated numerically so that the quantum yields can be simulated. Various alternative mechanisms to explain the photochemical results are considered. Finally experimental evidence for wall deactivation of the equilibrated triplet state at low pressures is presented and discussed.

A. Graphical Presentation of Results

The reciprocal quantum yield of the primary process as a function of HFB concentration is plotted for all wavelengths in Figures 8 to 17. The low pressure region is also shown where appropriate. Figures 18 and 19 show the data acquired at temperatures other than 25^{o} C.

B. General Observations

(i) At equivalent pressures the decomposition efficiency increases drastically with decrease in wavelength.

(ii) At all five wavelengths where photochemistry takes place, the reciprocal quantum yield at high pressure is a linear function of HFB concentration.

(iii) There is no evidence of the quantum yields either levelling off at high pressures at any wavelength or showing a large variation with temperature.

(iv) When the phosphorescence of HFB is completely quenched, the quantum yields remain unchanged.

(v) No photochemistry was observed with 405 nm or 436 nm radiation.

(vi) At lower pressures the plots become curved downwards. Futhermore there is no evidence to indicate that the slopes tend to zero at the pressures available here.

(vii) No quantum yield greater than 0.64 was recorded although HFB was irradiated at pressures as low as 500μ.

C. Proposed Mechanism

One set of processes that accounts satisfactorily for the observed results is

$$B + h\nu \longrightarrow {}^{1}_{2}B^{*}$$

$${}^{1}_{2}B^{*} \xrightarrow{k_1} {}^{3}_{?}B^{*} \qquad \text{(i)}$$

$${}^{1}_{2}B^{*} \xrightarrow{k_2} 2CO + C_2F_6 \qquad \text{(ii)}$$

$${}^{1}_{2}B^{*} + M \xrightarrow{\omega} {}^{1}_{1}B^{0} + M^{*} \qquad \text{(iv)}$$

$${}^{3}_{?}B^{*} + M \xrightarrow{\omega} {}^{3}_{1}B^{0} + M^{*} \qquad \text{(viii)}$$

$${}^{3}_{?}B^{*} \xrightarrow{k_5} 2CO + C_2F_6 \qquad \text{(ix)}$$

with B a ground state hexafluorobiacetyl molecule and M any molecule which causes vibrational equilibration. The super- and subscripts at the lefthand side of B refer to its multiplicity and its state within that multiplicity respectively. The right hand side superscripts, 0 and an asterisk denote molecules in equilibrium and non-equilibrium vibrational states, respectively.

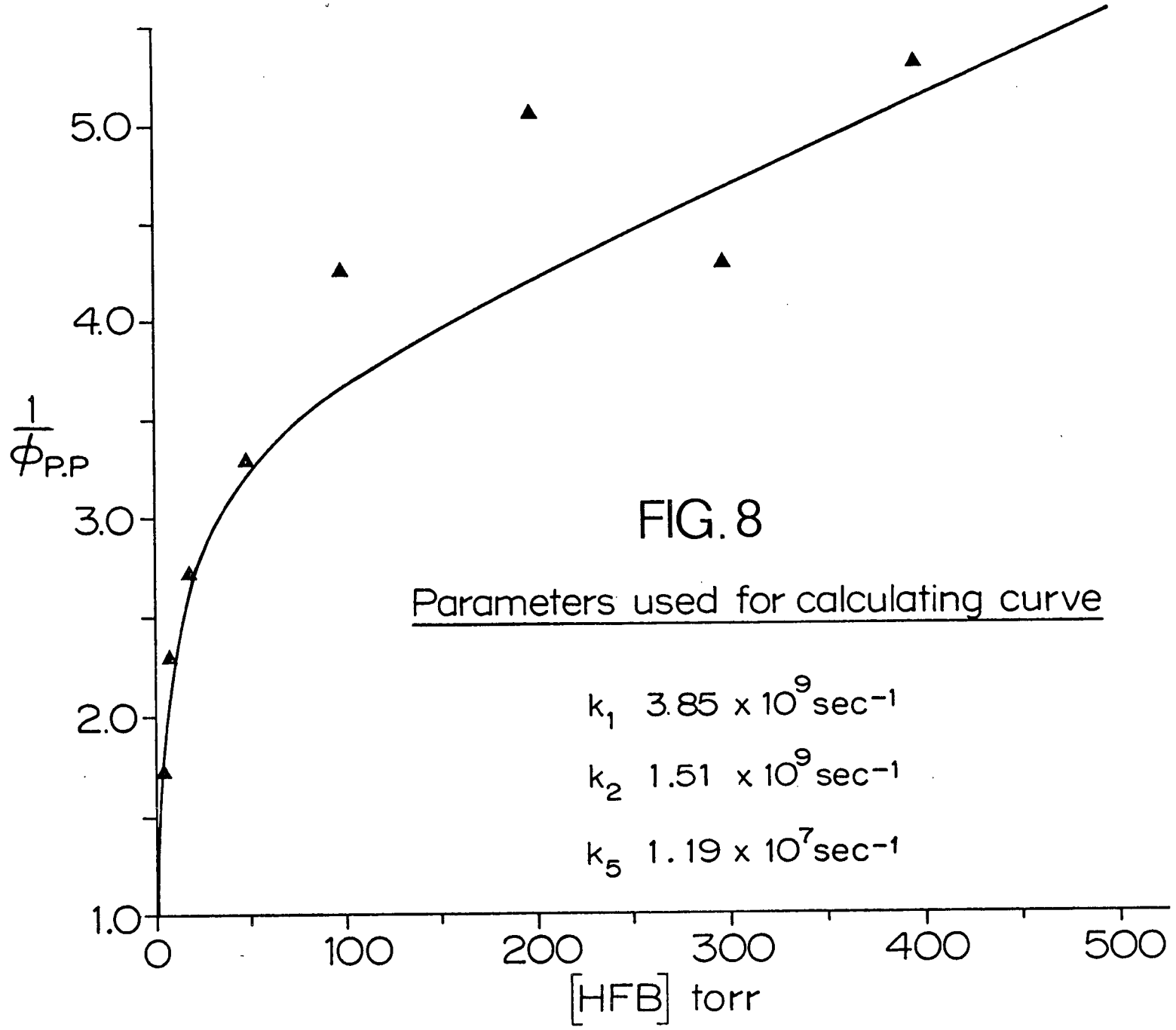

FIG. 8

Reciprocal quantum yields versus pressure -- 254 nm, 25 °C
High pressure region

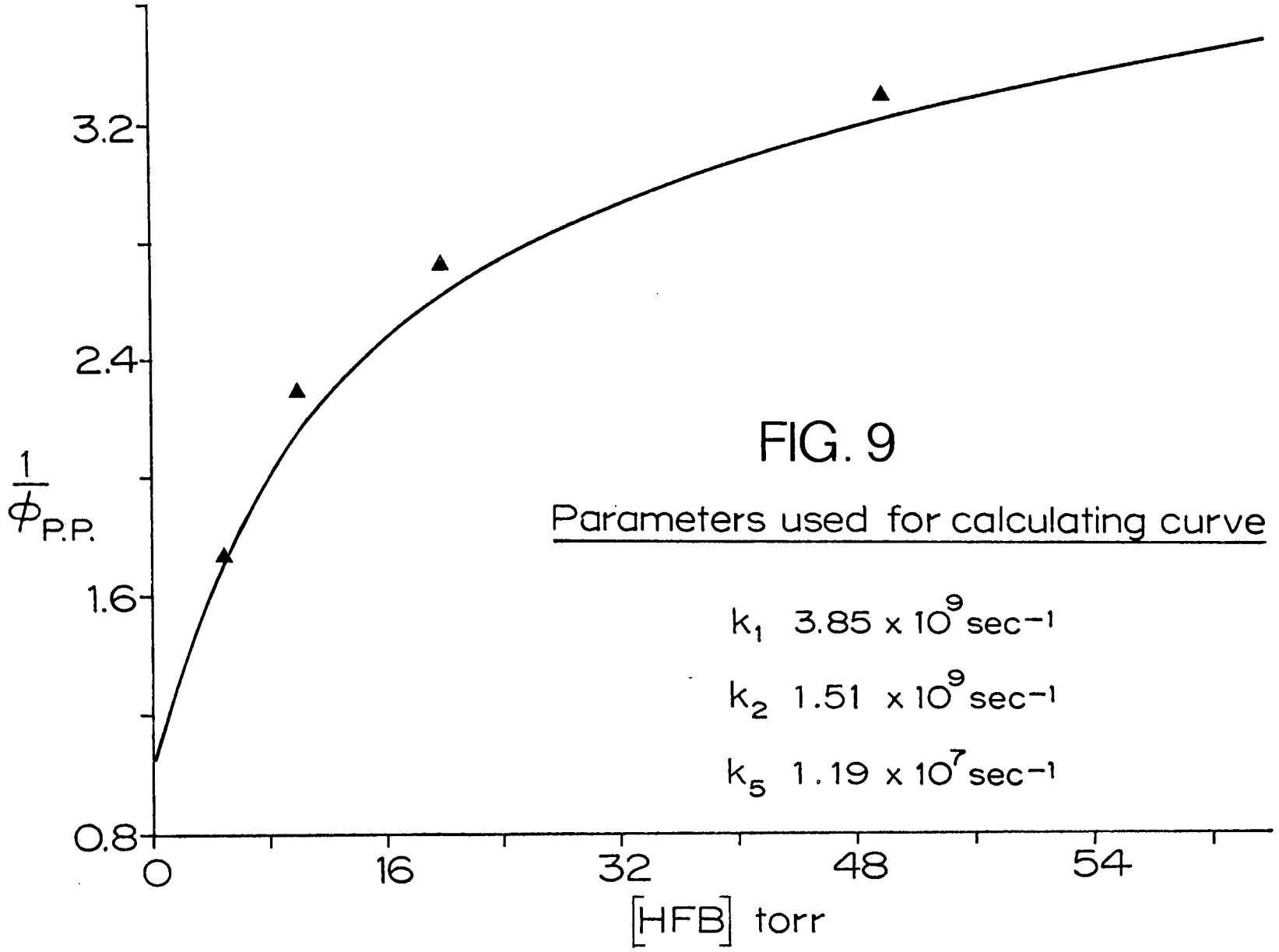

FIG. 9

Parameters used for calculating curve

k_1 $3.85 \times 10^9 sec^{-1}$

k_2 $1.51 \times 10^9 sec^{-1}$

k_5 $1.19 \times 10^7 sec^{-1}$

Reciprocal quantum yields versus pressure--254 nm, 25 °C
Low pressure region

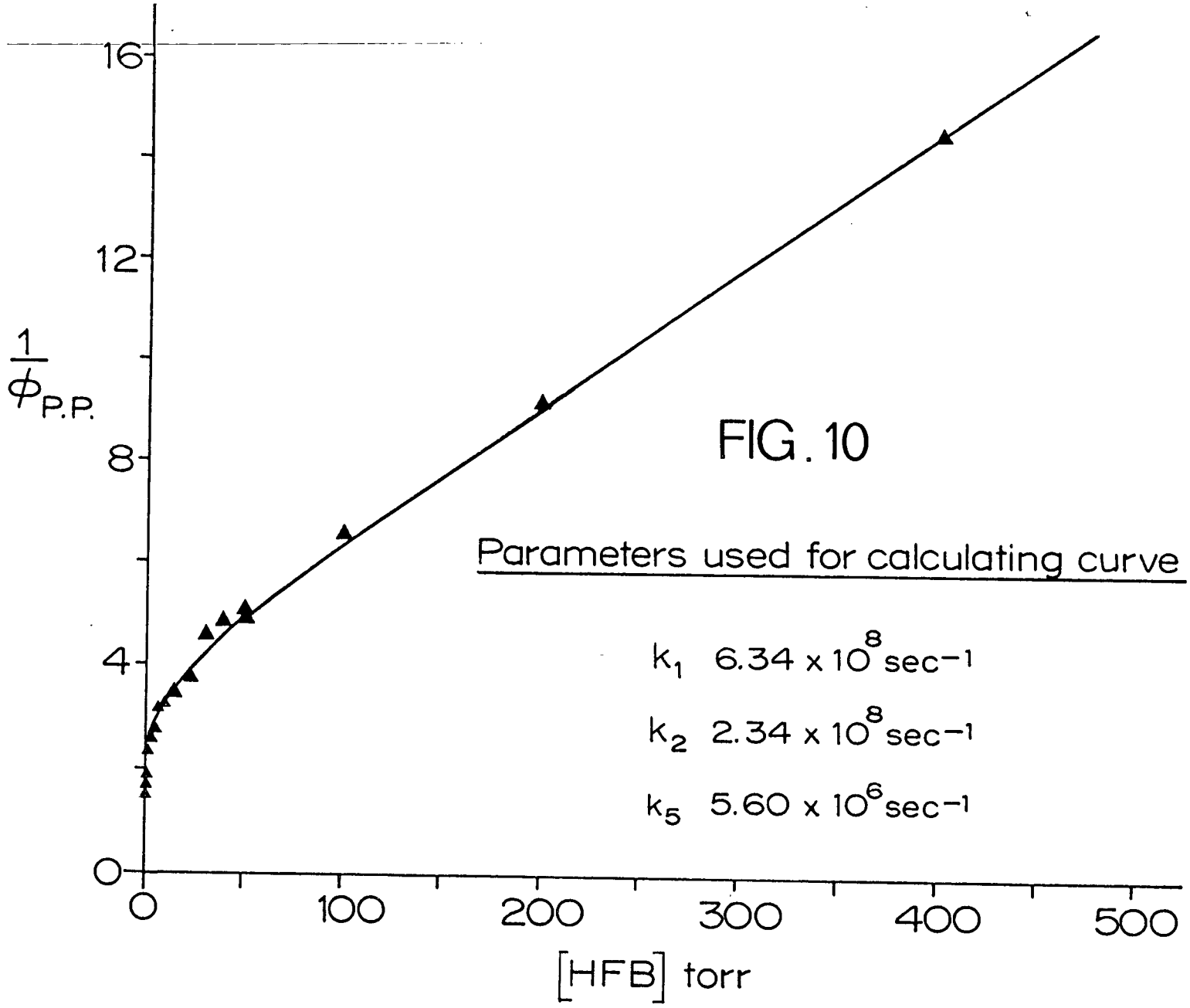

FIG. 10

Reciprocal quantum yields versus pressure-- 297 nm, 25 °C
High pressure region

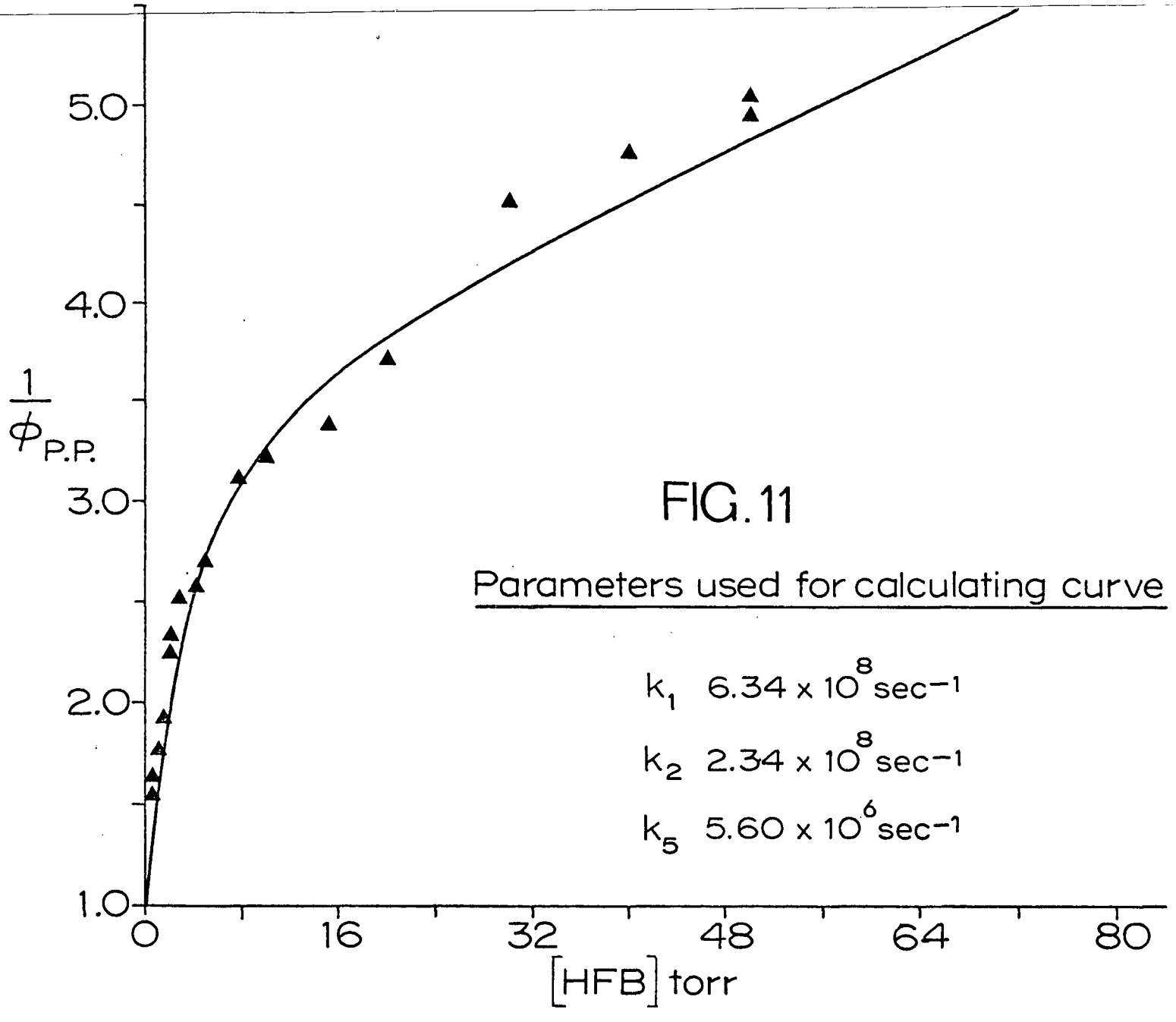

FIG. 11

Parameters used for calculating curve

k_1 $6.34 \times 10^8 sec^{-1}$

k_2 $2.34 \times 10^8 sec^{-1}$

k_5 $5.60 \times 10^6 sec^{-1}$

Reciprocal quantum yields versus pressure -- 297 nm, 25 °C
Low pressure region

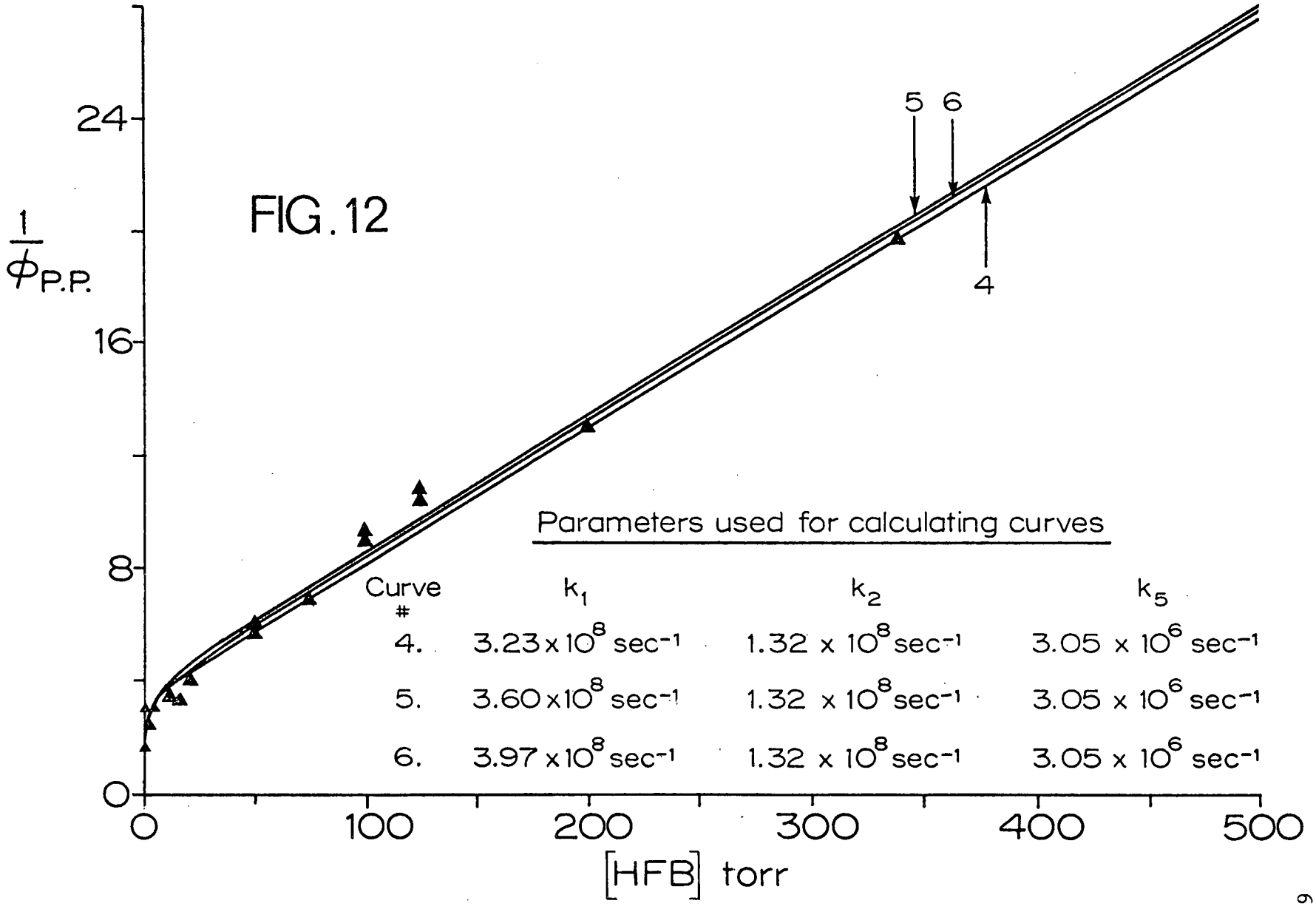

Reciprocal quantum yields versus pressure -- 313 nm, 25 °C
High pressure region

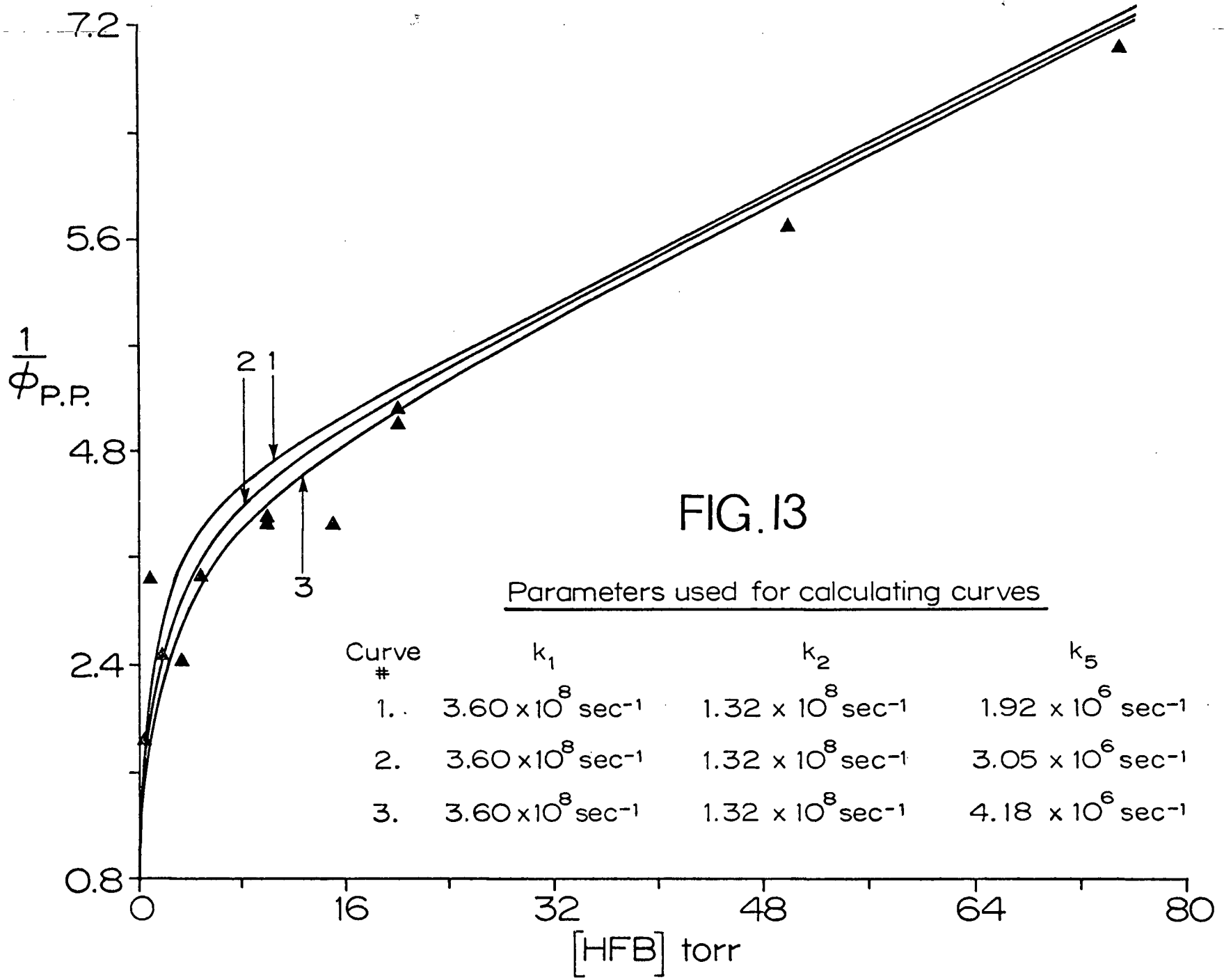

FIG. 13

Parameters used for calculating curves

Curve #	k_1	k_2	k_5
1.	3.60×10^8 sec^{-1}	1.32×10^8 sec^{-1}	1.92×10^6 sec^{-1}
2.	3.60×10^8 sec^{-1}	1.32×10^8 sec^{-1}	3.05×10^6 sec^{-1}
3.	3.60×10^8 sec^{-1}	1.32×10^8 sec^{-1}	4.18×10^6 sec^{-1}

Reciprocal quantum yields versus pressure-- 313 nm, 25 °C
Low pressure region

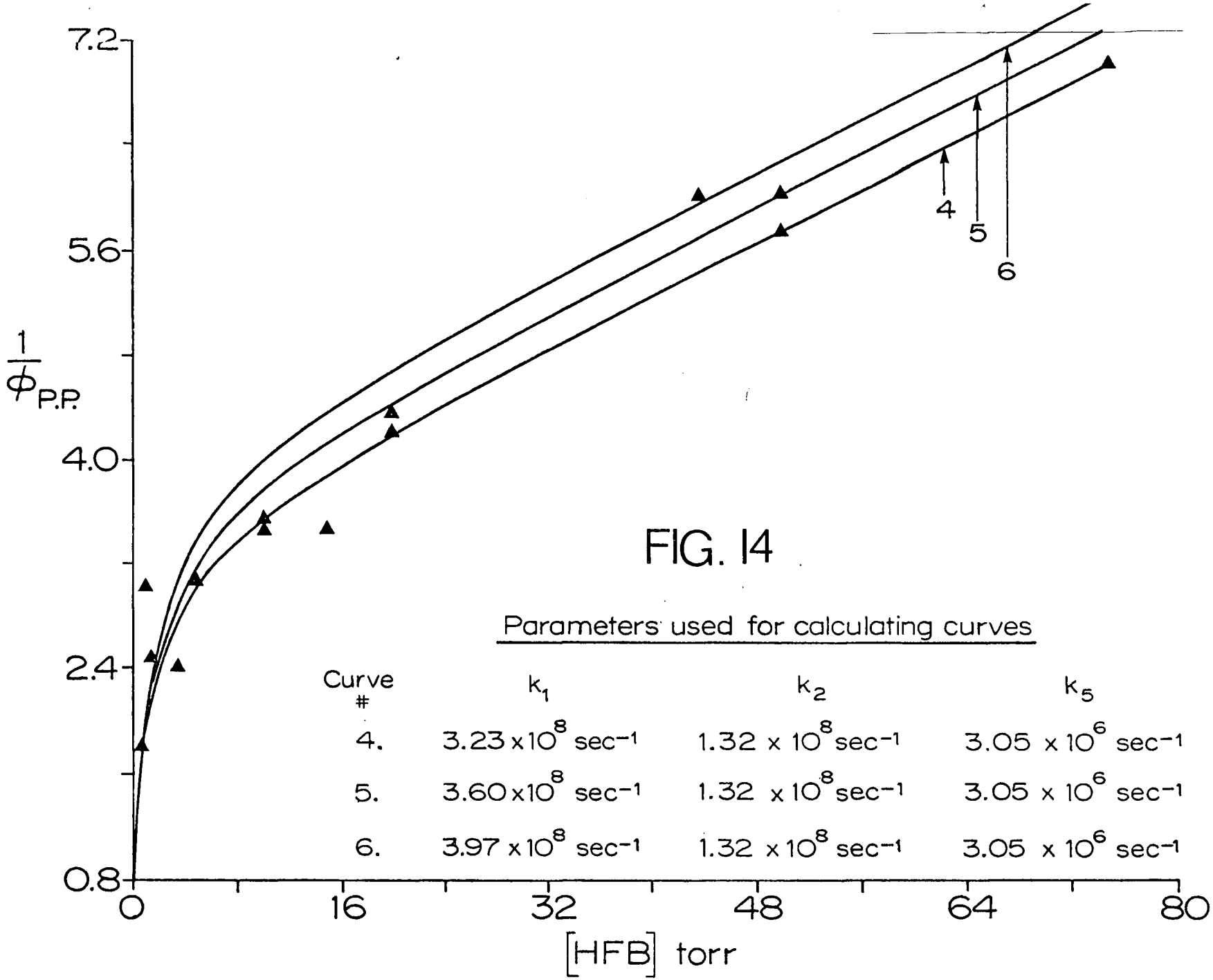

FIG. 14

Parameters used for calculating curves

Curve #	k_1	k_2	k_5
4.	3.23×10^8 sec^{-1}	1.32×10^8 sec^{-1}	3.05×10^6 sec^{-1}
5.	3.60×10^8 sec^{-1}	1.32×10^8 sec^{-1}	3.05×10^6 sec^{-1}
6.	3.97×10^8 sec^{-1}	1.32×10^8 sec^{-1}	3.05×10^6 sec^{-1}

Reciprocal quantum yields versus pressure -- 313 nm, 25 °C

Low pressure region

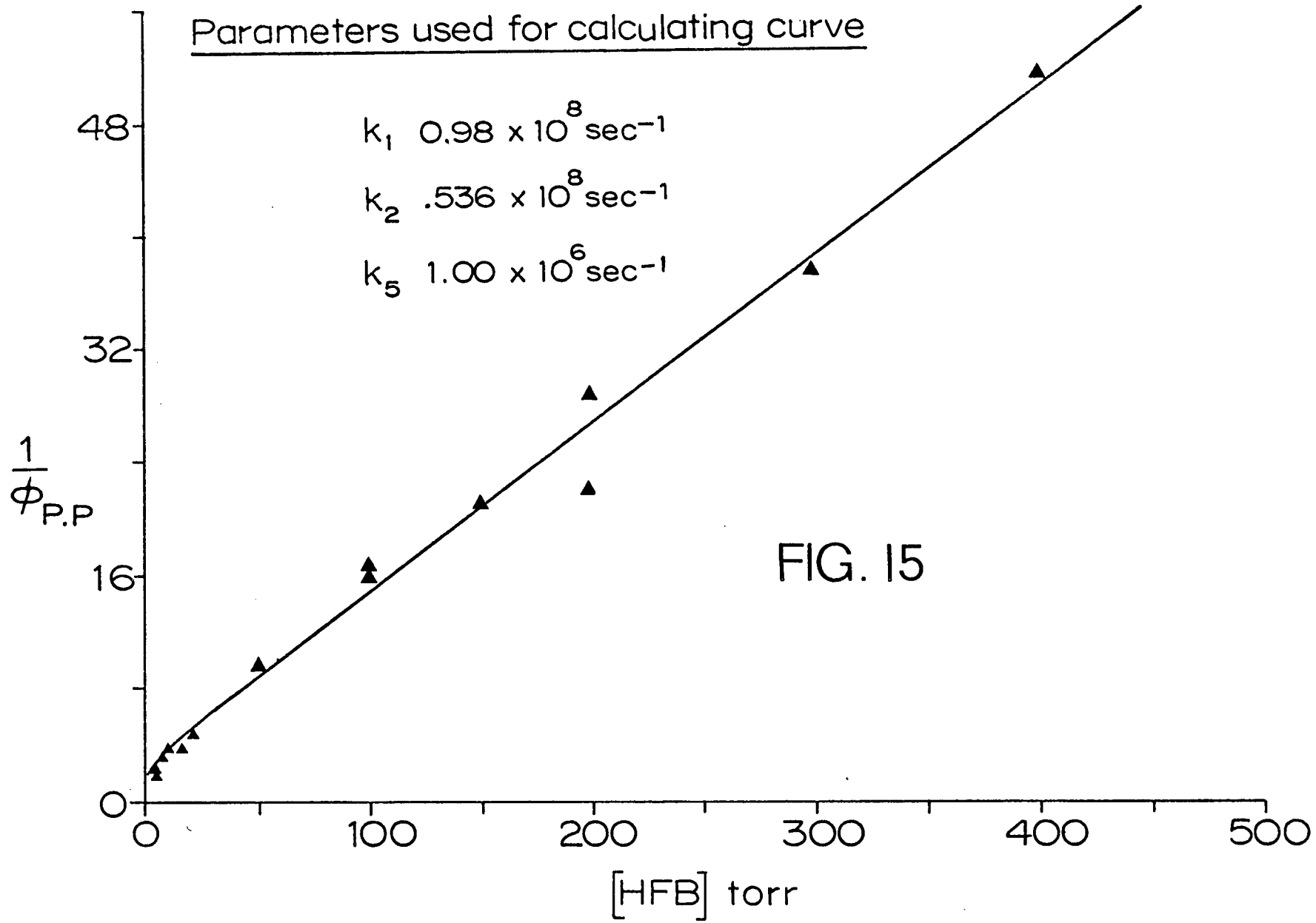

FIG. 15

Reciprocal quantum yields versus pressure -- 334 nm, 25°C
High pressure region

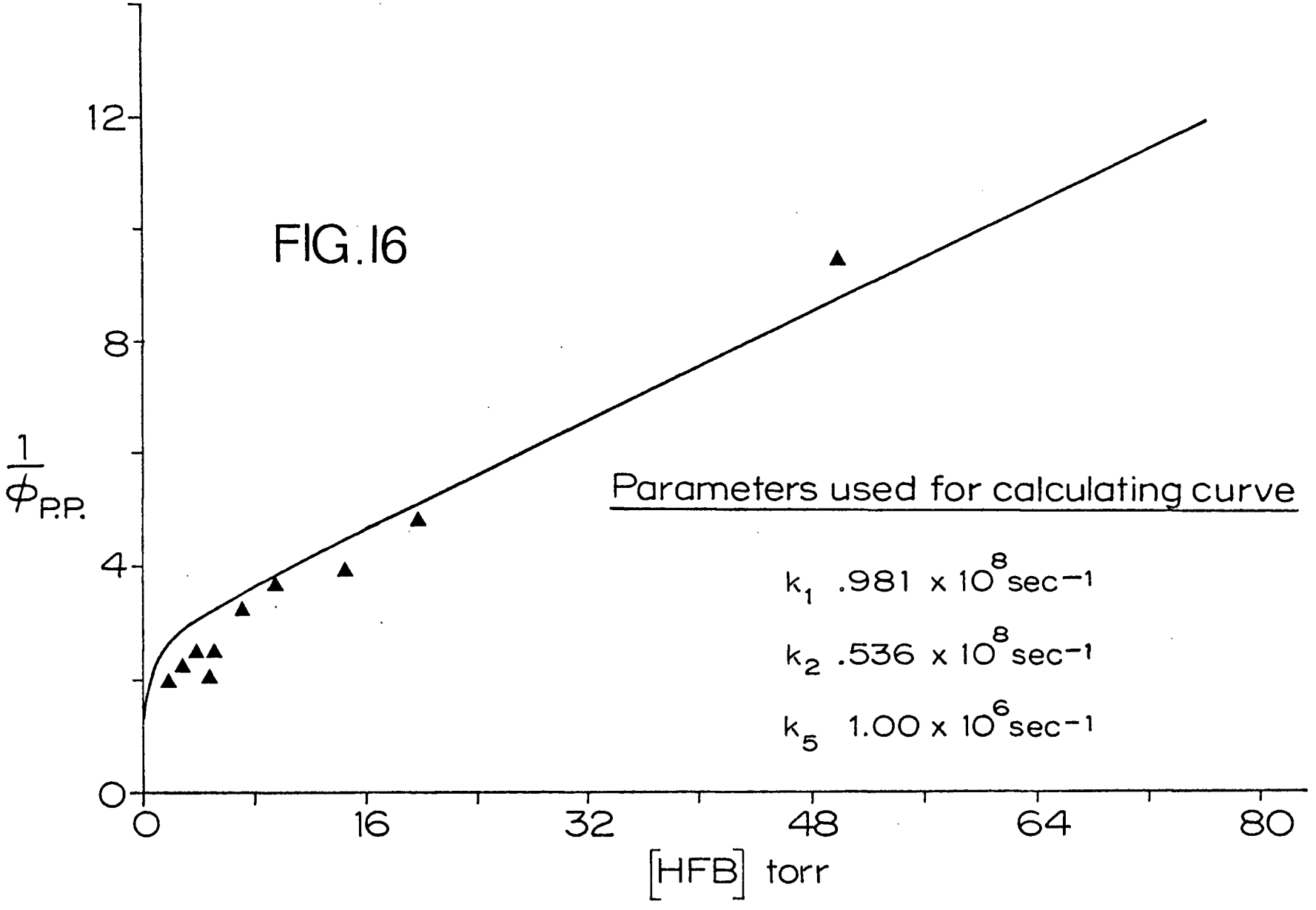

Reciprocal quantum yields versus pressure -- 334 nm, 25 °C
Low pressure region

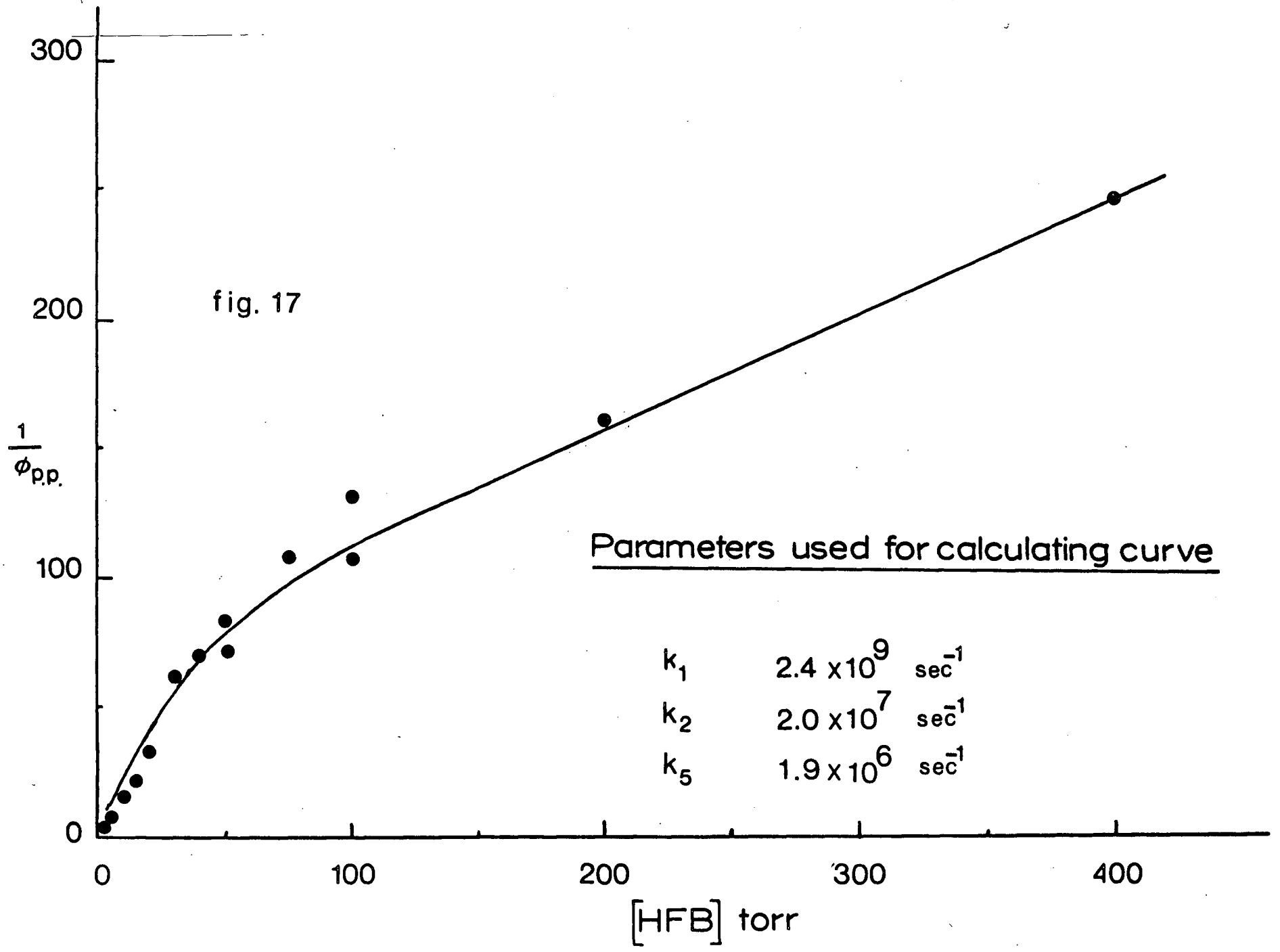

Reciprocal quantum yields versus pressure -- 366 nm, 25°C
High pressure region

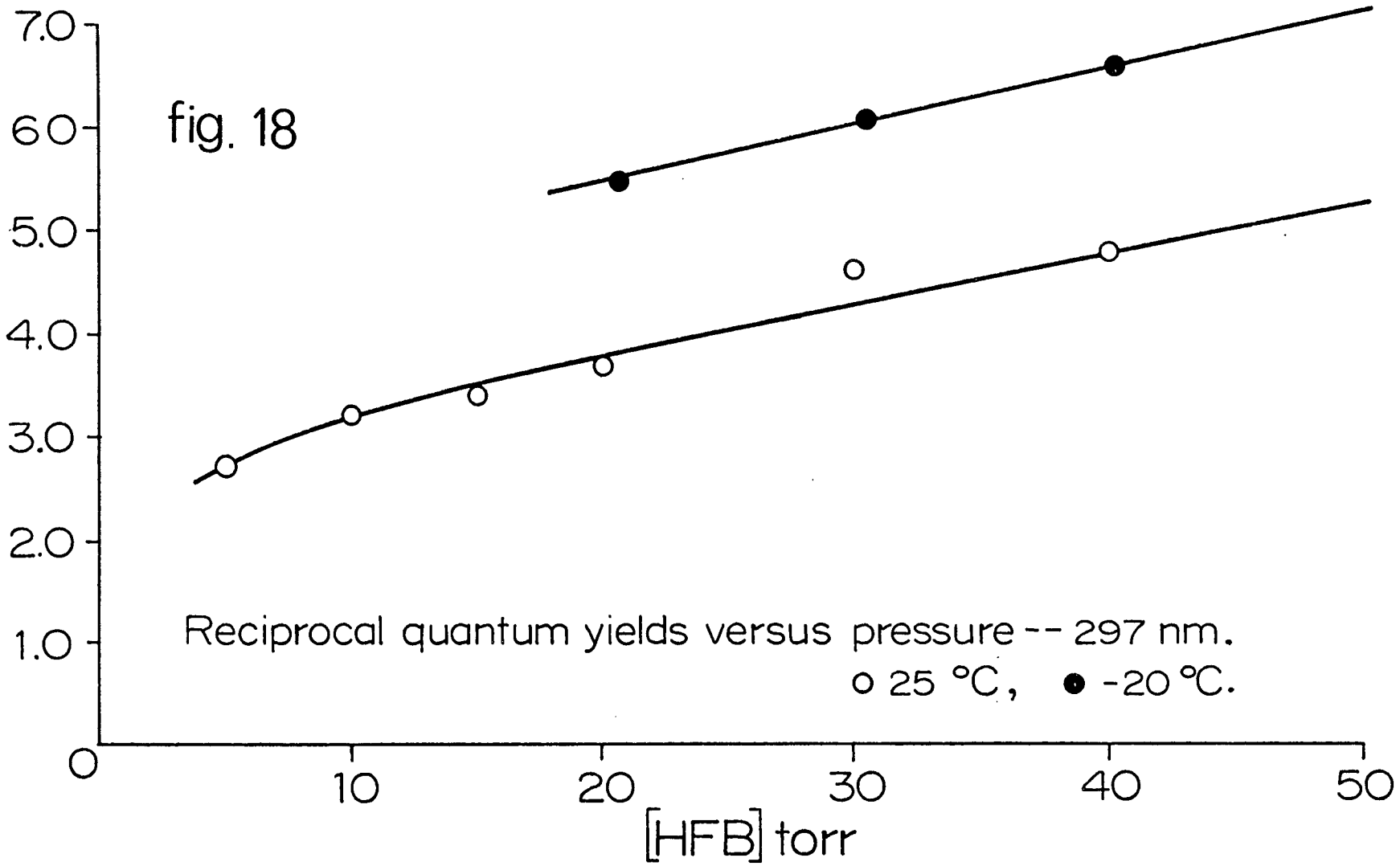
7.0
6.0
5.0
4.0
3.0
2.0
1.0
0
10
20
30
40
50
[HFB] torr
Reciprocal quantum yields versus pressure -- 297 nm.
o 25 °C, ● -20 °C.

fig. 18

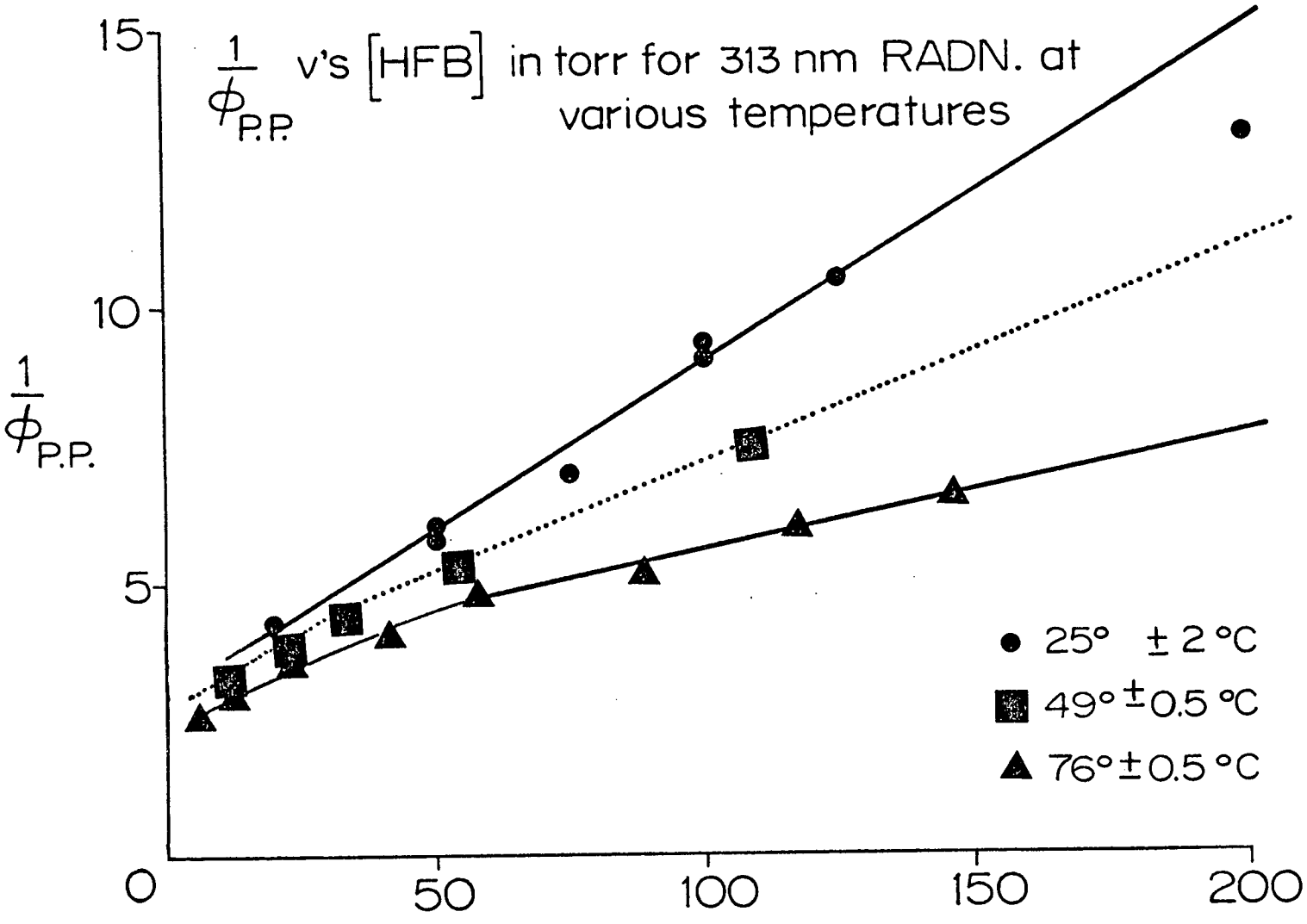
$\frac{1}{\phi_{P.P.}}$ v's [HFB] in torr for 313 nm RADN. at various temperatures
15
10
5
0
50
100
150
200
$\frac{1}{\phi_{P.P.}}$
● 25° ± 2 °C
■ 49° ± 0.5 °C
▲ 76° ± 0.5 °C
[HFB] in torr

fig. 19

The excited state involved in processes (viii) and (ix) is assumed to be the vibronic triplet formed on intersystem crossing from the vibronic level reached on excitation. Although the dissociating molecule (process (ix)) could be in any metastable state as far as the experimental evidence is concerned, it will be taken to be in the abovementioned vibronic triplet state in the discussion that follows.

From a steady-state treatment of the mechanism, the primary quantum yield for dissociation is given by:

$$\phi_{\text{Primary Process}} = \frac{k_2}{k_1 + k_2 + \omega M}$$

Molecules Decomposing from Non-equilibrated Singlet State

$$+ \frac{k_1}{k_1 + k_2 + \omega M} \times \frac{k_5}{k_5 + \omega M} \qquad (6)$$

Molecules Decomposing from Triplet State Having Originated from Non-Vibrationally Equilibrated Singlet State

Rearranging we find

$$\frac{1}{\phi_{P.P.}} = \frac{k_1 + k_2 + \omega M}{k_2 + \dfrac{k_1 k_5}{k_5 + \omega M}}$$

$$= \frac{\dfrac{k_1 + k_2}{k_2} + \dfrac{\omega M}{k_2}}{1 + \dfrac{k_1}{k_2 \left(1 + \dfrac{\omega M}{k_5} \right)}} \qquad \text{----------(7)}$$

At high pressure

$$\left(\frac{1}{\phi_{P.P.}} \right)_{M \to \infty} = 1 + \frac{k_1}{k_2} + \frac{\omega M}{k_2} \qquad \text{--------(8)}$$

Therefore, $1/\phi_{P.P.}$ vs. HFB conc. will be linear at high pressures with a slope and intercept given by ω/k_2 and $(1 + k_1 / k_2)$ respectively.

At low pressure

$$\left(\frac{1}{\phi_{P.P.}}\right)_{M \to 0} = 1 + \left(\frac{\omega + \frac{k_1 \omega}{k_5}}{k_1 + k_2}\right) M \text{---------(9)}$$

Therefore at low enough pressures the reciprocal quantum yields will tend toward unity.

D. Discussion

(i) Collisional Deactivation

It can be seen that the mechanism accounts for the essential features of the photochemical results. It assumes a single-step deactivation. This does not necessarily mean that the vibrationally equilibrated species ($^1_1B^0$) is formed directly from $^1_2B^*$ with unit efficiency, but simply that the first collision reduces the probability of dissociation to a negligible value. However, the recent work of Kutschke et al[4] on the pressure dependence of HFA photochemistry appears to give definite evidence that excess vibrational energy is

dissipated via a multistage cascade ("weak" collisional process). Ware's[7] lifetime measurements on HFA and Pitts'[38] photochemical data on trans-Crotonaldehyde support a similar conclusion.

Nevertheless, a kinetic description of the primary process which includes a complete multistage vibrational degradation becomes algebraically unmanagable with regard to evaluation of rate constants and diagnostic plots. Therefore, the strong collision approximation will be taken as a basis for discussion, bearing in mind the oversimplification so produced.

(ii) Mechanistic Considerations

The data are consistent with a mechanism that has photochemistry originating from two different states. One, the excited singlet state reached on excitation, is vibrationally excited while the other is postulated to be the vibrational level of the excited triplet reached on intersystem crossing (ISC) from the vibronic state reached on excitation.

At high pressures therefore, dissociation (process (ii)) competes directly with collisional degradation from the singlet state. Once vibrationally equilibrated, the

excited molecule can fluoresce (process (v)), cross over to the triplet manifold (process (vi)) or return to its ground state by some other radiationless process (process (vii)).

As the pressure is lowered ISC (process (i)) as well as dissociation of $^1_2B^*$ become more competitive with collisional deactivation. Consequently, the triplet state must be populated from the state reached on excitation. The pressure at which this competition becomes apparent depends on wavelength. The vibrationally excited triplet state molecule can then dissociate (process (ix)) or be collisionally degraded to the vibrationally equilibrated triplet. In this low pressure region (i.e. less than ca. 30 torr, but dependent on wavelength) photochemistry will take place from both states.

The fact that no photochemical products were detected with 405 nm or 436 nm radiation is interesting. The $S_1 \leftarrow S_0$ origin has been tentatively placed at 450 ± 30 nm.[1] Excitation with 436 nm and 405 nm radiation therefore, populates HFB in S_1 with little or no excess vibrational energy and with 7.1 kcal/mole, respectively. Consequently, it appears that the first excited state of HFB does not dissociate unless

it has at least 70 kcals of vibronic energy. The triplet formed by the intersystem crossing process from S_1 would also seem to be unreactive in this regard.

(iii) Photochemical Inertness of Equilibrated Triplet

No provision has been made here for dissociation following intersystem crossing from the equilibrated singlet state by analogy with HFA.[4] This omission follows from the negative quenching results with HFAM and the negative 436 nm photochemical results. The former suggests that the triplet mode responsible for photodecomposition is an excited vibrational state that has not yet equilibrated. Furthermore, the only slight change of gas phase emission intensity, ϕ_{phos} / ϕ_{fluor} ratio, and of τ_{phos} with temperature[39] confirms the absence of thermal-like decomposition of the equilibrated triplet state (at least at temperatures below 100° C). One would also expect a high pressure limiting yield ($\phi^{\infty}_{P.P.}$) independent of wavelength and strongly dependent on temperature if dissociation of the equilibrated triplet state was involved. Plots of $\phi_{P.P.}$ versus reciprocal HFB concentration (Figure 20) show that the high pressure quantum yields curve

towards zero at all wavelengths except 254 nm. Moreover the intercepts are different for each wavelength. It is not clear whether thermal-like dissociation is important at 254 nm or whether the yields would curve slowly to zero at higher pressures. Finally the temperature dependence of the quantum yields (Figures 18 and 19) is very slight (-20° C to $+80^{\circ}$ C).

(iv) Triplet Dissociation

Inspection of the reciprocal quantum yield plots (Figures 9, 11, 13 and 16) shows that curvature, attributed to triplet dissociation, is less pronounced with increasing wavelength. At 334 nm, for example, the curvature is slight (Figure 16). The data at 366 nm (Figure 17) suggest that triplet dissociation becomes noticeable at a relatively high pressure (i.e. ca. 50 torr).

(v) Light Intensity

The fact that the primary process is not a function of light intensity rules out the possibility of two triplet state molecules reacting to give the products as in biacetyl[26] -- at least in the intensity range used here (5×10^{14} to 3×10^{15} photons/cm^2/sec).

FIGURE 20

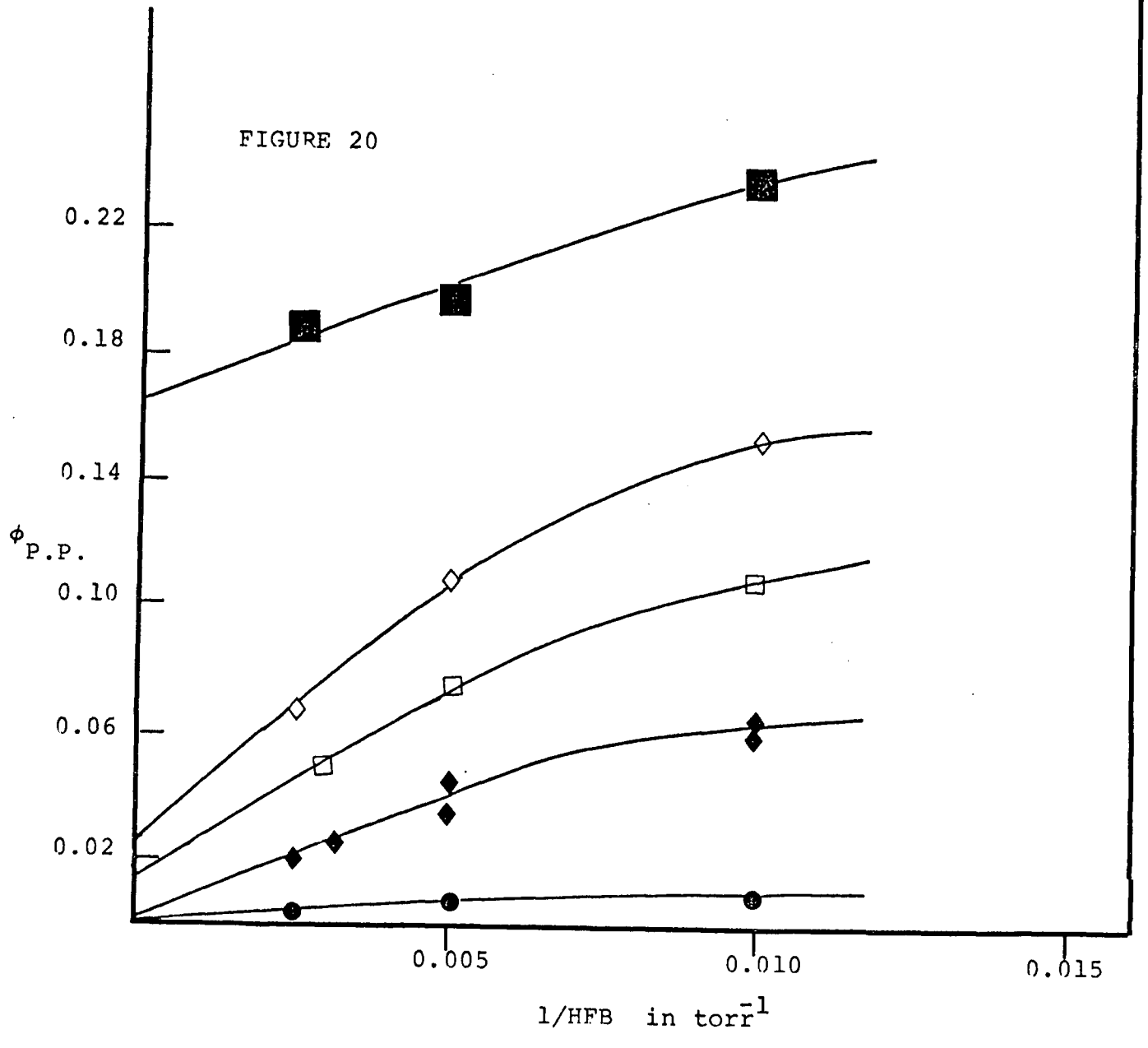

nm	Symbol
254	■
297	◇
313	□
334	◆
366	●

QUANTUM YIELDS VERSUS RECIPROCAL PRESSURES---HIGH PRESSURE REGION

(vi) Evaluation of Rate Constants

It has been shown that

$$\left(\frac{1}{\phi_{P.P.}}\right)_{M \to \infty} = 1 + \frac{k_1}{k_2} + \frac{\omega}{k_2} M \text{-----(8)}$$

so that at high pressure a plot of reciprocal quantum yields versus pressure will be linear with a slope and intercept given by ω/k_2 and $(1 + k_1 / k_2)$ respectively.

The method of least squares was therefore applied to the data (above approx. 40 torr) at each wavelength. The slopes and the intercepts are given in Tables 15 and 16. Taking the gas-kinetic collision diameter as 7.0Å , ω can be computed from kinetic theory as $\omega = 1.2 \times 10^{11}$ liter/mole/sec (6.42×10^{6} $torr^{-1}sec^{-1}$). k_2 and k_1 could therefore be calculated. Subsequently k_5 was computed using Equation (6) for each pressure (below approx. 20 torr) where an experimental quantum yield was available. An averaged k_5 was thus obtained for each wavelength. Some of the low pressure data at 313 nm (e.g. 1 torr and 15 torr) gave negative values for k_5, because of large experimental uncertainty in the quantum

TABLE 15

Rate Constants for Dissociation and Intersystem Crossing at 25° C

Wavelength nm	Slope[a] = ω/k_2 $torr^{-1}$	$k_2 \times 10^{-8}$ (sec^{-1})	intercept = $1 + k_1/k_2$	k_1/k_2	$k_1 \times 10^{-8}$ (sec^{-1})	$k_5 \times 10^{-6}$ (sec^{-1})
254	0.0043 ±0.0021	15.1	3.55	2.55 ±0.50	38.5	11.9 ±4.0
297	0.0274 ±0.0002	2.34	3.71	2.71 ±0.04	6.34	5.6 ±1.5
313	0.049 ±0.002	1.32	3.73	2.73 ±0.28	3.60	3.0 ±1.1
334	0.112 ±0.005	0.536	2.83	1.83 ±0.90	0.98	≤1.0
366	0. 32 ±0.04	0. 20	65.5	64.5 ±7.2	24	1.9

a. $\omega = 6.42 \times 10^6$ $torr^{-1}$ sec^{-1}

TABLE 16

Rate Constants for Dissociation and Intersystem Crossing at Various Temperatures

Wavelength nm	Temp °C	Slope[a] = ω/k_2 $torr^{-1}$	Intercept $(1 + k_1 / k_2)$	k_1 / k_2	k_2 (sec^{-1})	k_1 (sec^{-1})
313	+25	0.049 ±0.002	3.73	2.73 ±.28	1.32×10^8	3.60×10^8
313	+50	0.041 ±0.002	3.06	2.06 ±.13	1.56×10^8	3.21×10^8
313	+76	0.026 ±0.003	2.87	1.87 ±.27	2.45×10^8	4.59×10^8
297	-20	0.066 ±0.005	3.82	2.82 ±.18	0.96×10^8	2.72×10^8
297	+25	0.0274 ±0.0002	3.71	2.71 ±.04	2.34×10^8	6.34×10^8

yields, when treated in this way. The latter values for k_5 were ignored and so the quoted error limits are rather optimistic for this wavelength. The 334 nm data necessitate that only an upper limit on k_5 be given. Table 15 summarizes these results.

(vii) Simulation of Quantum Yield Results

The parameters given in Table 15 were used to evaluate reciprocal quantum yields at various pressures using Equation (6). The results, plotted as a smooth curve at each wavelength on the same Figure as the experimental data, are given in Figures 8 to 17. To determine what effect each parameter had on the overall quantum yield, parameters at one wavelength (313 nm) were varied within their quoted error limits. Very little change is noticed in the high pressure region (Figure 12). However in the low pressure region changes in k_1 (Figure 14) appear to have a larger effect on the quantum yield than changes in k_5 (Figure 13). This apparently larger effect may be due to using error limits for k_5 which are too small (c.f. section (vi), this chapter).

(viii) Variation of k_1, k_2 and k_5 with Wavelength

The experimental data indicate that the rates of dissociation of both the singlet vibronic state molecules (k_2) and the triplet vibronic state molecules (k_5) are a function of their energy content. These relationships are shown in Figure 21. The minimum energy necessary for singlet state dissociation lies between 405 nm (70.0 kcal) and 366 nm (78.0 kcal). The minimum exciting radiation necessary for triplet state dissociation lies between 405 nm and 334 nm (85.0 kcal).

The inclusion of k_1 (rate of intersystem crossing from the vibronic singlet level reached on excitation) was necessitated in McIntosh's work.[1] If intersystem crossing to the triplet is only via (vi), which competes with fluorescence from $^1_1B^0$, pressure dependencies within the singlet manifold should be duplicated by the phosphorescence as well. This was not found to be the case.[1] Also, ratios of ϕ_{phos}/ϕ_{fluor} are observed which are larger than the limiting high pressure value and which are functions of pressure and energy. The photochemical quantum yields found here are also consistent with a mechanism in which $^1_2B^*$ is

depleted by both intersystem crossing and dissociation in competition with collisional degradation. The relative importance of k_2 and k_1 has been assessed from the extrapolated intercept of the high pressure data in Figures 8, 10, 12, 15 and 17 (see Equation (8)).

The Rate Constants at 366 nm: A few comments concerning the large k_1/k_2 ratio at 366 nm (Table 15) are necessary. The point representing k_1 at 366 nm in Figure 21 is inconsistent with the values of k_1 at other wavelengths in the sense that it is an order of magnitude larger than is expected by extrapolation. McIntosh, in fact, found k_1 to be 6.5×10^7 sec^{-1}, which is in line with the other results (see Figure 21).

The plot of log k_2 against energy should in principle be sharply concave down at the low energy side, as the threshold is approached. For k_1 on the other hand, the intersystem crossing rate is probably not governed by a minimum energy. The value of k_1 for the equilibrated singlet is known[1] to be 2.8×10^7 $sec.^{-1}$ Thus the values of log k_1 approach this limiting value at low energy (see Figure 21).

The value of k_1 has been determined here indirectly so that the experimental uncertainty is quite large. According to Equation (8) the slope of high pressure data represents ω/k_2, and k_1 is found by

$$k_1 = (\text{Intercept} - 1)\frac{\omega}{\text{slope}}$$

The errors are thereby greatly magnified. For example, within error limits for each point of ±20%, one finds k_2 to be ± 30% but k_1 is uncertain by a factor of two! There is every reason therefore to suspect that k_1 at 366 nm is not anomalous but that the value of k_1 shown in Figure 21 is simply subject to large uncertainty.

The point representing k_5 at 366 nm in Figure 21 is likewise inconsistent with the values of k_5 at the other wavelengths insofar that it is expectedly too large. The value of k_5 has been computed using Equation (6) for each pressure below 30 torr where an experimental quantum yield is available. This procedure necessitates using the previously determined values of k_1 and k_2 so that the large errors in these parameters are reflected in the value of k_5. Consequently one finds k_5 varying by a factor of three. The value of k_5 shown in Figure 21 at 366 nm is therefore also subject to large uncertainty.

The Intersystem Crossing Rate Constant: As aforementioned the rate of intersystem crossing from the vibronic singlet level reached on excitation increases as the wavelength decreases (Figure 21). This behaviour of k_1 is consistent with the idea that as the molecules are raised to upper vibrational levels of the excited singlet state the hypervolume associated with the vibronic states increases and so the probability of contacting potential surface intersections increases. This is the first reported instance of the intersystem crossing rate constant being a strong function of the energy of the exciting radiation. A similar but smaller effect is however known for benzene. Ware and co-workers[40] have found that the nonradiative rate constant (assumed to be entirely due to intersystem crossing) is a function of the vibronic level in the $^1B_{2u}$ state into which the molecule is excited. Over an energy range of 1450 cm^{-1} the intersystem crossing rate constant varied by a factor of 1.3. For HFB the intersystem crossing rate constant is found to vary by a factor of about 70 over an energy range of 9000 cm^{-1}. In cases where triplet dissociation has been established[4,17] the intersystem crossing process appears to originate mainly from the vibrationally equilibrated singlet state. Consequently the wavelength of

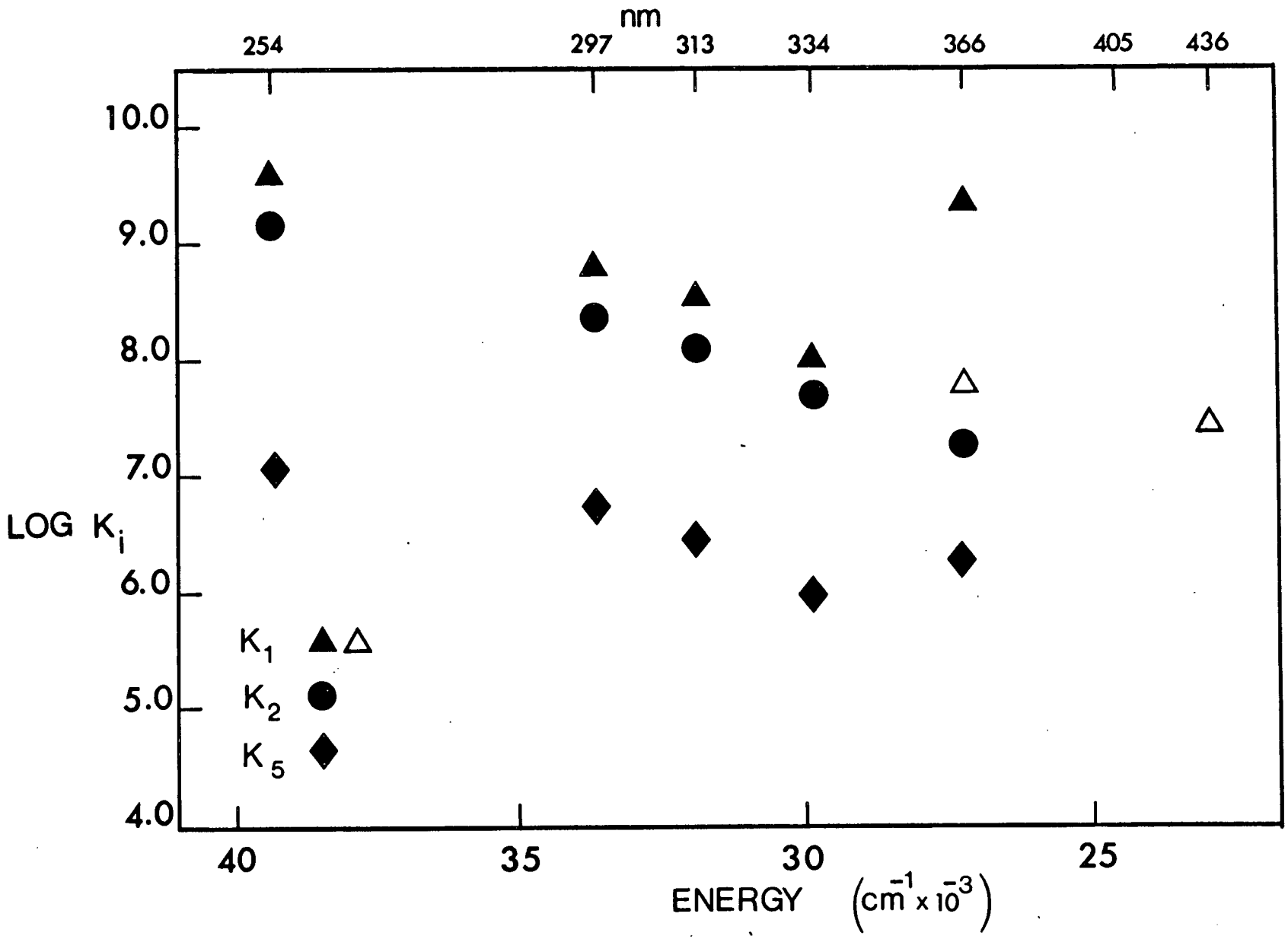

fig. 21 Log. of the various rate constants versus excitation energy. △ from McIntosh.[1]

the irradiating light has no effect on the intersystem crossing process for these systems.

(ix) Other Possible Mechanisms

(a) Involvement of the Vibrationally Excited Ground State:

It is possible that the excited singlet state, instead of crossing to the triplet manifold, crosses isoenergetically to a highly vibrationally excited level of the ground state. The wavelength dependence found here would then be observed if the rate of internal conversion depended on the vibrational level of the excited state $^{1}_{2}B^{*}$ or if the rate of dissociation depended on the vibrational level of the ground state.[41]

Experimentally, involvement of the ground state (like involvement of the vibronic triplet state) is difficult to substantiate as a path for photodecomposition. It can only be inferred by the elimination of every other possibility. Even so, quantitative documentation is sparse. Cyclo[1.3.5]heptatriene[8-9, 42-43] appears to be the only system for which the data are reasonably convincing. No carbonyl compound is known to photodissociate from the ground state.

The evidence for ground state participation in the photolysis of glyoxal[13,44] is, at best, indecisive.

(b) Vibrational Energy Distribution Function:

It has also been suggested that curvature in reciprocal quantum yield versus pressure plots can be explained on the basis of the width of the vibrational energy distribution function.[45] This function embodies both the thermal energy distribution factor of the ground electronic state and the energy profile of the absorbed light. Bowers[46] found for HFAM at 366 nm that the predicted "falloff" in $1/\phi_{P.P.}$ occurred mostly at much lower pressures than had been found experimentally by Wu and Rice.[37] He concluded that more than one electronic state might be involved.

Further discussion of this type of theoretical approach to HFB photochemistry must await evaluation of the normal mode frequencies of the ground state of HFB and an indication as to how they may change in the excited state.

(x) Wall Deactivation of the Equilibrated Triplet State

Finally, experimental evidence for another type of collisional deactivation is presented and discussed. This

deactivation involves the equilibrated triplet state of HFB at very low pressures (approximately one torr) interacting with the reaction cell wall.

Parmenter and Poland[18] found that there was a marked decrease in the quantum yield of biacetyl phosphorescence emission and the lifetime of the triplet in experiments at low pressures. They attributed these effects to the increasing importance of biacetyl triplet diffusion to and deactivation at the cell wall at low pressures.

More recently McIntosh[1] has observed that phosphorescence quantum yields of HFB decrease rapidly in the pressure region below 2 torr at 436 nm. Low pressure triplet lifetimes were thus required to confirm the effect for HFB.

Results and Discussion: The experimental set-up and apparatus for determining phosphorescence lifetimes of HFB is described in Chapter II. Figure 22 shows the difference (γ) between the reciprocals of the observed lifetimes ($1/\tau$) at low pressure and the lifetime extrapolated at high pressure ($1/\tau_0$) against HFB concentration. There is a marked deviation from the high pressure value for experiments in the region below

1 torr. Furthermore γ is found to be (within experimental error) a linear function of the reciprocal of the HFB pressuree (Figure 23). The results shown in Figures 22 and 23 are expected if wall deactivation of triplets is important at low pressures. The rate of diffusion is inversely proportional to the gas concentration[47] so that deactivation at the wall should also be inversely proportional to the pressure of the gas through which the triplets must diffuse to react at the wall. It is also expected that this effect will occur under the conditions used here somewhat below 1 torr. At this pressure the average distance which the triplet molecules can diffuse during their lifetime approaches the average distance from the cell wall at which the molecules are excited (approximately 1.5 cm).* These results parallel those obtained for biacetyl by Parmenter and Poland[18] and confirmed recently by Calvert and co-workers.[14] The latter workers have also shown that the isolated excited singlet state molecule undergoes a truly unimolecular ISC process with the same efficiency as in the collisionally perturbed system at high pressures. They found that the relative

*The time in seconds for the triplet molecule to diffuse a distance x cms. is given approximately by x^2/D, where D is the diffusion coefficient; $D = D_0/\text{pressure(Torr)}$.[48] For HFB $D_0 = 1.1 \times 10^{-2} cm^2/sec$. (Appendix B).

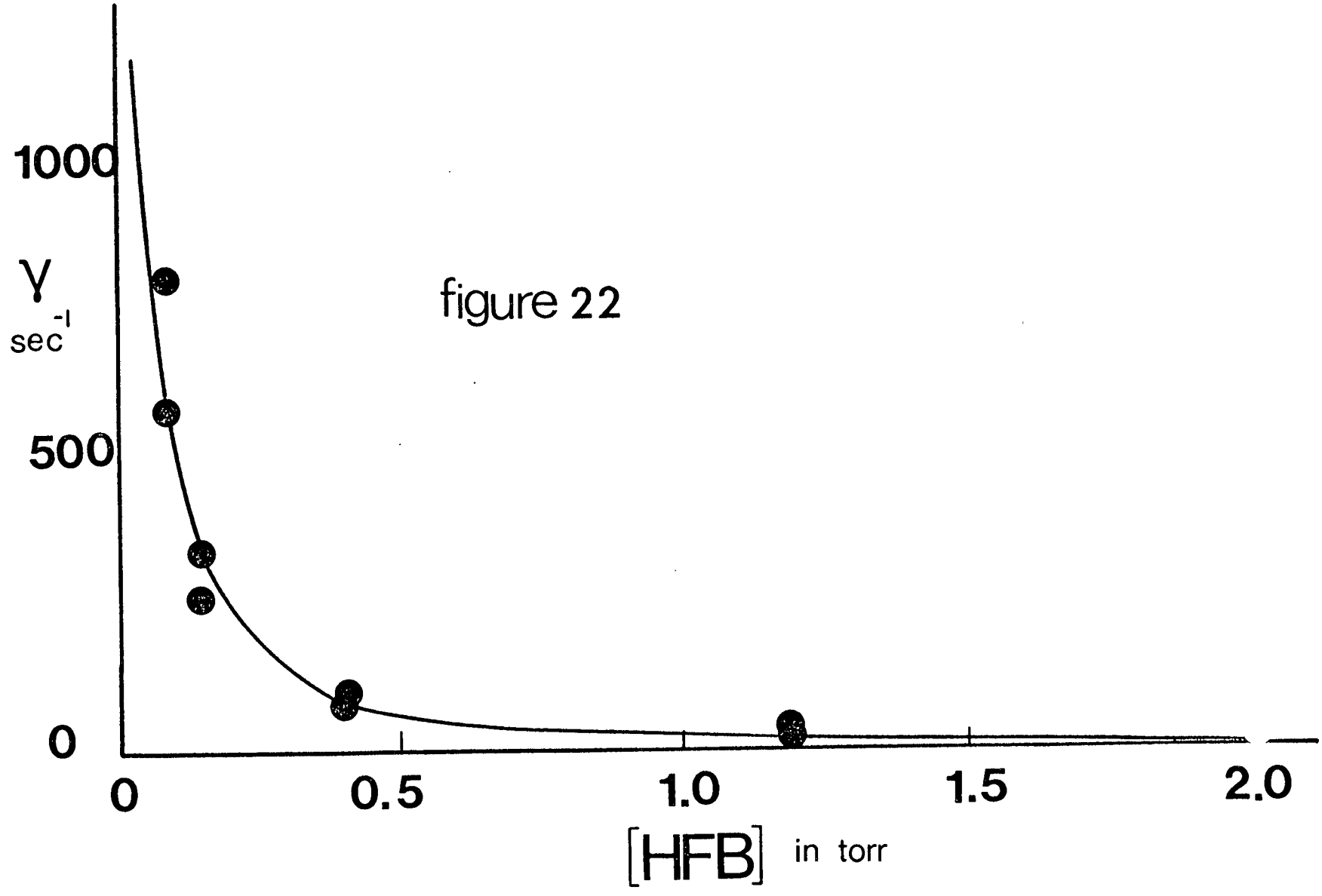

figure 22

DIFFERENCE (γ) BETWEEN THE RECIPROCALS OF THE OBSERVED LIFETIME (τ) AT LOW PRESSURES AND THE CONSTANT HIGH PRESSURE TRIPLET LIFETIME (τ_0) VERSUS HFB PRESSURE

DIFFERENCE (γ) BETWEEN THE RECIPROCALS OF THE OBSERVED LIFETIME (τ) AT LOW PRESSURES AND THE CONSTANT HIGH PRESSURE TRIPLET LIFETIME (τ_0) VERSUS RECIPROCAL HFB PRESSURE

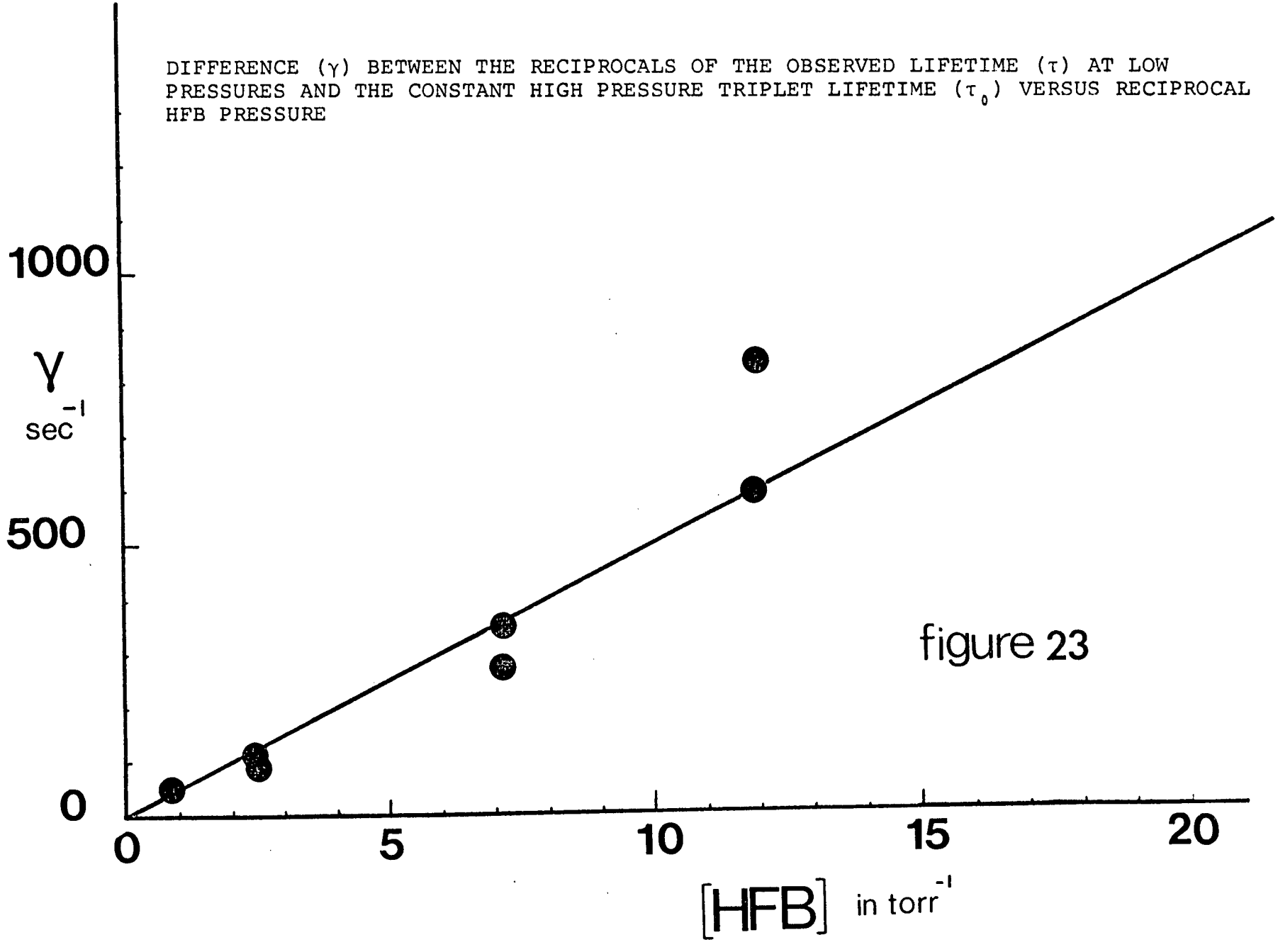

figure 23

phosphorescence quantum yield of biacetyl at 436.5 nm is invariant of pressure between 12.5 torr and 11.4μ . Collisional deactivation is negligible for singlet state biacetyl molecules below about 10 torr.[49] There is every reason to expect that the intersystem crossing reaction for HFB will also be truly unimolecular.

CHAPTER V

The Primary Process

In this chapter a detailed mechanism, incorporating all the known photochemical and photophysical data, is presented. Its scope and limitations are critically discussed. Various rate constants for photochemical and photophysical processes are evaluated and compared with those obtained previously. The fluorescence and photochemical yields are combined to demonstrate decomposition competing with collisional deactivation in the triplet manifold.

A. Detailed Mechanism

The processes necessary to account for the observed photochemical and photophysical results are as follows:

$$B + h\nu \longrightarrow {}^1_2B^*$$

$${}^1_2B^* \xrightarrow{k_1} {}^3_?B^* \qquad \text{(i)}$$

$${}^1_2B^* \xrightarrow{k_2} 2CO + C_2F_6 \qquad \text{(ii)}$$

$${}^1_2B^* \xrightarrow{k_f^*} B + h\nu_{fluor} \qquad \text{(iii)}$$

$${}^1_2B^* + M \xrightarrow{\omega} {}^1_1B^0 + M^* \qquad \text{(iv)}$$

$${}^1_1B^0 \xrightarrow{k_f} B + h\nu_{fluor} \qquad \text{(v)}$$

$${}^1_1B^0 \xrightarrow{k_{isc}} {}^3_1B^* \qquad \text{(vi)}$$

$$^{3}_{?}B^{*} + M \xrightarrow{\omega} {}^{3}_{1}B^{0} + M \quad \text{(viii)}$$

$$^{3}_{?}B^{*} \xrightarrow{k_5} 2CO + C_2F_6 \quad \text{(ix)}$$

$$^{3}_{1}B^{0} \xrightarrow{k_p} B + h\nu_{phos} \quad \text{(x)}$$

$$^{3}_{1}B^{0} \xrightarrow{k_{11}} B \quad \text{(xi)}$$

$$^{3}_{1}B^{0} + \text{wall} \xrightarrow{k_{wall}} B + \text{wall} \quad \text{(xiii)}$$

A few comments concerning the individual processes seem to be in order: intersystem crossing to the triplet manifold from the vibronic level reached on excitation (process (i)) is necessitated by McIntosh's emission results as well as the photochemical results reported in this work. As, if ISC to the triplet is only via process (vi), which competes with fluorescence from $^{1}_{1}B^{0}$, pressure dependencies within the singlet manifold should be reflected by the phosphorescence as well. However ϕ_{phos} with 405 nm and 366 nm excitation has become pressure independent at 20 torr HFB, yet ϕ_{fluor} is still increasing in this region.[1] Also, ϕ_{phos}/ϕ_{fluor} ratios are observed which are larger than the limiting high pressure value, and which are functions of pressure and energy.[1] The intercepts in the reciprocal quantum yield

versus pressure plots necessitates a mechanism which includes k_1 as a means of depleting (with k_2) the vibronic singlet state.

The data require a mechanism that has photochemistry originating from two different states - the vibronic singlet state (process (ii)) and the vibronic triplet state (process (ix)). At high pressures process (ii) competes directly with collisional degradation (process (iv)) from the singlet state. Once vibrationally equilibrated, the excited molecule can fluoresce (process (v)) or cross to the triplet manifold (process (vi)). As the pressure is lowered ISC (process (i)) and dissociation from the vibronic singlet state become more competitive with collisional deactivation and consequently the triplet state is populated from the level reached on excitation. This vibrationally excited triplet state molecule can dissociate (process (ix)) or be collisionally degraded to the vibrationally equilibrated triplet (process (viii)). The equilibrated triplet state can then either phosphoresce (process (x)) or return to the ground state by some radiationless conversion process (process (xi)).

Fluorescence must be possible from levels near those reached on excitation (process (iii)) as well as from an equilibrated state (process (v)) as McIntosh[1] found that at low pressures ϕ_{phos} decreases much faster than ϕ_{fluor}; ϕ_{phos} apparently rapidly decreases to zero as ϕ_{fluor} approaches a finite non zero value. Although wall deactivation (xiii) becomes a major consideration in the very low pressure region, it is unlikely to change these general conclusions. The ϕ_{phos} results at shorter wavelengths show the same features (as longer wavelengths) at higher pressures where wall-deactivation of the equilibrated triplet would be negligible.

B. Independent Evaluation of $(k_1 + k_2)$

McIntosh[1] has evaluated $(k_1 + k_2)$ at each wavelength using his fluorescence data. Table 17 reproduces his estimates together with the values found in the present work from the photochemical experiments. There is good agreement between the two values of the rate constants. This agreement substantiates the proposed mechanism; in particular the feature of the intersystem crossing process from the vibronic state reached on excitation (process (i)). The apparent discrepancy

in the 366 nm results is discussed in Chapter IV. It should be noted however that McIntosh has estimated k_2 at 366 nm to be 1.9×10^7 sec^{-1} while a value of 1.4×10^7 sec^{-1} is found in this work.

C. Evaluation of k_2 from the Full Mechanism

(i) Fluorescence/Photochemistry Ratio

From a steady-state treatment of the mechanism, the primary photochemical yield and the fluorescence yield are given by the expressions

$$\phi_{P.P.} = \frac{k_2}{k_1 + k_2 + \omega M + k_f^*} + \frac{k_1}{k_1 + k_2 + \omega M + k_f^*} \times \frac{k_5}{k_5 + \omega M} \quad \text{-----(11)}$$

and Equation (1) respectively. The ratio is

$$\frac{\phi_{fluor}}{\phi_{P.P.}} = \frac{\alpha\omega M + k_f^*}{k_2 + \frac{k_5}{k_5 + \omega M} \cdot k_1} \quad \text{-----(12)}$$

where $\alpha = \frac{k_f}{k_f + k_{ISC}} \equiv \phi_{fluor}^{\infty}$

Table 17

Rate Constants for the Sum of Singlet Dissociation and Intersystem Crossing from the Initially Populated Vibronic Singlet State.

Wavelength nm	$(k_1 + k_2) \times 10^{-8}$ sec^{-1} [a]	$(k_1 + k_2) \times 10^{-8}$ sec^{-1} [b]
254	53.6	-
297	8.68	13.0
313	4.92	3.7
334	1.52	2.2
366	24.2	0.84
405	-	0.61

[a] This work

[b] McIntosh[1]

At high pressures (12) becomes

$$\frac{\phi_{fluor}}{\phi_{P.P.}} = \frac{\alpha\,\omega M}{k_2} \qquad \text{----------(13)}$$

Combining the known value of α^1 with the slope of the ratio versus pressure plot gives k_2. This was done for each wavelength where appropriate data were available. Figure 24 shows a typical example. Table 18 gives the values of k_2 obtained by this method.

(ii) Phosphorescence/Photochemistry Ratio

The phosphorescence yield, from a steady-state treatment of the mechanism, is given by equation (2). Let

$$\frac{k_{ISC}}{k_{ISC} + k_f} = \phi^0_{ISC} \quad \text{and} \quad \frac{k_p}{k_p + k_{11}} = \beta$$

The ratio of the phosphorescence yield to the photochemical quantum yield is given by

$$\frac{\phi_{phos}}{\phi_{P.P.}} = \frac{\frac{\beta\ \omega M}{\omega M + k_5} \times \phi^0_{ISC} \times \omega M + \frac{\beta\ \omega M}{\omega M + k_5} \times k_1}{k_2 + k_1 \times \frac{k_5}{\omega M + k_5}}$$

$$= \frac{\beta\ \omega M \{\ \phi^0_{ISC}\ \omega M + k_1\ \}}{k_2\ \{\omega M + k_5\} + k_1\ k_5} \quad \text{----------(14)}$$

Now at high pressures

$$\omega M >> k_5$$

and $$k_2\ \omega M >> k_1\ k_5$$

$$\therefore \quad \frac{\phi_{phos}}{\phi_{P.P.}} = \frac{\beta(\phi^0_{ISC}\ \omega M + k_1)}{k_2}$$

$$= \frac{\beta\ \phi^0_{ISC}\ \omega}{k_2} \cdot M + \beta\frac{k_1}{k_2}$$

------(15)

A plot of this ratio against HFB pressure gives a slope equal to $\beta\frac{\phi^0_{ISC}\ \omega}{k_2}$. McIntosh[1] gives values of β and ϕ^0_{ISC} (0.086 and 0.9 respectively) so that k_2 can be determined. This was done for each wavelength where appropriate data were available. Figure 25 shows a typical example. Table 18 gives the values of k_2 obtained by this method.

(iii) Discussion

It can be seen from Table 18 that there is a good agreement between the various methods used in obtaining k_2. In particular, the absolute photochemical and photophysical quantum yields at high pressures (at least) are internally consistent. This lends credence to the proposed mechanism.

D. Complementary Aspects of this and Previous Work

McIntosh's quantum yield measurements were designed for a specific purpose - the absolute emission quantum yield of HFB at high pressure (250 torr) at various excitation wavelengths.[50] He therefore optimized his experimental arrangement with this in mind. In particular, the illuminating beam passed through the cm square cell within 1 mm of the side observation window. The triplet lifetime results

Table 18

Rate Constants for Singlet Dissociation

Wavelength nm	k_2 (Photochemistry only)	k_2 (Fluorescence & photochemistry)	k_2 (Phosphorescence & photochemistry)
297	2.34×10^8 sec^{-1}	2.10×10^8 sec^{-1}	2.58×10^8 sec^{-1}
313	1.32×10^8 sec^{-1}	1.14×10^8 sec^{-1}	1.24×10^8 sec^{-1}
334	0.54×10^8 sec^{-1}	0.52×10^8 sec^{-1}	0.56×10^8 sec^{-1}
366	0.20×10^8 sec^{-1}	0.053×10^8 sec^{-1}	0.050×10^8 sec^{-1}

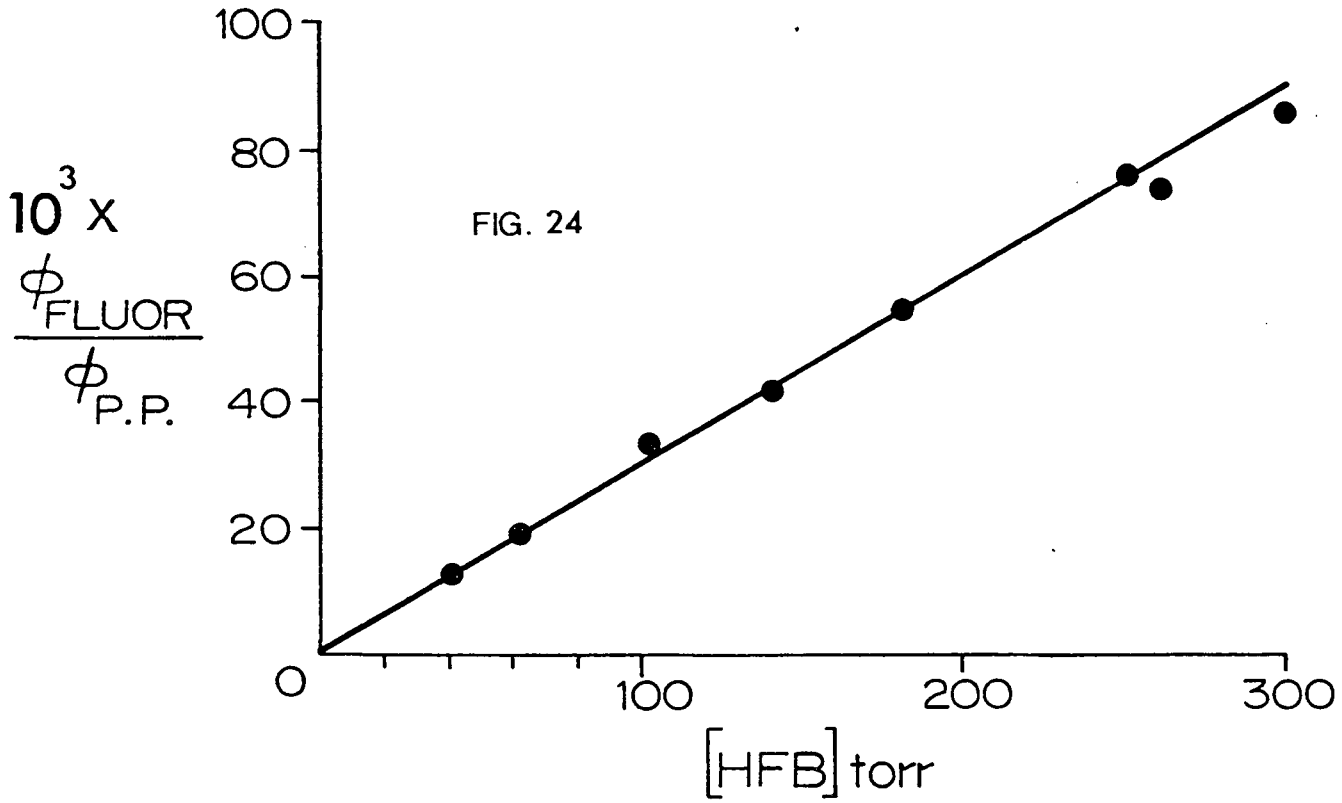

FIG. 24

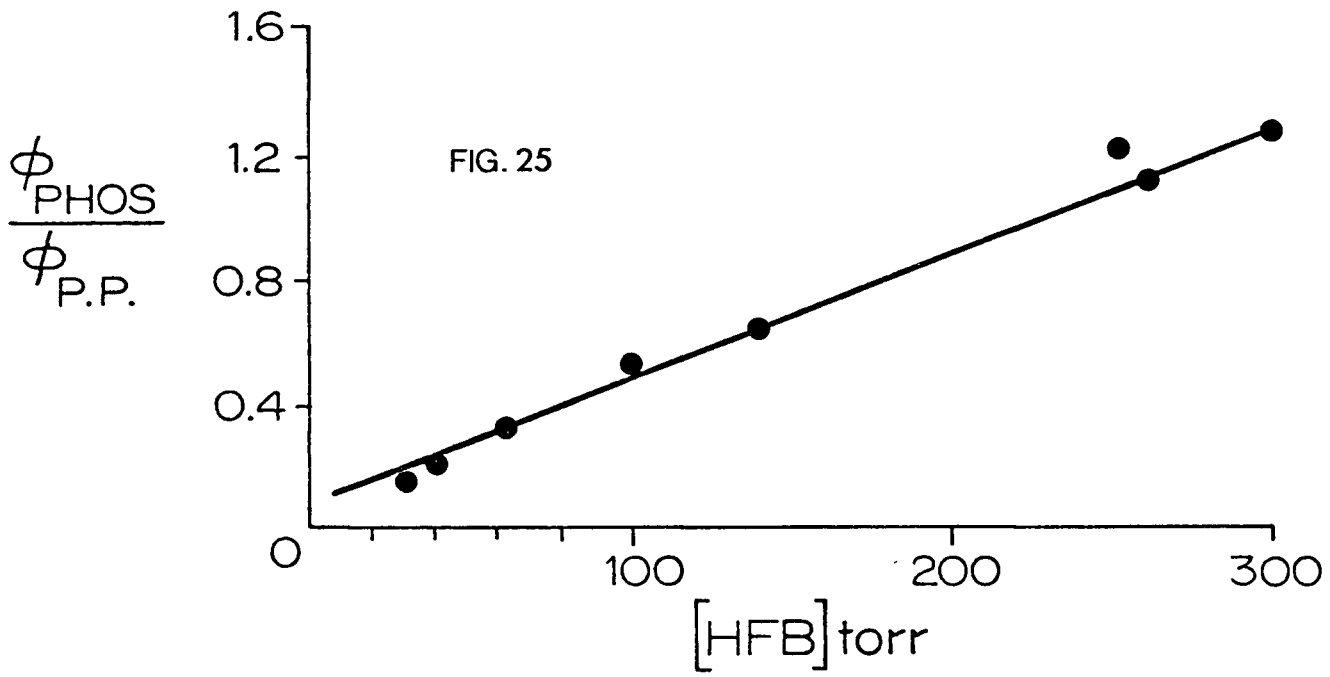

FIG. 25

FIG. 24 RATIO OF FLUORESCENCE YIELD TO PHOTOCHEMICAL YIELD VERSUS HFB PRESSURE AT 313 NM. HIGH PRESSURE REGION

FIG. 25 RATIO OF PHOSPHORESCENCE YIELD TO PHOTOCHEMICAL YIELD VERSUS HFB PRESSURE AT 313 NM. HIGH PRESSURE REGION

of the present work would indicate that his phosphorescence yields below about 5 or 10 torr are quantitatively open to question. His observation that ϕ_{phos} decreases as the pressure decreases is undoubtedly real as the shorter wavelength results display this same pressure dependence (as longer wavelengths) at higher pressures where wall-deactivation of the equilibrated triplet would be negligible. These pressure dependencies are caused by triplet dissociation competing favorably with collisional degradation. It is possible that if dissociation is absent (as at 436 nm) the limiting high pressure ϕ_{phos} will be maintained to very low pressures as in biacetyl.[14]

The fluorescence yields and the singlet dissociation yields are unaffected by the cell geometry because of the short lifetime of the singlet state ($\sim$ 50 nsec). The triplet dissociation yields are similarly unaffected.

The fluorescence and photochemical data can be combined to illustrate this competition in the triplet manifold:

(i) Fluorescence and Intersystem Crossing

The full expression for the fluorescence/photochemistry ratio, Equation (12), can be written in the form

$$\frac{\phi_{fluor}}{\phi_{P.P.}} = \frac{\alpha\ \omega M + k_f^*}{k_2 + \Omega k_1} \qquad \text{----------(16)}$$

where $\Omega = \frac{k_5}{k_5 + \omega M}$

At high pressures it is found that this ratio is linear with pressure (Page 107). As the pressure is lowered however, Ω changes from 0 to 1. Figure 26 shows the experimental data at 297 nm confirming this prediction. The difference between the extrapolated value and the experimentally determined value of $\phi_{fluor}/\ \phi_{P.P.}$ decreases below 30 torr. It appears that these two lines would converge at zero pressure as Equation (16) demands. The data at 313 nm show the same pressure dependence (Figure 27) beginning at a lower pressure and much less pronounced. No deviation from linearity is noticeable with 334 nm or 366 nm radiation even at the lowest pressures of HFB irradiated. Fluorescence data are unavailable with 254 nm exciting radiation.

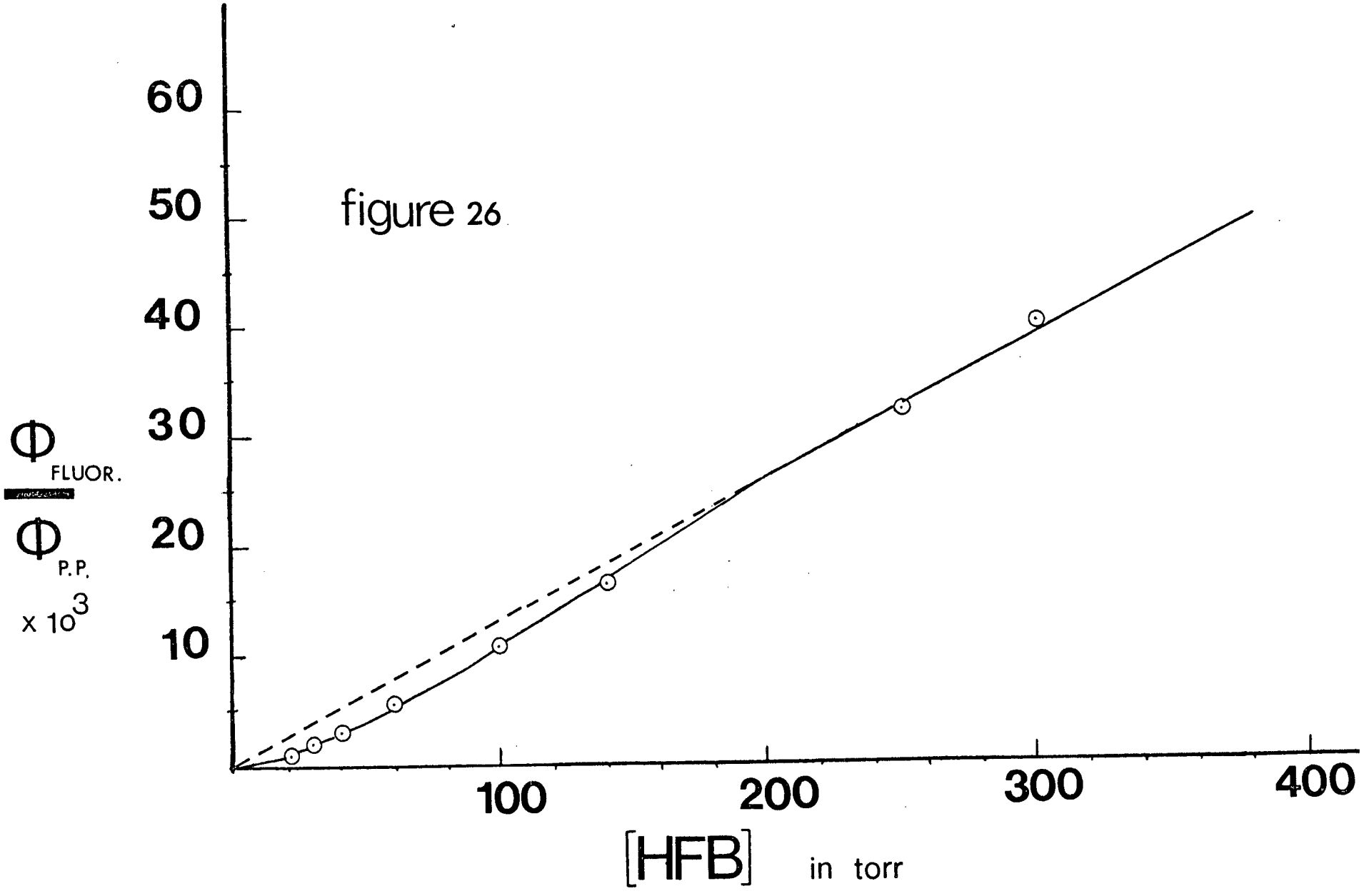

RATIO OF FLUORESCENCE YIELD TO PHOTOCHEMICAL YIELD VERSUS HFB PRESSURE AT 297 NM

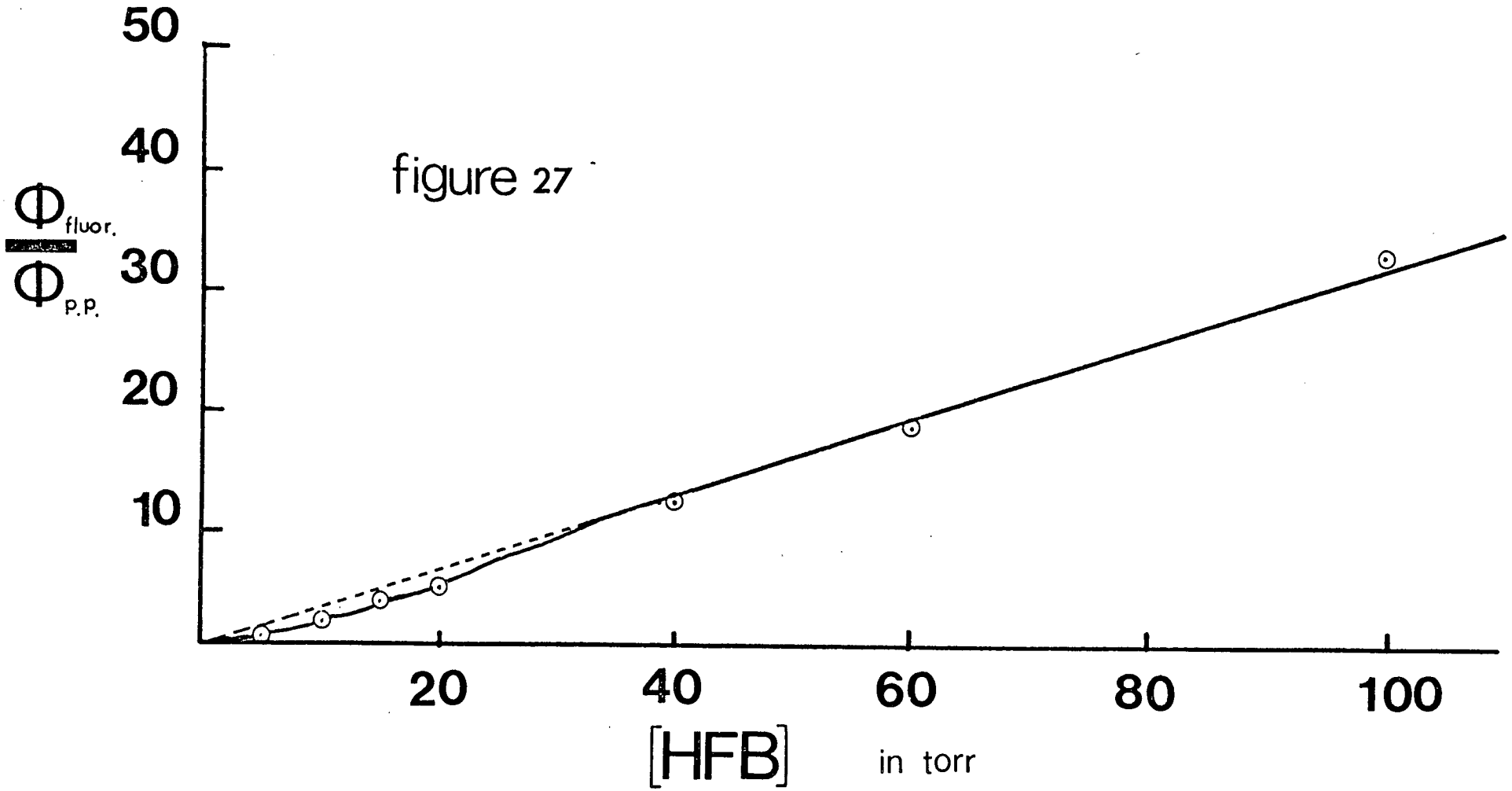

RATIO OF FLUORESCENCE YIELD TO PHOTOCHEMICAL YIELD VERSUS HFB PRESSURE AT 313 NM

Figure 26 shows that decomposition can compete with collisional deactivation in the triplet manifold below about 100 torr at 297 nm. As the wavelength is increased the vibrational energy of the triplet molecules formed decreases. The pressure at which this competition is evident therefore, decreases.

(ii) Limitations on Available Data

A question must now be answered: are the two independent sets of data (photochemistry and emission) complementary? The absolute uncertainty in the emission yields is given as 17%. Of course this would vary slightly depending on wavelength and pressure region being considered. The relative error for the photochemical yields is about 10% although this rises sharply under extreme conditions (e.g. very high pressures at 366 nm).

A fair reflection of these errors is achieved if the fluorescence and phosphorescence quantum yields are calculated using Equations (1) and (2) and plotted together with McIntosh's experimental data. The calculations involve using his values of ϕ^{∞}_{fluor} and ϕ^{∞}_{phos} and values of k_1, k_2 and k_5 taken from this work. A problem arises for ϕ_{phos} at

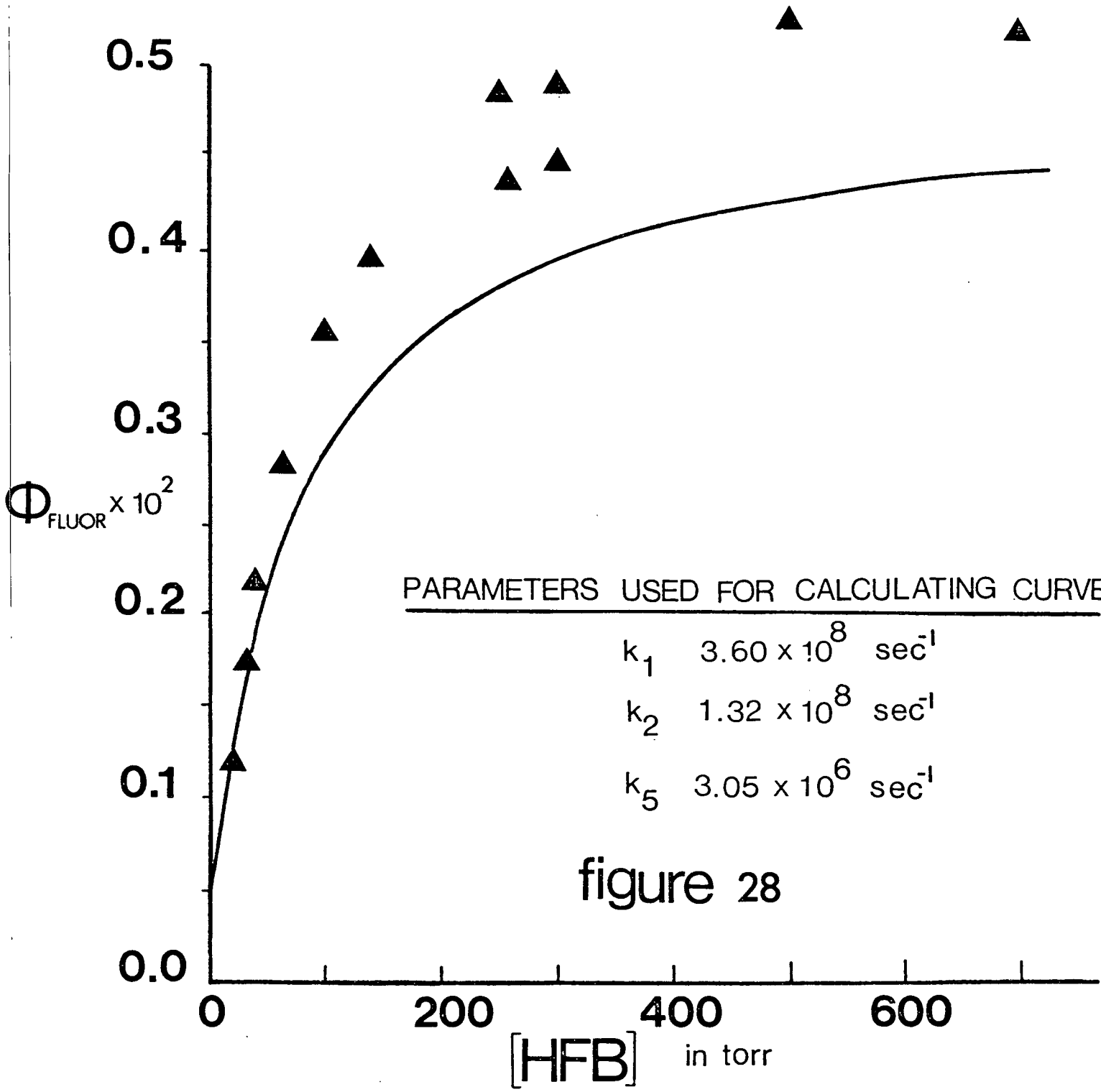

figure 28

FLUORESCENCE QUANTUM YIELD VERSUS HFB PRESSURE AT 313 NM
EXPERIMENTAL POINTS FROM McINTOSH[1]. SOLID LINE CALCULATED FROM PARAMETERS INDICATED

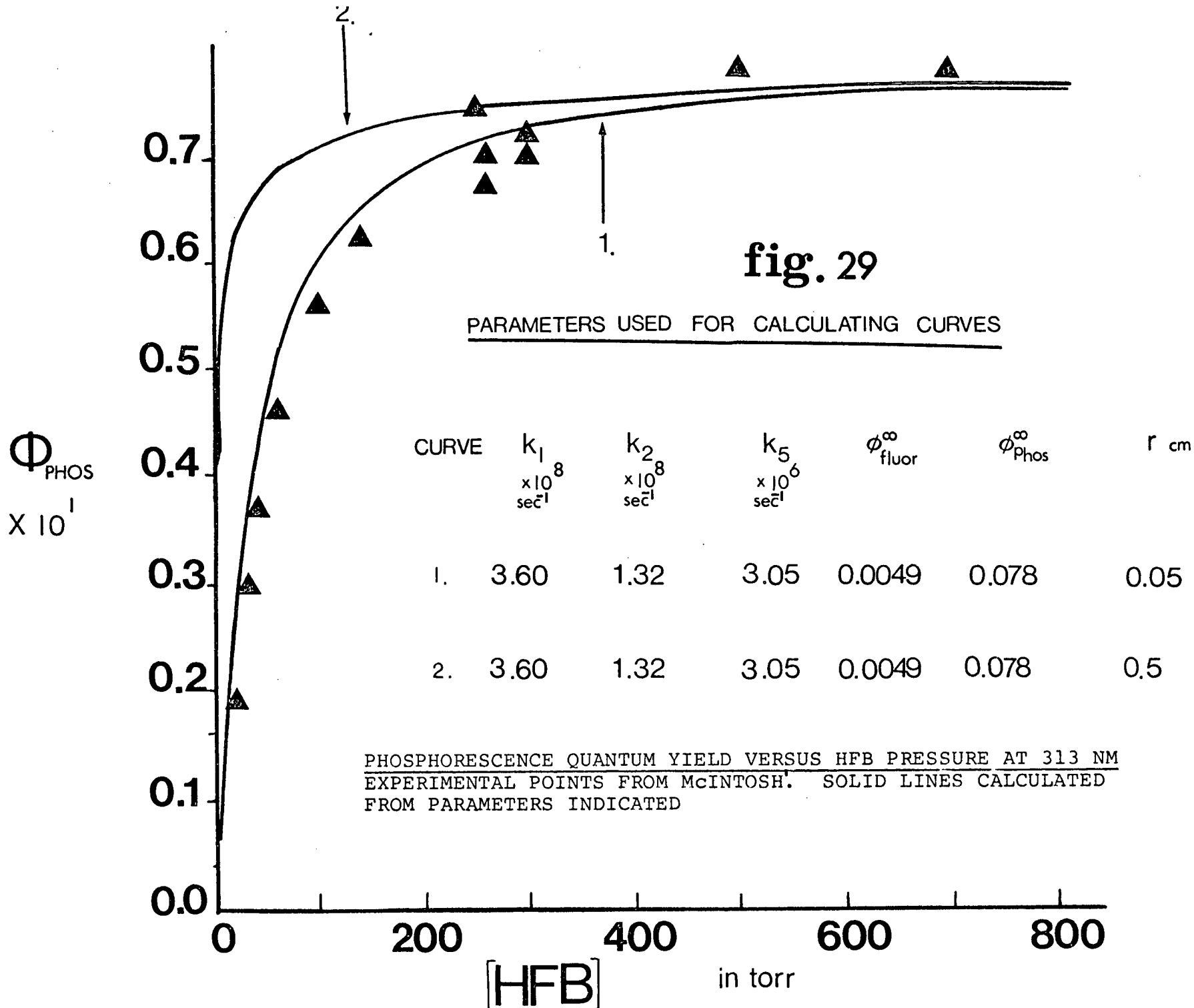

fig. 29

PARAMETERS USED FOR CALCULATING CURVES

CURVE	k_1 $\times 10^8$ sec^{-1}	k_2 $\times 10^8$ sec^{-1}	k_5 $\times 10^6$ sec^{-1}	ϕ^{∞}_{fluor}	ϕ^{∞}_{Phos}	r cm
1.	3.60	1.32	3.05	0.0049	0.078	0.05
2.	3.60	1.32	3.05	0.0049	0.078	0.5

PHOSPHORESCENCE QUANTUM YIELD VERSUS HFB PRESSURE AT 313 NM
EXPERIMENTAL POINTS FROM McINTOSH[1]. SOLID LINES CALCULATED FROM PARAMETERS INDICATED

low pressures where wall-deactivation becomes important (process (xiii)) as the effective cell radius (r) for McIntosh's experiment can only be estimated. Therefore this calculation was carried out with what are considered to be extreme values of r: 0.5 cm and 0.05 cm respectively (Appendix B). Gross assumptions are also made regarding the diffusion coefficient and the probability for wall reflection without deactivation. The results at 313 nm are given in Figures 28 and 29. It is evident that even at a pressure of 200 torr HFB a cell radius of 0.05 cm would necessitate wall deactivation being considered when reporting phosphorescence quantum yields. Plots at 297, 334 and 366 nm show the same trends. No emission yields are available at 254 nm.

Within the quoted experimental errors and limitations imposed on the calculated curves the two studies are seen to be entirely complementary.

E. Concluding Remarks - Suggestions for Further Work

This investigation has helped to establish the main features of the primary process in the photolysis of hexa-

fluorobiacetyl. Its potential as a model system is obvious - predictable photochemical products as well as emission from two different electronic states. Much remains to be done however, particularly in the low pressure region.

The technique of transient fluorometry[51] offers a very powerful tool to observe the initially-formed singlet state. By examining fluorescence decay as a function of exciting wavelengths at very low pressures information could be obtained regarding the non-radiative processes (primary dissociation and intersystem crossing) depleting the excited singlet state. Emission data at these same wavelengths and low pressures would also be very useful. The experimental arrangement will have to be such that wall-deactivation can be quantitatively eliminated. The variation of emission yields with pressure at very low pressures would indicate whether intersystem crossing is truly unimolecular and if HFB is in the "large molecule" limit discussed in the theories of unimolecular transitions.[10]

An interesting phenomenon has been noted for the HFB-HFAM energy transfer system. It is found that the phosphorescence lifetime of a mixture of 50 torr HFB and 500 torr

hexafluoroethane (HFE) is very slightly temperature dependent while the quenched lifetime of the same mixture by HFAM has a negative temperature dependence below room temperature, i.e. the rate of quenching increases as the temperature decreases. It should prove interesting to investigate this effect further for other systems.

B I B L I O G R A P H Y

1. J.S.E. McIntosh, Primary Photphysical Processes in Hexafluorobiacetyl. Ph.D. Thesis, University of British Columbia, 1969

2. P.G. Bowers, The Primary Photochemical Process in Hexafluoroacetone Vapour. Ph.D. Thesis, the University of British Columbia, 1964

3. G.B. Porter and B.T. Connelly, J. Chem. Phys., 33, 81, (1960)

4. D.A. Whytock and K.O. Kutschke, Proc. Roy. Soc., A306, 503, (1968); A. Gandini and Kutschke, ibid., 511; Gandini, Whytock and Kutschke, ibid., 529; ibid., 537; ibid., 541.

5. G.B. Porter and K. Uchida, J. Phys. Chem., 70, 4079, (1966)

6. A.N. Strachan, R.K. Boyd and K.O. Kutschke, Can. J. Chem., 42, 1345, (1964)

7. A.M. Halpern and W.R. Ware, J. Chem. Phys., 53, 1969, (1970)

8. R. Atkinson and B.A. Thrush, Chem. Phys. Letters, 3, 684, (1969)

9. R. Atkinson and B.A. Thrush, Proc. Roy. Soc., A316, 123 (1970)

10. G.W. Robinson, J. Chem. Phys., 47, 1967, (1967); B.R. Henry and M. Kasha, Ann. Rev. Phys. Chem., 19, 161, (1968); J.B. Birks and I.H. Munro, Progr. React. Kinet., 4, 239, (1967); J. Jortner, S.A. Rice, and R.M. Hochstrasser, Advan. Photochem., 7, 149, (1969)

11. A.V. Buettner, J. Chem. Phys., 46, 1398, (1967)

12. W.A. Noyes and I. Unger, Singlet and Triplet States: Benzene and Simple Aromatic Compounds, in Advances in Photochemistry, vol. 4, eds. W.A. Noyes, G.S. Hammond and J.N. Pitts, Jr., Interscience Publishers, 1966.

13. R.B. Cundall and A.S. Davies, Primary Processes in the Gas Phase Photochemistry of Carbonyl Compounds, in Progress in Reaction Kinetics, vol. 4, ed. G. Porter, Pergamon Press, 1967.

14. H.W. Sidebottom, C.C. Badcock, J.G. Calvert, B.R. Rabe and E.K. Damon, J. Am. Chem. Soc., 94, 13,(1972)

15. G. Porter, Reactivity, Radiationless Conversion and Electron Distribution in the Excited State, in Reactivity of the Photoexcited Organic Molecule, Proceedings of the Thirteenth Conference on Chemistry at the University of Brussels, October 1965, Interscience, 1967.

16. G.B. Porter, J. Chem. Phys., 32, 1587, (1960)

17. H. Ishikawa and W.A. Noyes, Jr., J. Am. Chem. Soc., 84, 1502, (1962); J. Chem. Phys., 37, 591, (1962)

18. C.S. Parmenter and H.M. Poland, J. Chem. Phys., 51, 1551, (1969)

19. E. Drent and J. Kommandeur, Chem. Phy. Letters, 8, 303, (1971)

20. J.G. Calvert and J.N. Pitts, Jr., Photochemistry, Wiley, New York, 1966; W.A. Noyes, Jr., G. B. Porter and J.E. Jolley, Chem. Rev., 56, 49, (1956)

21. J.R. Majer, C. Olavesen and J.C. Robb, J.Chem. Soc. (B), 48, (1971)

22. J.R. Majer, C. Olavesen and J.C. Robb, J. Chem. Soc. (A), 893, (1969)

23. P.B. Ayscough and E.W.R. Steacie, Proc. Roy. Soc. A234, 476, (1956)

24. I.M. Whittemore and M. Szwarc, J. Phys. Chem., 67, 2492, (1963)

25. W.J. Reid, Primary Photochemical Processes in Hexafluorobiacetyl at 313 nm, M.Sc. Thesis, the University of British Columbia, 1970.

26. W.A. Noyes, W.A. Mulac and M.S. Matheson, J. Chem. Phys., 36, 880, (1962)

27. A. Gandini, D.A. Whytock and K.O. Kutschke, Berichte der Bunsengesellschaft fur physikalische Chemie, 72, 296, (1968)

28. L.O. Moore and J.W. Clark, U.S. Patent 3,055,913 (1962); ibid., J. Org. Chem., 30, 2472, (1965)

29. G. Urry and W.H. Urry, Rev. Sci. Inst. 27, 819, (1956)

30. C.G. Hatchard and C.A. Parker, Proc. Roy. Soc., A235, 518, (1956)

31. C.A. Parker, Photoluminescence of Solutions, Elservier Publishing Company, 1968.

32. Noyes and Leighton, The Photochemistry of Gases, Reinhold, 1941.

33. R.E. Hunt and T.L. Hill, J. Chem. Phys., 15, 111, (1947)

34. J.S.E. McIntosh, private communication.

35. J.S.E. McIntosh and G.B. Porter, J. Chem. Phys., 48, 5475, (1968)

36. R.E. Rebbert and P. Ausloos, J. Am. Chem. Soc., 87, 1847, (1965)

37. E-C. Wu and O.K. Rice, J. Phys. Chem., 72, 542, (1968)

38. J.W. Coomber and J.N. Pitts, Jr., J. Am. Chem. Soc., 91, 4955, (1969)

39. W.J. Reid, unpublished results.

40. W.R. Ware, B.K. Selinger, C.S. Parmenter and M.W. Schuyler, Chem. Phys. Letts., 6, 342, (1970)

41. Calvert and Pitts, Photochemistry, p. 660

42. R. Srinivasan, J. Amer. Chem. Soc., 84, 3432, (1962)

43. R. Srinivasan, Photochemistry of Conjugated Dienes and Trienes, in Advances in Photochemistry, vol. 4, eds. W.A. Noyes, G.S. Hammond and J.N. Pitts, Interscience Publishers, 1966

44. C.S. Parmenter, J. Chem. Phys., 41, 658, (1964)

45. P.G. Bowers, J. Chem. Soc. (A), 466, (1967); ibid., Can. J. Chem., 46, 307, (1968)

46. Ibid., J. Phys. Chem., 74 , 952, (1970)

47. J.O. Hirschfelder, C.F. Curtiss and R.B. Bird, Molecular Theory of Gases and Liquids, Wiley, New York, 1964.

48. S.W. Benson, The Foundations of Chemical Kinetics, McGraw-Hill Book Co., New York, 1960.

49. H.M. Poland, Fluorescence and Phosphorescence from Biacetyl and Glyoxal, Ph.D. Thesis, Indiana University, 1969.

50. J.S.E. McIntosh, Ph.D. Thesis, University of British Columbia, Chapter VI, 1969.

51. E.W. Schlag, S. Schneider, and S.F. Fisher, Ann. Rev. Phys. Chem., 22, 465, (1971); W.R. Ware, Transient Luminescence Measurements, in Creation and Detection of Excited States, vol. 1, ed. A. Lamola, Marcel Dekker, New York, 1971.

52. M. Kovacs, D.R. Rao and A. Javen, J. Chem. Phys., 48, 3339, (1968)

53. H.M. Poland, Ph.D. Thesis, Indiana University, Page 30, 1969.

A P P E N D I X

A. Window Corrections

Because of the large transmission losses from the silica-air interfaces of the reaction vessel and the actinometer cell, it was necessary to apply a correction factor to obtain the absolute intensity of the absorbed radiation.[32-33] For convenience all windows were assumed to have identical losses from reflection.

Let α be the fraction of light lost in passing through a window.

Evacuated cell:-

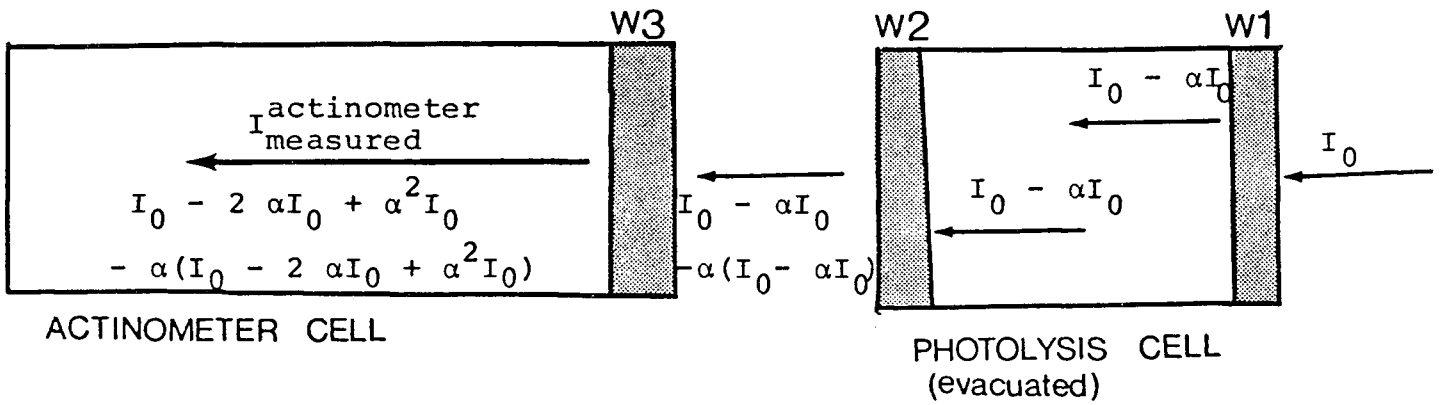

$$I^{\text{actinometer}}_{\text{measured (no gas)}} = I_0 - 2\alpha I_0 + \alpha^2 I_0 - \alpha I_0 + 2\alpha^2 I_0 - \alpha^3 I_0$$

$$= I_0 - 3\alpha I_0 + 3\alpha^2 I_0$$

$$= I_0 (1 - 3\alpha + 3\alpha^2)$$

$$= I_0 (1 - 3\{\alpha - \alpha^2\})$$

$$\therefore \quad I_0 = \frac{I^{\text{actinometer}}_{\text{measured (no gas)}}}{1 - 3(\alpha - \alpha^2)}$$

However, we want to measure the intensity of radiation just inside the front window (W_1).

$$\text{i.e.} \quad I_0 - \alpha I_0 \equiv I$$

$$I \equiv I_0 - \alpha I_0 = I_0 (1 - \alpha)$$

$$\therefore \quad I = \frac{I^{\text{actinometer}}_{\text{measured (no gas)}}}{1 - 3(\alpha - \alpha^2)} \times (1 - \alpha)$$

It was found that the transmission properties of the quartz windows (Chapter 2, Section E) at the various wavelengths were in excellent agreement with the variation in

reflection as calculated using the index of refraction of fused quartz, assuming Fresnel's Law and an air - SiO_2 - air interface.

B. Wall Deactivation

It is assumed that wall-deactivation is responsible for all low pressure effects on the equilibrated triplet state. The diffusion equations developed initially by Javen et al[52] and subsequently by Poland[49] for a similar problem concerning wall-deactivation of triplet biacetyl are used. The geometry of her experiments are similar to ours. In both cases diffusion to the walls occurs in a cylindrical cell uniformly filled with the excited diffusing species.

The rate constant for deactivation on the wall, k_{wall}, is given by

$$k_{wall} = \frac{\mu^2 D}{r^2}$$

where $k_{wall} = \tau_{wall}^{-1}$ and τ_{wall} is the lifetime that the excited species would have if it decayed only by diffusion to the wall. D is the usual diffusion coefficient, r is the

cell radius and μ is given by the solution of the boundary condition

$$\mu J_1(\mu) - \frac{(\bar{v}\, r)}{2D} \quad \frac{(1 - \beta) J_0(\mu)}{(1 + \beta)} = 0$$

J_0 and J_1 are zero and first order Bessel functions.[49]

D was calculated from[47]

$$D = {}^1/_3 \times \bar{v}\ (MFP)$$

where MFP = Free Mean Path and $\bar{v}$ and β are the mean speed and probability for wall reflection with deactivation respectively. D was calculated to be 0.011 $cm^2 sec^{-1}$. β was chosen to be 0.1.[53]